

# **Large-Scale Optimization for Interdependent Infrastructure Systems**

by

Geunyeong Byeon

A dissertation submitted in partial fulfillment  
of the requirements for the degree of  
Doctor of Philosophy  
(Industrial and Operations Engineering)  
in the University of Michigan  
2020

Doctoral Committee:

Professor Jon Lee, Co-Chair  
Professor Pascal Van Hentenryck, Co-Chair  
Professor Marina A. Epelman  
Assistant Professor Ruiwei Jiang  
Assistant Professor Johanna Mathieu

Geunyeong Byeon

[gbyeon@umich.edu](mailto:gbyeon@umich.edu)

ORCID iD: 0000-0003-3324-1831

© Geunyeong Byeon 2020

To my family.

## ACKNOWLEDGEMENTS

I would like to thank those who provided assistance in this research and support throughout my time working on this dissertation. First and foremost, I would like to express my deepest gratitude to my advisor, Pascal, for his guidance of my research and genuine support. Working with Pascal in the past four years is the greatest privilege of my life; His brilliant advice helped me in all the time of research and enlightened me on how to communicate with others. Besides his research guidance, I have been constantly inspired by his passion, energy, patience, and open-mindedness, which has influenced various aspects of me in invaluable ways.

I would also like to express my profound gratitude to Prof. Jon Lee. I have been truly amazed by how he cares about the people around him. It was his endless caring and support that led me to go through some difficult times during my graduate years. He is also a wonderful teacher; I enjoyed every minute of his lectures. I am also sincerely thankful to Prof. Marina Epelman for her genuine support and her passion for teaching. What I have learned from her, inside and outside the classroom, as a student and as her teaching assistant will continuously inspire me. I am also very grateful to Profs. Ruiwei Jiang, Johanna Mathieu, and Siqian Shen for their caring and excellent courses from which I learned a great deal. I am also sincerely thankful to Prof. Brian Denton for his warm support; He is a phenomenal leader who embraces each individual in the department with respect and care. I also would like to extend my gratitude to two of my brilliant collaborators, Russell and Harsha in Los Alamos National Laboratory, for their valuable comments on research and kind support. I believe the only way that I can give back what these amazing people have given me is to transfer their caring to other people, especially students who would be in the same shoes that I had been in.

My Ph.D. life has been delightful as I have come to know many friendly staff members and my fellow students in the Industrial and Operations Engineering department. My sincere gratitude goes to Cathy Boblitt, Matt Irelan, Christopher Konrad, Tina Picano Sroka, Matthew-Remy Aguirre, Hideaki Nakao, Connor Riley, Byron Tasseff, Miao Yu, Xian Yu, Huiwen Jia, and Thomas Chen. My special thanks to Minseok Ryu, Sol Lim, Youngchan Jang, Seokjoo Kwak, and Seokhyun Chung.

Last but not least, I own my deepest thanks to my family for their unwavering love and support.

In addition, I gratefully acknowledge partial support from the DOE-OE Smart Grid R&D Program through the Grid Modernization Laboratory Consortium project *LPNORM* and NSF grant NSF-1638331.

# TABLE OF CONTENTS

|  |             |
|--|-------------|
| <b>Dedication</b> . . . . .  | <b>ii</b>   |
| <b>Acknowledgments</b> . . . . .   | <b>iii</b>  |
| <b>List of Figures</b> . . . . .   | <b>vii</b>  |
| <b>List of Tables</b> . . . . .  | <b>viii</b> |
| <b>List of Abbreviations</b> . . . . .   | <b>ix</b>   |
| <b>Abstract</b> . . . . .  | <b>xi</b>   |
| <b>Chapter</b>   |             |
| <b>1 Introduction</b> . . . . .  | <b>1</b>    |
| 1.1 Preliminaries . . . . .  | 2           |
| 1.1.1 Background on Application Areas . . . . .  | 2           |
| 1.1.2 Decomposition Techniques . . . . .   | 7           |
| 1.2 Thesis Overview . . . . .  | 11          |
| <b>2 Communication-Constrained Expansion Planning for Resilient Distribution Systems</b> . . . . . | <b>14</b>   |
| 2.1 Introductory Remarks . . . . .   | 14          |
| 2.2 Literature Review . . . . .  | 17          |
| 2.3 Mathematical Modeling: the ORDPDC . . . . .  | 18          |
| 2.3.1 Linearization of the ORDPDC . . . . .  | 26          |
| 2.4 Case Study . . . . .   | 28          |
| 2.4.1 Data Description . . . . .   | 28          |
| 2.4.2 Impact of Grid Topology . . . . .  | 30          |
| 2.4.3 Impact of the Communication Network . . . . .  | 30          |
| 2.4.4 Load Flow Analysis of the Linearization of the ORDPDC . . . . .                              | 33          |
| 2.5 Solution Approaches . . . . .  | 34          |
| 2.5.1 Benchmark Approaches: Scenario-Based and Scenario Decomposition . . . . .                    | 34          |
| 2.5.2 Proposed Approach: Branch-and-Price Algorithm . . . . .                                      | 35          |
| 2.6 Performance Analysis of the Branch and Price Algorithm . . . . .                               | 39          |
| 2.6.1 Computational Performance . . . . .  | 40          |
| 2.6.2 Solution Quality at the Root Node. . . . .   | 40          |

|          |  |            |
|----------|--|------------|
| 2.6.3    | Benefits of the Accelerating Schemes . . . . .   | 41         |
| 2.7      | Concluding Remarks . . . . .   | 43         |
| <b>3</b> | <b>Unit Commitment with Gas Awareness . . . . .</b>  | <b>44</b>  |
| 3.1      | Introductory Remarks . . . . .   | 44         |
| 3.2      | Mathematical Modeling: the UCGNA . . . . .   | 46         |
| 3.2.1    | The Electricity Transmission System . . . . .  | 46         |
| 3.2.2    | The Natural Gas Transmission System . . . . .  | 49         |
| 3.2.3    | Physical and Economic Couplings . . . . .  | 51         |
| 3.2.4    | Bilevel Formulation . . . . .  | 53         |
| 3.3      | Solution Approach . . . . .  | 56         |
| 3.4      | Case Study . . . . .   | 57         |
| 3.4.1    | Data Description . . . . .   | 57         |
| 3.4.2    | Impact of the Gas-Awareness . . . . .  | 58         |
| 3.5      | Discussion on the UCGNA . . . . .  | 63         |
| 3.6      | Concluding Remark . . . . .  | 65         |
| <b>4</b> | <b>Benders Subproblem Decomposition for Discrete-Continuous Bilevel Problems 67</b>          | <b>67</b>  |
| 4.1      | Introductory Remarks . . . . .   | 67         |
| 4.2      | Literature Review . . . . .  | 70         |
| 4.3      | MIP reformulation . . . . .  | 72         |
| 4.4      | A Dedicated Benders Decomposition Method for MIBPSD . . . . .                                | 73         |
| 4.4.1    | Interpretation of Benders Cuts . . . . .   | 76         |
| 4.5      | MIBPSD with Additional Upper Level Constraints on Dual Variables of<br>Lower Level . . . . . | 77         |
| 4.6      | Sequence-Independent BSP Decomposition . . . . .   | 78         |
| 4.7      | Acceleration Schemes for the Dedicated Benders Method . . . . .                              | 79         |
| 4.7.1    | Normalizing Benders Feasibility Cuts . . . . .   | 79         |
| 4.7.2    | An In-Out Approach . . . . .   | 82         |
| 4.8      | Performance Analysis of the Dedicated Benders Method . . . . .                               | 83         |
| 4.8.1    | Test Instances . . . . .   | 83         |
| 4.8.2    | Computational Performance . . . . .  | 84         |
| 4.8.3    | Benefits of the Acceleration Schemes . . . . .   | 87         |
| 4.8.4    | Benefits of the Decomposition Method . . . . .   | 89         |
| 4.9      | Concluding Remarks . . . . .   | 90         |
| <b>5</b> | <b>Conclusions . . . . .</b>   | <b>93</b>  |
|          | <b>Appendices . . . . .</b>  | <b>95</b>  |
|          | <b>Bibliography . . . . .</b>  | <b>105</b> |

## LIST OF FIGURES

### Figures

|      |   |    |
|------|---|----|
| 1.1  | Notations for the 3-Phase Power Flow Equations. . . . .   | 3  |
| 2.1  | The Cyber-Physical Network for Electricity Distribution. Solid lines represent power lines and dotted lines represent communication links. . . . .  | 19 |
| 2.2  | Notations for the Power Flow Equations. . . . .   | 22 |
| 2.3  | The Single-Commodity Flow Model for $\tilde{G}$ (red-colored squares denote control centers). . . . .   | 24 |
| 2.4  | The Piecewise-Linear Inner Approximation of a Circle. . . . .   | 28 |
| 2.5  | The urban and rural distribution systems which contain three copies of the IEEE 34 system to mimic situations where there are three normally independent distribution circuits that support each other during extreme events. These test cases include 109 nodes, 118 generators, 204 loads, and 148 edges. . . . . | 29 |
| 2.6  | Statistics on the Optimal Grid Designs. . . . .   | 31 |
| 2.7  | Optimal Designs of the Rural and Urban Networks (3% damage level). . . . .  | 31 |
| 2.8  | Optimal Design of Network NETWORK123 (20% damage level). . . . .  | 32 |
| 2.9  | Cost Analysis For the Number of Communication Centers . . . . .   | 32 |
| 2.10 | Optimal Designs of the Rural Network under 3% Damage and Various Communication Network Configurations. . . . .  | 33 |
| 2.11 | Comparison of Computation Times: SBD versus BnP. . . . .  | 41 |
| 2.12 | Comparison of Convergence Rates (rural network, 6% level of damage). . . . .  | 43 |
| 3.1  | Results for the Normal Operating Conditions of the Electrical Power System ( $\eta_e = 1$ ), where $x$ -axis represents $\eta_g$ . . . . .  | 59 |
| 3.2  | Results for the Stressed Electrical Power System ( $\eta_e = 1.3$ ), where $x$ -axis represents $\eta_g$ . . . . .  | 60 |
| 3.3  | Results for the Highly-Stressed Electrical Power System ( $\eta_e = 1.6$ ), where $x$ -axis represents $\eta_g$ . . . . .   | 61 |
| 3.4  | Results for the Highly-Stressed Condition $(\eta_e, \eta_g) = (1.6, 2.3)$ . . . . .   | 62 |
| 4.1  | D vs G. . . . .   | 87 |
| 4.2  | Statistics on Computation Times for Cut Generation. . . . .   | 90 |
| 4.3  | Convergence Behaviors of D and B. . . . .   | 91 |

## LIST OF TABLES

### Tables

|     |  |    |
|-----|--|----|
| 2.1 | The Parameters of the ORDPDC. . . . .  | 20 |
| 2.2 | The Variables of the ORDPDC. . . . .   | 21 |
| 2.3 | Impact of the Communication Network on Optimal Grid Designs. . . . .   | 33 |
| 2.4 | Numerical Stability of the BnP Algorithm. . . . .  | 41 |
| 2.5 | Branching Tree Statistics. . . . .   | 41 |
| 2.6 | Comparison to a Column Generation with Dual Stabilization. . . . .   | 42 |
| 2.7 | Benefits of the Accelerating Schemes. . . . .  | 42 |
|     |  |    |
| 3.1 | Parameters of the Electricity System. . . . .  | 47 |
| 3.2 | Variables of the Electricity System. . . . .   | 47 |
| 3.3 | Parameters of the gas system . . . . .   | 49 |
| 3.4 | Variables of the gas system . . . . .  | 49 |
| 3.5 | Parameters for the Electricity and Gas Coupling. . . . .   | 51 |
| 3.6 | Variables for the Electricity and Gas Coupling. . . . .  | 51 |
| 3.7 | Statistics on Committed Generators for the Stressed Electrical Power System<br>( $\eta_e = 1.6$ ): The first 7 columns display the number of committed generators<br>with respect to its fuel type, where (O) Oil, (C) Coal, (G) Gas, (H) Hydro, (R)<br>Refuse, (N) Nuclear, (E) Others, and the last two columns show the number<br>of committed GFPPs in each pricing zone, where (T) Transco Zone 6 Non NY<br>and (L) Transco Leidy Line. . . . . | 61 |
| 3.8 | Solution Statistics for (B), where Column (i) denotes the final objective value<br>of (B) for each instance and Column (ii) represents the optimality gap (time<br>limit: one hour) . . . . .  | 63 |
|     |  |    |
| 4.1 | Computational Performance Comparison ( $\eta_p = 1$ ). . . . .   | 85 |
| 4.2 | Computational Performance Comparison ( $\eta_p = 1.3$ ). . . . .   | 85 |
| 4.3 | Computational Performance Comparison ( $\eta_p = 1.6$ ). . . . .   | 86 |
| 4.4 | Benefits of the Acceleration Schemes ( $\eta_p = 1$ ). . . . .   | 88 |
| 4.5 | Benefits of the Acceleration Schemes ( $\eta_p = 1.3$ ). . . . .   | 88 |
| 4.6 | Benefits of the Acceleration Schemes ( $\eta_p = 1.6$ ). . . . .   | 89 |

## LIST OF ABBREVIATIONS

**AC** Alternating Current

**BnC** Branch-and-Cut

**BnP** Branch-and-Price

**DG** Distributed Generation

**DSR** Distribution System Restoration

**ED** Economic Dispatch

**GFPPs** Gas-Fueled Power Plants

**ILP** Integer Linear Programming

**KKT** Karush-Kuhn-Tucker

**LP** Linear Programming

**MIBP** Mixed-Integer Bilevel Programming

**MIBPSD** Mixed-Integer Bilevel Programming with Strong Duality in lower-level

**MILP** Mixed-Integer Linear Programming

**MIP** Mixed-Integer Programming

**MISOCP** Mixed-Integer Second-Order Cone Program

**ORDPDC** Optimal Resilient Design Problem for Distribution and Communication Systems

**PDE** Partial Differential Equations

**RCS** Remotely Controlled Switches

**SBD** Scenario-Based Decomposition

**SD** Scenario Decomposition

**SDP** Semidefinite Program

**SOCP** Second-Order Cone Program

**UC** Unit Commitment

**UCGNA** Unit Commitment problem with Gas Network Awareness

## ABSTRACT

The primary focus of this thesis is to develop decomposition methods for solving large-scale optimization problems, especially those arising in interconnected infrastructure systems. Several factors (e.g., the Internet-of-Things) are driving infrastructure systems to become more interdependent. As a result, these complex systems are increasingly exposed to a variety of risks and demand elaborate optimization modeling that allows risk-informed decision-making. The resulting optimization models, however, are often of large-scale and have computationally challenging properties. In this regard, this thesis studies how to formulate optimization models mitigating their risks and develop decomposition methods for solving these models with improved computational properties.

We first present a network planning problem for electricity distribution grids and their associated communication networks. The problem is formulated as a two-stage mixed-integer linear program and is of large-scale, since it captures hundreds of potential disaster scenarios as well as grids' dependencies on the communication systems. To deal with its vast size, we develop a branch-and-price algorithm that features a tight lower bound and various acceleration schemes that address degeneracy. The model and algorithm were evaluated on a variety of test cases, the results of which demonstrate the impact of the risk-aware planning decisions as well as the computational benefits of the proposed solution approach.

Next, we propose a unit scheduling problem of electric grids. We introduce gas network awareness into the scheduling problem to alleviate risks from natural gas networks. The resulting optimization model is formulated as a bi-level optimization problem. To address

inherent computational challenges in solving bilevel problems, we develop a dedicated Benders decomposition method for solving a certain class of bilevel problems (discrete-continuous bilevel problems), which subsumes the proposed model. The algorithm features a Benders subproblem decomposition technique that breaks down the Benders subproblem into two more tractable problems. We test the model and the solution approach on a practically-relevant network data set. The results demonstrate that the risk-aware operational decision is instrumental in avoiding disruptions caused by gas system insecurity. It is also demonstrated that the proposed decomposition algorithm not only improves the computational performance of existing solution methods but also allows intuitive interpretation of Benders cuts.

# CHAPTER 1

## Introduction

Modern infrastructure systems continue to grow in their size and complexity, and in interdependencies among them. For instance, electric grids are getting larger and more complicated for supporting the increasingly digital and automated society, which also drives these grids to be closely connected to other infrastructure systems [1]. As a result, infrastructure systems become more involved and subjected to a broader range of risks [2] and, accordingly, necessitate elaborate planning and operations models for preventing and managing risks.

Risk-informed planning and operations decisions can be made through advanced optimization models. An optimization model may leverage huge volumes of data (e.g., historical disturbance data) and/or incorporate system interdependencies for finding better decisions aware of risks. The resultant optimization models, however, are usually of large scale and challenging to solve due to their inherent non-convexity brought by physics governing the system and/or binary decision variables, as well as the large system size and a variety of technical requirements for system reliability. Moreover, additional complexities added for embracing a large amount of data and/or different objectives among interconnected systems further aggravate the computational burden greatly.

To cope with the difficulty in handling a large number of variables and/or constraints of an optimization problem, *decomposition methods* have been developed as early as the 1960s [3, 4]. These methods typically solve a large problem by iteratively (i) solving a set of smaller problems, either in parallel or sequentially, and (ii) exchanging information necessary for optimality among these problems. *Column generation* and *Benders decomposition* methods are two widely used decomposition methods for solving large-scale (mixed-integer) linear optimization problems [5, 6]. These methods, however, are often found ineffective in solving real-world problems, especially when (i) the decomposed problems exhibit bad computational behavior (e.g., numerical issues) or when (ii) some undesirable properties of the decomposed problems (e.g., degeneracy) harm the quality of the informa-

tion exchanged among these problems. Accordingly, many real-world applications call for further advancements in these methods, possibly by exploiting problem structures.

In this regard, this thesis proposes optimization models that allow risk-informed decision-making for complex interconnected systems as well as their solution approaches, which advance the existing decomposition methods. In particular, this thesis studies two problems arising in *energy infrastructure*, especially electric grids and natural gas transmission systems, and two decomposition techniques for solving the problems—column generation and Benders decomposition. The main focus of this research is to (i) use optimization frameworks for alleviating the risks faced by the energy systems by making better planning and operations decisions and (ii) develop acceleration schemes that improve the computational performance of the decomposition methods.

For the rest of this chapter, we review basic concepts on the application areas and decomposition methods in Section 1.1 and give an overview of this dissertation in Section 1.2.

## 1.1 Preliminaries

This thesis studies optimization problems arising in energy infrastructure, especially electric grids and natural gas transmission systems, and develops their solution methods that build upon two widely-used decomposition methods—column generation and Benders decomposition. In Sections 1.1.1 and 1.1.2, we lay out some background on the application areas and the decomposition techniques that are helpful for the understanding of the remaining thesis; We refer to [7] for more details on the electric power systems, to [8] on the gas system, and to Chapter 13 of [9] along with references therein for the decomposition techniques.

### 1.1.1 Background on Application Areas

Electric grids and natural gas transmission systems are two examples of energy systems that are designed for supplying energy (e.g., electricity and natural gas, respectively) to consumers. In this section, we briefly describe the main components of these systems and explain their system-governing physical laws that are essential for analyzing the systems.

**Electric Grids.** An electric grid consists of (i) a variety of *generating units* that produce electricity, most of which is located at some distant power plants away from populated areas, (ii) high-voltage *transmission lines* that deliver the electricity generated at remote

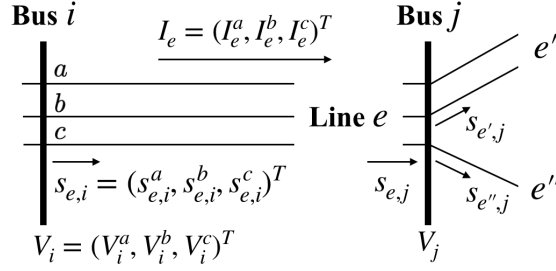


Figure 1.1: Notations for the 3-Phase Power Flow Equations.

power plants to populated regions, (iii) low-voltage *distribution lines* where the delivered electricity is distributed across end-users (e.g., households and businesses), and (iv) *substations* where the electricity is stepped up to a high-voltage level or stepped down to a low-voltage level for the different stages of electricity delivery (i.e., transmission and distribution). The part of an electric grid for transmitting electricity from remote sources to populated areas is referred to as a *transmission grid*, and that for distributing electricity over customers is called a *distribution grid*.

Planning and operating these grids is a challenging decision-making task due to a myriad of objectives and a variety of technical and nontechnical constraints the systems involve [10]. As such, optimization concepts and algorithms have been used in electric power systems to mathematically formalize and support their complex decision-making [11]. For example, in electricity day-ahead wholesale markets in the United States, two optimization problems named Unit Commitment (UC) problem and Economic Dispatch (ED) problem are being solved every day to clear the market and determine the most economical operating schedule of generating units while ensuring a reliable supply of electricity [12]. Other examples include transmission switching [13], expansion planning [14], and their various variants (e.g., with security constraints and/or uncertainty characterization), to name a few. For these optimization problems to yield practical solutions, an accurate mathematical model for analyzing electric power flow needs to be embedded in these problems.

Electric power is generated at power plants as three-phase Alternating Current (AC), which is a set of three sinusoidal currents with equal magnitudes and equally-spaced phase angles that are 120 degrees apart from each other. The flow of steady-state three-phase AC power over the transmission and distribution grids, then, is governed by *Ohm's law* and the *power flow balance equation*; The former states that relationship between the current flowing through a conductor and the voltage change across the conductor, and the latter requires that the sum of incoming power flows to each node of the network must equal the outgoing flows.

Let  $G = (N, E)$  be an undirected graph that represents an electric grid, where  $N$  and  $E$  denote the set of nodes and edges of the grid, respectively, which are also referred to as *buses* and *lines* in electric grid analysis. Let  $\mathcal{P} = \{a, b, c\}$  denote the three-phases of the grid  $G$ . For each bus  $i \in N$ , let  $V_i = (V_i^k)_{k \in \mathcal{P}_i}$  represent the sinusoidal three-phase voltage at the bus, where  $\mathcal{P}_i$  denotes the set of phases on the bus; For each line  $e = (i, j) \in E$ , let  $I_e = (I_e^k)_{k \in \mathcal{P}_e}$  represent the sinusoidal three-phase current passing through the line and let  $s_{e,i} = (s_{e,i}^k)_{k \in \mathcal{P}_e}$  denote the complex three-phase power on  $i$ -end of the line, where  $\mathcal{P}_e$  represents the set of phases on the line. Each line  $e \in E$  is characterized by a phase impedance matrix  $Z_e$ . The notations also use a superscript  $\mathcal{P}' \subseteq \mathcal{P}$  to represent the *projection* or the *extension* of a vector to the space of  $\mathcal{P}'$ . For example, if  $\mathcal{P}_i = \{a, b, c\}$  and  $\mathcal{P}' = \{a, b\}$ , then  $V_i^{\mathcal{P}'} = (V_i^a, V_i^b)^T$ . If  $\mathcal{P}_i = \{a, c\}$  and  $\mathcal{P}' = \{a, b, c\}$ , then  $V_i^{\mathcal{P}'} = (V_i^a, 0, V_i^c)^T$ . Some notations are illustrated in Figure 2.2.

With these notations and the sinusoidal steady-state assumption, Ohm's law states the relationship between  $I_e$ ,  $V_i$ ,  $V_j$ , and  $Z_e$  on each line  $e = (i, j) \in E$  as follows:

$$V_j^{\mathcal{P}_e} = V_i^{\mathcal{P}_e} - Z_e I_e. \quad (1.1)$$

Further, the power balance equation can be expressed as follows:

$$s_{e,i} = \text{diag}(V_i^{\mathcal{P}_e} I_e^H), \forall i \in \delta(e), e \in E, \quad (1.2a)$$

$$g_i^k - d_i^k = \sum_{e \in \delta(i)} s_{e,i}^k, \forall k \in \mathcal{P}_i, i \in N, \quad (1.2b)$$

where  $\delta(e)$  and  $\delta(i)$  represent the set of end-buses of line  $e$  (i.e.,  $\delta(e) = \{i, j\}$  for  $e = (i, j) \in E$ ) and the set of lines attached to bus  $i$ , respectively, and superscript  $H$  indicates the conjugate transpose;  $g_i^k$  and  $d_i^k$  denote the complex power generated and consumed on phase  $k \in \mathcal{P}_i$  at bus  $i$ , respectively. As indicated in Equation (1.2a), the complex power on each phase  $k \in \mathcal{P}_e$  is the product of the voltage and the complex conjugate of the current on phase  $k$ , and Equation (1.2b) requires the sum of incoming flows equals the sum of the outgoing flows at each bus.

Transmission grids consist primarily of balanced three-phase loads, placing the same electricity demand on each phase. In this case, the analysis can be done on a single phase, since the voltages and currents in the other two phases have the same magnitude as those in the analyzed phase with angles apart from each other by  $120^\circ$ . Assuming a single phase network, we represent the sinusoidal voltage at bus  $i$  as the rectangular form  $V_i = |V_i|(\cos \theta_i + \mathbf{i} \sin \theta_i)$  where  $\mathbf{i} = \sqrt{-1}$  (i.e.,  $V_i = |V_i| \angle \theta_i$  in the polar form); Let  $Z_e \in \mathbb{C}$  be the complex impedance on each line  $e \in E$  and let  $Y_e := 1/Z_e = G_e + \mathbf{i}B_e$  denote the

admittance of line  $e$ . Then, by combining Equations (1.1) and (1.2a), we have the following equations:

$$s_{e,i} = V_i \bar{I}_e \quad (1.3a)$$

$$= V_i (\bar{V}_i - \bar{V}_j) \bar{Y}_e \quad (1.3b)$$

$$= p_{e,i} + \mathbf{i}q_{e,i}, \quad (1.3c)$$

where

$$p_{e,i} = |V_i| \{ |V_i| G_e - |V_j| [G_e \cos(\theta_i - \theta_j) + B_e \sin(\theta_i - \theta_j)] \}, \quad (1.3d)$$

$$q_{e,i} = |V_i| \{ -|V_i| B_e - |V_j| [G_e \sin(\theta_i - \theta_j) - B_e \cos(\theta_i - \theta_j)] \}. \quad (1.3e)$$

On the other hand, distribution grids contain single-phase loads that unbalance the system (i.e., currents on each phase are not exactly  $120^\circ$  apart from one another and may have different magnitudes), thus the three-phase representation in Equations (1.1) and (1.2) is more appropriate to analyze the system. These equations describing how electric power flows (i.e., Equations (1.1) and (1.2) for the distribution grids and Equations (1.3) and (1.2) for the transmission systems) are often referred to as *power flow equations*.

Note that, in either case (i.e., transmission or distribution grids), the power flow equations are nonconvex (see, e.g., Equation (1.2a) and (1.3)); The nonconvexity makes optimization problems embedding the power flow equations very challenging to solve to global optimality. Therefore, there has been a considerable effort made to tightly approximate or relax the power flow equations with convex constraints; See recent surveys in [15, 16, 17]. The most widely used approximation method for balanced three-phase networks is the DC power flow approximation, which have been applied to various applications including long-term planning and wholesale electricity market operations [16]. The DC power flow approximation replaces Equation (1.3) expressed in the per-unit system as the following linear equations

$$p_{e,i} = -B_e(\theta_i - \theta_j), \quad q_{e,i} = 0, \quad (1.4)$$

by (i) ignoring the line resistance (implying  $G_e = 0$ ), (ii) using the small angle difference between adjacent nodes and the sine function approximation near zero  $\sin(\theta_i - \theta_j) \approx \theta_i - \theta_j$ , (iii) assuming near-nominal voltage magnitudes  $|V_i| \approx 1$  for all  $i \in N$ , and (iv) ignoring reactive power  $q_{e,i}$ . A more advanced linear approximation that incorporates both reactive power and voltage magnitudes is proposed in [18].

Meanwhile, a convex relaxation of the power flow equations for balanced three-phase networks is first proposed in [19] as a Second-Order Cone Program (SOCP) for radial net-

works and in [20] as a Semidefinite Program (SDP) for mesh networks [21]. The work in [22] studied the exactness of the SDP approach and more relevant details can be found in [23, 24] and references therein. Other SOCP representations of the power flow equations include relaxations [25, 26, 27] and approximations [28, 29, 30]. For unbalanced multi-phase networks, [21] proposed convex relaxations and linear approximation for radial networks, which is delineated in Section 2.3.1.1.

**Natural Gas Transmission Systems.** A natural gas transmission system moves natural gas from the gas wellhead to end-users. It consists of (i) *pipelines* along which natural gas travels toward customers after being gathered and processed in distant source areas, (ii) a series of *compressor stations* that increase the pressure of natural gas to keep the flow going forward, and (iii) *control valves* that restrict the flow or reduce the pressure of gas for flow redirection or some maintenance tasks.

Gas flow is governed by physical laws of fluid dynamics, which can be captured by a set of Partial Differential Equations (PDE) that evolve over both time and space along the pipeline [31, 32]. During the last century, most gas flow analysis assumed isothermal steady-state [8], which requires the temperature across a pipeline and the gas withdrawal over a day to have a little variation. One and mostly used isothermal steady-state model is the Weymouth equations, which is a set of simplified equations obtained by assuming a constant friction factor and horizontal pipelines [33, 34, 35].

Let  $\mathcal{G} = (\mathcal{V}, \mathcal{A})$  be a directed graph that represents a natural gas pipeline network, where  $\mathcal{V}$  and  $\mathcal{A}$  denote the set of nodes and arcs of the network, respectively. The set of arcs consists of the set of pipelines  $\mathcal{A}_p$  (passive lines), and compressor stations  $\mathcal{A}_c$  and control valves  $\mathcal{A}_v$  (active lines). For each node  $i \in \mathcal{V}$ , let  $\pi_i$  be the squared nodal pressure, and let  $\phi_a$  represent the gas flow on arc  $a = (i, j) \in \mathcal{A}$ , which takes a positive value if gas moves from  $i$  to  $j$  and a negative value, otherwise.

With these notations, the Weymouth equation approximates the relationship between the gas mass flux and the pressure drop along a passive line (i.e., pipeline)  $a \in \mathcal{A}_p$  as follows:

$$\pi_i - \pi_j = w_a \phi_a |\phi_a|, \quad (1.5)$$

where the parameter  $w_a$  is a Weymouth factor which depends on the physical characteristics of the pipeline (more details on the factor can be found in [8]). Further, the mass should be conserved as follows:

$$q_i = \sum_{a:(i,j) \in \mathcal{A}} \phi_a - \sum_{a:(j,i) \in \mathcal{A}} \phi_a, \quad \forall i \in \mathcal{V}, \quad (1.6)$$

where  $q_i$  denotes the gas mass flux injection/demand at vertex  $i$ .

Note that the Weymouth equation is nonconvex and challenges optimization problems that embed the gas flow equations from both computational and solution quality standpoints. Thus, several studies proposed convex approximations/relaxations of the equations. Suppose the direction of gas flow is fixed, then we can assume w.l.o.g.  $\phi_a \geq 0, \forall a \in \mathcal{A}$ . In this case, the Weymouth equation can be relaxed as the following SOC constraint:

$$\pi_i - \pi_j \geq w_a \phi_a^2, \quad (1.7)$$

by relaxing the equality in Equation (1.5) with inequality. The work in [35] proposed this relaxation and its extension to bidirectional flows which introduces auxiliary binary variables indicating the flow direction. Other approximation/relaxation schemes for handling the nonconvexity include mixed-integer piecewise linear approximations [36, 37, 38, 39], a Mixed-Integer Quadratically-Constrained Quadratic Program (MIQCQP) relaxation [40], a MISOCP relaxation [41], and a mixed-integer SDP relaxation [42]. For transient flow analysis, we refer the reader to [43] and references therein.

### 1.1.2 Decomposition Techniques

Column generation and Benders decomposition methods are two widely-used decomposition techniques for solving large-scale (mixed-integer) linear programs. Both methods build upon some problem reformulation schemes that allow distributed solution approaches: *Dantzig-Wolfe reformulations* for column generation and a *projection-based reformulation* for Benders decomposition.

**Column Generation** Column generation is useful when solving an Integer Linear Programming (ILP) problem with some complicating constraints. Consider the following ILP problem with an  $n$ -dimensional variable vector:

$$z = \min\{c^T x : Dx \geq d, Bx \geq b, x \in \mathbb{Z}_+^n\}. \quad (1.8)$$

Suppose that the constraint set  $Dx \geq d$  complicates the problem and optimizing a linear objective function over  $P := \{x \in \mathbb{Z}_+^n : Bx \geq b\}$  is relatively tractable.

Dantzig-Wolfe reformulation is a reformulation scheme for Problem (1.8) that utilizes some alternative representation of  $P$ , which is specified in a counterpart theorem of Minkowski's theorem for ILP:

**Theorem 1.1.1** ([9]). *Every discrete set  $P$  in the form of  $\{x \in \mathbb{Z}_+^n : Bx \geq b\}$  can be*

represented with  $P = \text{proj}_x(Q)$ , where

$$Q = \left\{ (x, \lambda, \mu) \in \mathbb{R}^n \times \mathbb{Z}_+^{|\mathcal{J}|} \times \mathbb{Z}_+^{|\mathcal{R}|} : x = \sum_{j \in \mathcal{J}} \lambda_j \hat{x}^j + \sum_{r \in \mathcal{R}} \mu_r \hat{v}^r, \sum_{j \in \mathcal{J}} \lambda_j = 1 \right\},$$

where  $\{\hat{x}^j\}_{j \in \mathcal{J}}$  is a finite set of integer points in  $P$  and  $\{\hat{v}^r\}_{r \in \mathcal{R}}$  is the set of extreme rays (scaled to be integral) of  $\text{conv}P$ , with  $\mathcal{J}$  and  $\mathcal{R}$  being the corresponding index sets.

Suppose  $P$  is bounded (i.e.,  $\mathcal{R} = \emptyset$ ), then by replacing  $P$  in Problem (1.8) with  $Q$ , we have the following extended reformulation of the ILP problem with a variable vector  $\lambda \in \{0, 1\}^{|\mathcal{J}|}$ :

$$z^{DW} = \min \sum_{j \in \mathcal{J}} (c^T \hat{x}^j) \lambda_j \quad (1.9a)$$

$$\text{s.t.} \sum_{j \in \mathcal{J}} (D \hat{x}^j) \lambda_j \geq d, \quad (1.9b)$$

$$\sum_{j \in \mathcal{J}} \lambda_j = 1, \quad (1.9c)$$

$$\lambda_j \in \{0, 1\}, \forall j \in \mathcal{J}. \quad (1.9d)$$

Note that any point in  $Q$  is a convex combination of some integral extreme points of  $P$ . Therefore, it can be shown that the LP relaxation  $z_{LP}^{DW}$  of Problem (1.9) has the same value as  $\min\{c^T x : Dx \geq d, x \in \text{conv}(P), x \in \mathbb{R}_+^n\}$ , which is (potentially much) stronger than the LP relaxation of (1.8). Note that, however, Problem (1.9) has exponentially many variables.

Column generation is a method for solving the LP relaxation of the Dantzig-Wolfe reformulation (i.e., Problem (1.9)) by generating variables (i.e., columns) iteratively. Suppose we have a subset of points  $\mathcal{J}^k \subseteq \mathcal{J}$  at iteration  $k$  with Problem (1.9) restricted as follows (called the Restricted Master Linear Problem (RMLP)):

$$z_k^{RMLP} = \min \sum_{j \in \mathcal{J}^k} (c^T \hat{x}^j) \lambda_j \quad (1.10a)$$

$$\text{s.t.} \sum_{j \in \mathcal{J}^k} (D \hat{x}^j) \lambda_j \geq d, \quad (1.10b)$$

$$\sum_{j \in \mathcal{J}^k} \lambda_j = 1, \quad (1.10c)$$

$$\lambda_j \geq 0, \forall j \in \mathcal{J}^k. \quad (1.10d)$$

Suppose Problem (1.10) has an optimal dual solution  $(\pi^k, \sigma^k)$  where  $\pi^k$  corresponds to Constraint (1.10b) and  $\sigma^k$  is associated with Constraint (1.10c). With the dual information of the current optimal basis of Problem (1.10), we can check whether there is a variable  $\lambda_j$  for some  $j \in \mathcal{J} \setminus \mathcal{J}^k$  with negative reduced cost, meaning that the variable has a potential to enter the current optimal basis (i.e., improving the current objective value).

This checking procedure can be performed by solving the following so-called *pricing problem*:

$$\min \{ -\sigma^k + (c - (\pi^k)^T D)^T x : x \in P \}, \quad (1.11)$$

which aims to find  $x \in P$  that yields the smallest reduced cost. If the pricing problem yields an optimal solution  $\hat{x}^j$  for some  $j \in \mathcal{J} \setminus \mathcal{J}^k$  with a negative objective value, then the method adds the corresponding variable  $\lambda_j$  and its associated column to Problem (1.10). The method repeats this procedure until the pricing problem has a nonnegative objective value.

**Benders Decomposition** Consider the following Mixed-Integer Linear Programming (MILP) problem:

$$z^{MIP} = \min \{ c^T x + h^T y : Gx + Hy \geq d, (x, y) \in \mathbb{Z}^n \times \mathbb{R}_+^p \}. \quad (1.12)$$

Consider a function  $f(\cdot)$  defined as follows:

$$f(\hat{x}) := \min \{ h^T y : Hy \geq d - G\hat{x}, y \in \mathbb{R}_+^p \}, \quad (1.13)$$

which describes the optimal objective value of a continuous problem obtained from Problem (1.12) by fixing its integer variable as some vector  $\hat{x} \in \mathbb{Z}^n$ . Note that if  $\hat{x} \notin \text{proj}_x Q$  where  $Q = \{(x, y) \in \mathbb{R}^n \times \mathbb{R}_+^p : Gx + Hy \geq d\}$ , then Problem (1.13) is infeasible (i.e.,  $f(\hat{x}) = +\infty$  by convention). Otherwise,  $f(x)$  takes a finite value. Accordingly, we let  $D_f := \text{proj}_x Q$  be the domain of  $f$ .

Using this function  $f$  and its domain  $D_f$ , Problem (1.12) can be expressed as follows:

$$z^{MIP} = \min_{x \in \mathbb{Z}^n} \{ c^T x + f(x) : x \in D_f \}, \quad (1.14)$$

which can, in turn, be written as

$$z^{MIP} = \min_{x \in \mathbb{Z}^n} \{ c^T x + t : x \in D_f, (x, t) \in P_f \} \quad (1.15)$$

where  $P_f = \{(x, t) : t \geq f(x)\}$  is the epigraph of  $f$ . Note that if  $x \in D_f$ , then by LP

duality we have:

$$f(x) = \max_{u \in \mathbb{R}_+^m} \{u^T(d - Gx) : H^T u \leq h\} \quad (1.16)$$

$$= \max_{k \in \mathcal{J}} (u^k)^T (d - Gx) \quad (1.17)$$

where  $\{u^j\}_{j \in \mathcal{J}}$  is the set of extreme points of  $U = \{u \in \mathbb{R}_+^m : H^T u \leq h\}$  and  $\mathcal{J}$  is the corresponding index set. Therefore, for  $x \in D_f$ ,  $P_f$  can be described by the following set of linear inequalities, called optimality cuts:

$$t \geq (u^j)^T (d - Gx), \quad \forall j \in \mathcal{J},$$

In addition,  $D_f = \text{proj}_x(Q)$  can also be expressed by a set of linear inequalities, according to Farkas' Lemma, as follows:

$$D_f = \{x \in \mathbb{R}^n : (v^r)^T (d - Gx) \leq 0, \forall r \in \mathcal{R}\}, \quad (1.18)$$

where  $\{v^r\}_{r \in \mathcal{R}}$  is the set of extreme rays of  $U$  and  $\mathcal{R}$  is the associated index set.

Accordingly, we obtain the following reformulation:

$$z^{MIP} = \min c^T x + t \quad (1.19)$$

$$\text{s.t. } (u^j)^T (d - Gx) \leq t, \forall j \in \mathcal{J}, \quad (1.20)$$

$$(v^r)^T (d - Gx) \leq 0, \forall r \in \mathcal{R}, \quad (1.21)$$

$$x \in \mathbb{Z}_n, t \in \mathbb{R}, \quad (1.22)$$

which is a ILP problem with a very large number of constraints.

Instead of explicitly having complete expression of the epigraph  $P_f$  and the domain  $D_f$ , Benders decomposition iteratively discovers  $P_f$  and  $D_f$  through some procedure. At each iteration  $k$ , suppose that we have some subsets  $\mathcal{J}^k \subseteq \mathcal{J}$  and  $\mathcal{R}^k \subseteq \mathcal{R}$ , and that  $(x^k, t^k)$  is obtained by solving the following relaxed problem:

$$\min c^T x + t \quad (1.23)$$

$$\text{s.t. } (u^j)^T (d - Gx) \leq t, \forall j \in \mathcal{J}^k, \quad (1.24)$$

$$(v^r)^T (d - Gx) \leq 0, \forall r \in \mathcal{R}^k, \quad (1.25)$$

$$x \in \mathbb{Z}_n, t \in \mathbb{R}. \quad (1.26)$$

Then, we can check the optimality and feasibility of  $x^k$  by solving Problem (1.13) with  $x$

fixed as  $x^k$ . There are two cases:

- (i)  $f(x^k) = +\infty$ , meaning that Problem (1.13) is infeasible for given  $x^k$ . Then, we can obtain a new extreme ray  $v^r$  for some  $r \in \mathcal{R} \setminus \mathcal{R}^k$  with  $(v^r)^T(d - Gx^k) > 0$ , using the resultant dual solution of Problem (1.13). The violated constraint  $v^r(d - Gx) \leq 0$ , called a feasibility cut, is added to Problem (1.13), (i.e.,  $\mathcal{R}^{k+1} = \mathcal{R}^k \cup \{r\}$ ).
- (ii) Problem (1.13) has a finite optimum with an optimal dual solution  $u^j$  for some  $j \in \mathcal{J} \setminus \mathcal{J}^k$ . If  $f(x^k) = (u^j)^T(d - Gx^k) > t^k$ , then add the violated constraint  $t \geq (u^j)^T(d - Gx)$ , called an optimality cut to Problem (1.13), (i.e.,  $\mathcal{J}^{k+1} = \mathcal{J}^k \cup \{j\}$ ).

The Benders decomposition repeats this procedure until it has no violated constraint (i.e.,  $f(x^*) \leq t^*$ ).

## 1.2 Thesis Overview

This thesis is organized as follows: Chapter 2 studies how to harden and modernize electricity distribution systems for building resiliency against natural disasters. Smart-grid technologies (e.g., distributed generation and remotely controlled switches) have emerged as important tools to improve the resiliency of distribution grids against extreme weather-related disturbances. Therefore it becomes important to study how best to place them on the grid in order to meet some resiliency criteria, while minimizing costs and capturing their dependencies on the associated communication systems that sustain their distributed operations. To address this need, we formulate the optimal resilient planning problem as a two-stage mixed-integer optimization problem using a number of potential disaster scenarios generated from historical data. The problem captures both the physical laws of distribution systems and the communication connectivity of the smart grid components. We propose an exact branch-and-price algorithm, which is a hybrid of branch-and-bound and column generation methods, for solving the problem; The proposed algorithm features a strong lower bound and a variety of acceleration schemes to address degeneracy. We evaluate the optimization model and the branch-and-price algorithm on a variety of test cases with varying disaster intensities and network topologies. The results demonstrate the importance of informing expansion plans of system interdependencies, as well as the computational benefits of the proposed solution approach which outperformed state-of-the-art solution methods (e.g., scenario-based decomposition methods [44, 45]) and an advanced branch-and-price algorithm (e.g., with a stabilized column generation [46]) significantly.

In Chapter 3, we investigate how to enhance risk awareness in electricity system operations against a dangerous link between the electricity and natural gas systems. Recent

changes in the fuel mix for electricity generation and, in particular, the increase in gas-fueled power plants have created significant interdependencies between the electrical power and natural gas transmission systems. However, despite their physical and economic couplings, these networks are still operated independently, with asynchronous market mechanisms. This mode of operation may lead to significant economic and reliability risks in congested environments as revealed by the 2014 polar vortex event experienced by the northeastern United States. To mitigate these risks, we explore the idea of introducing gas network awareness into an operational model of the electricity system, which is known as the unit commitment problem. Under the assumption that the power system operator has some (or full) knowledge of gas demand forecast and the gas network, we propose a tri-level optimization problem where natural gas zonal prices are given by the dual solutions of natural-gas flux conservation constraints and commitment decisions are subject to bid-validity constraints that ensure the economic viability of the committed gas-fired power plants. This tri-level program can be reformulated as a bilevel mixed-integer second-order cone program which motivated us to develop a dedicated Benders decomposition discussed in Chapter 4. The approach is validated on a case study for the Northeastern United States [47] that can reproduce the gas and electricity price spikes experienced during the early winter of 2014. The results on the case study demonstrate that gas awareness in unit commitment is instrumental in avoiding the peaks in electricity prices while keeping the gas prices to reasonable levels.

The bilevel model proposed in Chapter 3 challenges existing solution methods and motivated us to develop an advanced decomposition method for bilevel optimization. Bilevel optimization formulates a variety of real-world problems as they are suited to model hierarchical decision-making processes that arise in many applications such as in pricing, network design, and infrastructure defense planning [48, 49, 50, 51]. In spite of the wide applicability, algorithmic development for solving bilevel optimization problems has been sparse, due to its inherent complexity; Even the simplest subclass of bilevel problems where the upper and lower levels are both linear is NP-hard [52]. Accordingly, in Chapter 4, we propose a dedicated Benders decomposition method for solving a class of bilevel optimization problems where the upper level problem features some integer variables while the lower level problem enjoys strong duality, which subsumes the model presented in Chapter 3. The method decomposes the Benders subproblem into two more tractable, sequentially solvable problems that can be interpreted as the upper and the lower level problems. We show that the Benders subproblem decomposition carries over to an interesting extension of bilevel problems, which connects the upper level solution with the lower level dual solution, and discuss some special cases of bilevel problems that allow sequence-independent sub-

problem decomposition. Several acceleration schemes are discussed and a computational study demonstrates the computational benefits of the proposed method over an up-to-date commercial solver and the standard Benders method.

The results in Chapters 2, 3, and 4 are included in the papers [\[53, 54, 55\]](#).

## CHAPTER 2

# Communication-Constrained Expansion Planning for Resilient Distribution Systems

### 2.1 Introductory Remarks

The last decades have highlighted the vulnerability of the current electric power system to weather-related extreme events. Between 2007 and 2016, outages caused by natural hazards, such as thunderstorms, tornadoes, and hurricanes, amounted to 90 percent of major electric disturbances, each affecting at least 50,000 customers (derived from Form OE-417 of U.S. DOE). It is also estimated that 90 percent of all outages occur along distribution systems [56]. Moreover, the number of weather-related outages is expected to rise as climate change increases the frequency and intensity of extreme weather events [56]. Accordingly, it is critical to understand how to harden and modernize distribution grids to prepare for potential natural disasters.

Distributed Generation (DG) is one of the advanced technologies that can be utilized to enhance grid resilience. DG refers to electric power generation and storage performed by a collection of distributed energy resources. DG decentralizes the electric power distribution by supplying power to the loads closer to where it is located. The potential of DGs is realized via a system approach that views DGs and associated loads as a microgrid [57]. A microgrid is often defined as a small-scale power system on medium- or low- voltage distribution feeder that includes loads and DG units, together with an appropriate management and control scheme supported by a communication infrastructure [58]. When faults occur in the main grid, microgrids can be detached from the main grid and act in island mode to serve critical loads by utilizing local DGs or work in the grid-connected mode to provide ancillary services for the bulk system restoration [59]. Remotely Controlled Switches (RCS), another advanced technology, can be used to increase the grid flexibility by controlling the grid topology through a communication network and facilitate microgrid formations in emergencies. Other than the aforementioned operational enhancement

measures, a grid can also be hardened physically by installing underground cables and/or upgrading the overhead lines with stronger materials, which reduces the physical impact of catastrophic events [60].

A critical issue in building resilient distribution grids is to determine where to place such advanced devices (i.e., DGs, RCSs, and underground cables) and which existing lines to harden. It is also important to understand the dependency between the distribution grid and its associated communication network, which is critical to the effective operation of a modernized grid during emergency situations and is also vulnerable to extreme events [61, 62, 63, 64].

To address this pivotal and pressing issue, this chapter introduces the Optimal Resilient Design Problem for Distribution and Communication Systems (ORDPDC). The ORDPDC determines how to harden and modernize an interdependent network to ensure its resilience against extreme weather events. Like recent papers (e.g., [44, 65]), the ORDPDC takes into account a set of disaster scenarios, each defining a set of power system components that are damaged during an extreme event. These scenarios are generated from probabilistic models of how power system components respond to hazard-specific stress (e.g., wind speed and flood depth) that are derived from historical data. The ORDPDC considers the following upgrade options: a set of hardening options on existing power lines and communication links and a set of new components that can be added to the system—new lines, new communication pathways, remotely controlled switches, and distributed generation. The objective of the ORDPDC is to find the cheapest set of upgrade options that can be placed on the grid in order to guarantee that a minimal amount of critical and non-critical load be served in each scenario. These guarantees are called the resiliency criteria.

The ORDPDC is modeled with a two-stage stochastic mixed integer program. The first stage decides an upgrade profile and the second stage decides how to utilize the DGs, RCSs, and power lines/communication links, whose availability is decided in the first-stage, to restore critical loads up to resiliency criteria (e.g., 98 %) in each disaster scenario. For each scenario, the second stage is viewed as a restoration model that identifies how to reconfigure the grid. Within this second stage problem, the physics of power flows is modeled with the steady-state, unbalanced three phase AC power flow equations and constraints that ensure that the radial structure of distribution grids is maintained. When the grid is reconfigured due to some disturbances, each island or microgrid must be connected to at least one control center that coordinates its DGs and loads and operates its RCSs. This communication requirement is modeled with a single-commodity flow model.

Several solution methods can be used to solve the ORDPDC, taking advantage of its block diagonal structure. [44] proposed a Scenario-Based Decomposition (SBD) algorithm

that restricts attention to a smaller set of scenarios and adds new ones on an as needed basis (see Section 2.5.1). However, in the worst case, the SBD algorithm must solve the large-scale ORDPDC as a whole. Another Scenario Decomposition (SD) algorithm was proposed by [45] that explores solutions to each subproblem as candidate primal feasible solutions for the overall problem (see Section 2.5.1). However, a strong performance of the SD algorithm is guaranteed only when the probability that an  $\epsilon$ -optimal solution of the overall problem (for small enough  $\epsilon > 0$ ) becomes the optimal solution to a realization is strictly positive. Hence, in the worst case, it may explore all feasible solutions of each subproblem. Branch-and-Price (BnP), which combines column generation and branch-and-bound, is another solution method for approaching large-scale mixed-integer programming [5]. Although widely successful on many applications, it may suffer from degeneracy and long-tail effects as problems become larger. To address these difficulties, several stabilization techniques have been proposed and proven to be effective in many applications (e.g., [46, 66, 67]). Nevertheless, the high degree of degeneracy and the significant scale of the ORDPDC create significant challenges for the dual stabilization techniques.

To address these computational challenges, this chapter proposes a BnP algorithm that systematically exploits the structure of the ORDPDC. The algorithm starts with a compact reformulation that results in strong lower bounds on the test cases and pricing subproblems that are naturally solved in parallel. Moreover, the BnP algorithm tackles the degeneracy inherent in the ORDPDC through a variety of acceleration schemes for the pricing subproblems: A pessimistic reduced cost, an optimality cut, and a lexicographic objective. The resulting BnP algorithm produces significant computational improvements compared to existing approaches.

The key contributions of this chapter can be summarized as follows:

- The chapter proposes the first planning model for resilient distribution networks that combines the use of advanced technologies (e.g., DGs, RCSs, and undergrounding) with traditional hardening options and captures the dependencies between the distribution grid and its associated communication system.
- The chapter proposes an exact BnP algorithm for solving the ORDPDC, which systematically exploits the ORDPDC structure to obtain strong lower bounds and address its significant degeneracy issues.
- The chapter evaluates the impact of grid and communication system topologies on potential expansion plans. It also reports extensive computational results demonstrating the benefits of the proposed BnP algorithm on the test cases.

The remainder of this chapter is organized as follows. Section 2.2 reviews related work on the ORDPDC. Section 2.3 formalizes the ORDPDC and presents a tight linear approximation. Section 2.4 analyzes the behavior of the model on the case studies. Section 2.5 describes solution approaches for solving the ORDPDC, where Section 2.5.1 briefly reviews the SBD and SD algorithms and Section 2.5.2 presents the new BnP algorithm. Lastly, Section 2.6 reports on the computational performance of the proposed algorithm. Section 2.7 concludes the chapter.

## 2.2 Literature Review

There has been a considerable progress in advancing methods that address weather-related issues at distribution level [59]. Many studies develop post-fault Distribution System Restoration (DSR) models to bring power back as soon as possible and restore critical loads after a severe outage. Recently, DGs, RCSs, and redundant lines were utilized to leverage microgrids in load restoration. Most of the studies assume the existence of those devices beforehand [68, 69, 70, 71]. [72] proposed a DSR model that utilizes the placement of dispatchable DGs. The above-mentioned studies however propose post-contingency models. To facilitate these novel restoration methods, the devices should be placed in suitable places in advance. This chapter focuses on the optimal placement of those devices so that the grid survives potential weather-related events.

Only a limited number of studies have discussed how to optimally add resilience to distribution networks. Most relevant is the work by [65] and [44] who propose multi-scenario models for making a distribution grid resilient with respect to a set of potential disaster scenarios. They propose decomposition-based exact and heuristic solution approaches. However, these studies do not take into account the grid's functional dependencies on the associated communication network. Accordingly, the possible faults in the communication network are not considered and the upgrade options only consider the power grid, not the communication network. [73] proposed a two-stage robust optimization model by utilizing a bi-level network interdiction model that identifies the critical components to upgrade for the resilience against the  $N - K$  contingency criterion. However, as pointed out in [65], in practice, the computational complexity of this approach grows quickly with the number of allowable faults. The study also did not explicitly consider the dependency on the communication network: A DG can supply power to the node it is placed on and its children if they are not damaged by the attack. [74] and [75] discuss how to place RCSs in distribution systems, but only single fault scenarios are assumed, which is not suitable for capturing weather-related extreme events.

As the instrumentation of the grid increases, frameworks for modeling its dependence on communication networks from a resilience viewpoint have been studied [63, 76]. [58] proposed a hierarchical control system, which assumes the existence of a controller in each microgrid to allow the coordination among distributed generation units in the microgrid, while multiple microgrids are organized by a central management controller. On the other hand, distributed control systems are applied to microgrids where there are many devices with their own controllers. Accordingly, [68] assumed that RCSs have local communication capabilities to exchange information with neighboring switches over short-range low-cost wireless networks and proposed a global information discovery scheme to get the input parameters for a DSR model. However, the assumption that RCSs are installed in all lines is premature for current distribution systems. [72] proposed a two-layered communication framework where the lower-layer cyber network supports microgrids where local control systems are installed, while the upper-layer network is composed of multiple local control systems that only communicate with their neighboring counterparts. The study can be viewed as a hybrid of centralized and decentralized framework: At a microgrid level, it is operated in a centralized fashion, while the upper-level network is operated in a decentralized manner. However, it did not consider fault scenarios in communication networks. This chapter only assumes the lower-layer cyber network proposed in [72] by dynamically allocating a local control system to each microgrid in islanding mode. Moreover, this chapter also considers potential faults in the communication system.

To the best of our knowledge, this chapter proposes, for the first time, an exact optimization algorithm for expanding an integrated distribution grid and communication network through the placement of new DGs and RCSs and the hardening of existing lines in order to ensure resilience against a collection of disaster scenarios.

## 2.3 Mathematical Modeling: the ORDPDC

The ORDPDC considers an unbalanced three-phase distribution grid coupled with a communication network, as illustrated in Figure 2.1. In the figure, blue- and red-colored arrows represent regular and critical loads. Nodes in the communication networks may control a generator or a switch in the distribution network, as indicated by dotted lines. The figure also highlights how the line phases are interconnected at the buses and the communication centers that will send instructions to generators and switches remotely.

Let  $G = (V, E)$  be an undirected graph that represents a distribution grid and its available upgrade options:  $V$  and  $E$  denote the set of buses and the set of distribution lines. The communication network, along with its potential upgrade options, is represented by a undi-

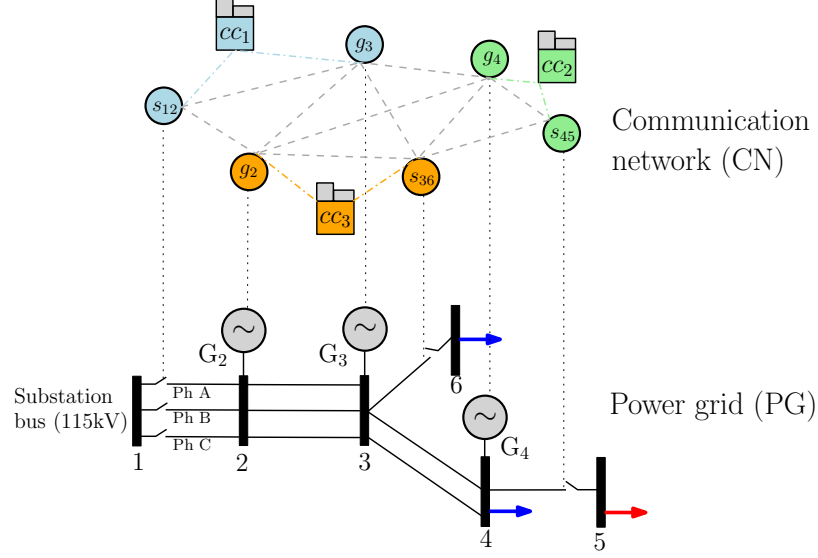


Figure 2.1: The Cyber-Physical Network for Electricity Distribution. Solid lines represent power lines and dotted lines represent communication links.

rected graph  $\tilde{G} = (\tilde{N}, \tilde{E})$ , where  $\tilde{N}$  and  $\tilde{E}$  are the set of communication nodes and a set of communication links. A communication node is either a control point or an intermediate point. Each control point is associated with some device in  $G$  and some nodes in  $\tilde{N}$  are designated as control centers.

The power grid  $G$  depends on its communication network  $\tilde{G}$  in the following way: A device in  $G$  (e.g., a generator or a RCSs) is operable only when its associated control point can receive a signal from some control center in  $\tilde{G}$ . This modeling enables islands to form and to be operated independently only when at least one control center can communicate to the island and, in particular, its generator(s).

Let  $\mathcal{G} = (\mathcal{N}, \mathcal{E})$  be the integrated system of  $G$  and  $\tilde{G}$  with  $\mathcal{N} = N \cup \tilde{N}$  and  $\mathcal{E} = E \cup \tilde{E}$ . Let  $\mathcal{D}$  be a set of damage scenarios for  $\mathcal{G}$  indexed with  $\mathcal{S} := \{1, \dots, |\mathcal{D}|\}$ . Each scenario  $s \in \mathcal{S}$  is a set of edges of  $\mathcal{E}$  that are damaged under  $s$ . The goal of the ORDPDC is to find an optimal upgrade profile for the cyber-physical system  $\mathcal{G}$  that is resilient with respect to the damage scenarios in  $\mathcal{D}$ . The upgrade options include a) the building of new edges in  $\mathcal{E}$  (i.e., distribution lines or communication links); b) the building of RCSs on some lines in  $E$  to provide operational flexibility; c) the hardening of existing edges in  $\mathcal{E}$  to lower the probability of damage, and d) the building of DGs at some buses of the grid.

The ORDPDC is a two-stage mixed integer stochastic program. The first-stage variables represent potential infrastructure enhancements for the coupled network  $\mathcal{G}$  and the second-stage variables capture how upgrades serve the loads in each disaster scenario.

Table 2.1 specifies the input data for the ORDPDC problem, while Table 2.2 describes

Table 2.1: The Parameters of the ORDPDC.

|  |   |
|--|---|
| $G = (N, E)$   | an undirected extended distribution grid with available upgrade options   |
| $\mathcal{U} := \mathcal{U}^0 \cup \mathcal{U}^n$            | a set of generators, indexed with $l$   |
| $\mathcal{U}^0$  | a set of existing generators  |
| $\mathcal{U}^n$  | a set of generators that can be installed   |
| $i(l) \in N$   | the bus in which the generator $l \in \mathcal{U}$ is located   |
| $\mathcal{U}_i \subseteq \mathcal{U}$                        | the set of generators connected to bus $i \in N$  |
| $E_V \subseteq E$  | a set of transformers   |
| $\beta_e$  | maximum flow variation allowed between different phases on line $e \in E_V$   |
| $\mathcal{C} \subseteq 2^{ E }$                              | a collection of a set of edges which forms a cycle with a distinct node set   |
| $\mathcal{P}_e, \mathcal{P}_i, \mathcal{P}_l$                | a set of phases on line $e \in E$ , bus $i \in N$ , and generator $l \in \mathcal{U}$ , respectively                  |
| $T_e^k$  | a thermal limit on line $e \in E$ for phase $k \in \mathcal{P}_e$   |
| $\underline{V}_i^k, \overline{V}_i^k$                        | lower and upper bound on voltage magnitude at bus $i \in N$ on phase $k \in \mathcal{P}_i$                            |
| $Z_e = R_e + \mathbf{i} X_e$                                 | phase impedance matrix of line $e \in E$  |
| $\mathcal{L} \subseteq N$                                    | a set of buses with critical loads  |
| $D_{i,p}^k + \mathbf{i} D_{i,q}^k$                           | complex power demand at bus $i \in N$ on phase $k \in \mathcal{P}_i$  |
| $\eta_c, \eta_t$   | resiliency criteria in percentage for critical and total loads respectively   |
| $\underline{g}_{l,p}^k + \mathbf{i} \overline{g}_{l,q}^k$    | complex power generation capacity of generator $l \in \mathcal{U}$ on phase $k \in \mathcal{P}_l$                     |
| $\tilde{G} = (\tilde{N}, \tilde{E})$                         | an extended associated communication network with potential upgrade options   |
| $\tilde{N}_c := \tilde{N}_t \cup \tilde{N}_u$                |   |
| $\tilde{N}_t \subseteq \tilde{N}$                            | a set of control points for switches  |
| $\tilde{N}_u \subseteq \tilde{N}$                            | a set of control points for generators  |
| $\tilde{i}(e) \in \tilde{N}_t, \tilde{i}(l) \in \tilde{N}_u$ | the control point in $\tilde{G}$ of a switch $e \in \mathcal{E}_t$ and a generator $l \in \mathcal{U}$ , respectively |
| $\tilde{i}_d \in \tilde{N}$                                  | an artificial dummy node in $\tilde{G}$   |
| $\mathcal{G} = (\mathcal{N}, \mathcal{E})$                   | the integrated system of $G$ and $\tilde{G}$  |
| $\mathcal{E}_x := \mathcal{E}_x^0 \cup \mathcal{E}_x^n$      |   |
| $\mathcal{E}_x^0 \subseteq \mathcal{E}$                      | a set of existing lines and links   |
| $\mathcal{E}_x^n \subseteq \mathcal{E}$                      | a set of lines and links that can be installed  |
| $\mathcal{E}_t := \mathcal{E}_t^0 \cup \mathcal{E}_t^n$      |   |
| $\mathcal{E}_t^0 \subseteq E$                                | a set of lines in which a switch is installed   |
| $\mathcal{E}_t^n \subseteq E$                                | a set of lines in which a switch can be installed   |
| $\mathcal{E}_h \subseteq E$                                  | a set of lines or links that can be hardened  |
| $c_e^x$  | installation cost of $e \in \mathcal{E}_x^n$  |
| $c_e^t$  | installation cost of switch on $e \in \mathcal{E}_t^n$  |
| $c_e^h$  | line hardening cost of $e \in \mathcal{E}_h$  |
| $c_l^u$  | installation cost of $l \in \mathcal{U}^n$ on the corresponding bus   |
| $\mathcal{D}$  | a collection of sets of damaged lines for each scenario, indexed with $\mathcal{S} := \{1, \dots,  \mathcal{D} \}$    |

the model variables. The formulation assumes that all new and hardened lines come with switches (i.e.,  $\mathcal{E}_x^n \cup \mathcal{E}_h \subseteq \mathcal{E}_t^0$ ) which reflects current industry practice. Throughout this chapter, an edge  $e \in \mathcal{E}$  is represented as an ordered pair  $(e_h, e_t)$  for some  $e_h, e_t \in \mathcal{N}$  and  $\delta(e) = \{e_h, e_t\}$ . The set of all edges incident to a node  $i \in \mathcal{N}$  is denoted by  $\delta(i)$ . The notation  $x_{\mathcal{A}}$  represents the projection of a vector  $x$  to the space of some index set  $\mathcal{A}$ , i.e.,  $(x_a)_{a \in \mathcal{A}}$ : For instance,  $x_{\mathcal{E}_x^s} = (x_e^s)_{e \in \mathcal{E}_x^s}$ .

Table 2.2: The Variables of the ORDPDC.

| <b>Binary variables</b>                                    |  |
|--|--|
| $x_e$  | 1 if $e \in \mathcal{E}_x^n$ is built  |
| $t_e$  | 1 if a switch is built on $e \in \mathcal{E}_t^n$  |
| $h_e$  | 1 if $e \in \mathcal{E}_h$ is hardened   |
| $u_l$  | 1 if a generator $l \in \mathcal{U}^n$ is built.   |
| For each disaster scenario $s \in \mathcal{S}$ ,           |  |
| $z_e^s$  | 1 if $e \in \mathcal{E}$ is active during $s$  |
| $x_e^s$  | 1 if $e \in \mathcal{E}_x$ exists during $s$   |
| $t_e^s$  | 1 if a switch on $e$ is used or not during $s$   |
| $h_e^s$  | 1 if $e \in \mathcal{E}_h$ is hardened during $s$  |
| $u_l^s$  | 1 if a generator $l \in \mathcal{U}^n$ is available during $s$   |
| $y_e^s$  | 1 if $i, j \in N$ can be disconnected, for $e = (i, j) \in C$ , $C \in \mathcal{C}$ , during $s$               |
| $b_e$  | 1 if the real power on line $e = (i, j) \in E$ flows from $j$ to $i$ during $s$                                |
| $b'_e$   | 1 if the reactive power on line $e = (i, j) \in E$ flows from $j$ to $i$ during $s$                            |
| <b>Continuous variables</b>                                |  |
| For each disaster scenario $s \in \mathcal{S}$ ,           |  |
| $d_i^{s,k} = d_{i,p}^{s,k} + \mathbf{i} d_{i,q}^{s,k}$     | amount of power delivered at bus $i \in N$ on phase $k \in \mathcal{P}_i$ during $s$                           |
| $g_l^{s,k} = g_{l,p}^{s,k} + \mathbf{i} g_{l,q}^{s,k}$     | amount of power generation of $l \in \mathcal{U}$ on phase $k \in \mathcal{P}_l$ during $s$                    |
| $s_{e,i}^{s,k} = p_{e,i}^{s,k} + \mathbf{i} q_{e,i}^{s,k}$ | power flow on $i$ -end of line $e \in E$ , where $i \in \delta(e)$ , on phase $k \in \mathcal{P}_e$ during $s$ |
| $V_i^{s,k}$  | complex voltage at bus $i \in N$ on phase $k \in \mathcal{P}_i$ during $s$                                     |
| $I_e^{s,k}$  | complex current on line $e \in E$ on phase $k \in \mathcal{P}_e$ during $s$                                    |
| $v_i^{s,k}$  | squared voltage magnitude at bus $i \in N$ on phase $k \in \mathcal{P}_i$ during $s$                           |
| $f_e^s$  | the amount of artificial flow on $e \in \tilde{E}$ during $s$  |
| $\gamma_{\tilde{i}}^s$                                     | indicator of connectivity of control point $\tilde{i} \in \tilde{N}$ to some control center during $s$         |

The presentation uses  $w = (x_{\mathcal{E}_x^n}, t_{\mathcal{E}_t^n}, h_{\mathcal{E}_h}, u_{\mathcal{U}^n})$  to denote upgrade profiles,  $m$  the dimension of  $w$ ,  $c = (c_{\mathcal{E}_x^n}^x, c_{\mathcal{E}_t^n}^t, c_{\mathcal{E}_h}^h, c_{\mathcal{U}^n}^u) \in \mathbb{R}^m$  the cost vector, and  $w^s = (x_{\mathcal{E}_x^n}^s, t_{\mathcal{E}_t^n}^s, h_{\mathcal{E}_h}^s, u_{\mathcal{U}^n}^s)$  feasible upgrade profiles for each scenario  $s \in \mathcal{S}$ . For each  $s \in \mathcal{S}$ ,  $\mathcal{Q}(s)$  denotes the set of upgrade profiles that enable the grid to maintain the predetermined load satisfaction (resiliency) level  $\eta_c, \eta_t$  (e.g.,  $\eta_c = 0.98$  and  $\eta_t = 0.5$ ) under disaster scenario  $s$ .

With these notations, the ORDPDC is formulated as follows:

$$(P) \quad \min \quad c^T w \quad (2.1a)$$

$$\text{s.t.} \quad w \geq w^s, \quad \forall s \in \mathcal{S}, \quad (2.1b)$$

$$w^s \in \mathcal{Q}(s), \quad \forall s \in \mathcal{S}, \quad (2.1c)$$

$$w \in \{0, 1\}^m. \quad (2.1d)$$

Problem (P) tries to find the optimal upgrade profile  $w^* = (x_{\mathcal{E}_x^n}^*, t_{\mathcal{E}_t^n}^*, h_{\mathcal{E}_h}^*, u_{\mathcal{U}^n}^*)$  that ensures resilient operations for each disaster scenario. Constraint (2.1b) ensures that an upgrade profile is feasible if it dominates a feasible solution  $w^s \in \mathcal{Q}(s)$  for each scenario  $s$ , i.e., if the grid survives each of the extreme events in  $\mathcal{S}$ .

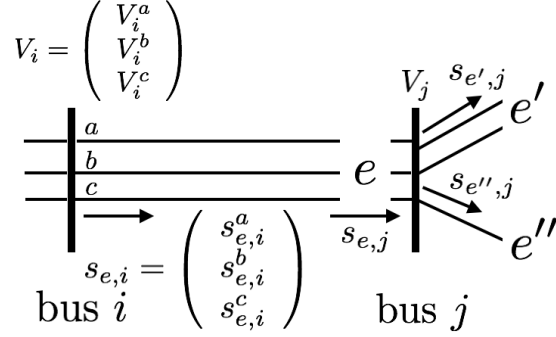


Figure 2.2: Notations for the Power Flow Equations.

The set  $\mathcal{Q}(s)$  is specified by resiliency constraints that are expressed in terms of the AC power flow equations, load satisfaction requirements, the communication network, and the grid topology:

$$\mathcal{Q}(s) = \{w^s \in \{0, 1\}^m : (2), (3), (2.5), (5), \text{ and } (2.8)\}$$

where Constraints (2), (3), (2.5), (5), and (2.8) are stated in detail in the following. The variables in each  $\mathcal{Q}(s)$  are indexed by  $s$ . For simplicity, this section omits index  $s$ .

**Power Flow Constraints.** Let  $\mathcal{P} = \{a, b, c\}$  denote the three phases of the network. For each bus  $i \in N$ , define  $V_i = (V_i^k)_{k \in \mathcal{P}_i}$  and, for each line  $e \in E$ , define  $I_e = (I_e^k)_{k \in \mathcal{P}_e}$  and  $s_{e,i} = (s_{e,i}^k)_{k \in \mathcal{P}_e}$ . The notations also use a superscript  $\mathcal{P}' \subseteq \mathcal{P}$  to represent the *projection* or the *extension* of a vector to the space of  $\mathcal{P}'$ . For example, if  $\mathcal{P}_i = \{a, b, c\}$  and  $\mathcal{P}' = \{a, b\}$ , then  $V_i^{\mathcal{P}'} = (V_i^a, V_i^b)^T$ . If  $\mathcal{P}_i = \{a, c\}$  and  $\mathcal{P}' = \{a, b, c\}$ , then  $V_i^{\mathcal{P}'} = (V_i^a, 0, V_i^c)^T$ .

$$-M(1 - z_e) \leq V_j^{\mathcal{P}_e} - (V_i^{\mathcal{P}_e} - Z_e I_e) \leq M(1 - z_e), \quad \forall e = (i, j) \in E, \quad (2.2a)$$

$$s_{e,i} = \text{diag}(V_i^{\mathcal{P}_e} I_e^H), \quad \forall e \in E, i \in \delta(e), \quad (2.2b)$$

$$\sum_{l \in \mathcal{U}_i} g_l^k - d_i^k = \sum_{e \in \delta(i)} s_{e,i}^k, \quad \forall i \in N, k \in \mathcal{P}_i \quad (2.2c)$$

$$(p_{e,i}^k)^2 + (q_{e,i}^k)^2 \leq (T_e^k)^2 z_e, \quad \forall e \in E, i \in \delta(e), k \in \mathcal{P}_e, \quad (2.2d)$$

$$\underline{V}_i^k \leq |V_i^k| \leq \overline{V}_i^k, \quad \forall i \in N, k \in \mathcal{P}_i. \quad (2.2e)$$

$$-b_e T_e^k \leq p_{e,i}^k \leq T_e^k (1 - b_e), \quad \forall e = (i, j) \in E, k \in \mathcal{P}_e, \quad (2.2f)$$

$$-b'_e T_e^k \leq q_{e,i}^k \leq T_e^k (1 - b'_e), \quad \forall e = (i, j) \in E, k \in \mathcal{P}_e, \quad (2.2g)$$

For each line  $e = (i, j) \in E$ , Ohm's law for 3-phase lines states the relationship  $V_j^{\mathcal{P}_e} = V_i^{\mathcal{P}_e} - Z_e I_e$  between  $I_e$ ,  $V_i$ , and  $V_j$ . For each line  $e \in E$  and bus  $i \in \delta(e)$ , the electric power flow equation  $s_{e,i} = \text{diag}(V_i^{\mathcal{P}_e} I_e^H)$  describes the relationship between  $s_{e,i}$ ,  $V_i^{\mathcal{P}_e}$ , and  $I_e$ , where superscript  $H$  indicates the conjugate transpose. In Constraint (2.2a), the big-M method is used to apply Ohm's law only for available lines; the big-M can be set as  $\max_{j' \in \{i,j\}, k \in \mathcal{P}_e} \bar{V}_{j'}^k - \min_{j' \in \{i,j\}, k \in \mathcal{P}_e} \underline{V}_{j'}^k$ . Equation (2.2c) is the balance equation for power flow at each bus  $i \in N$ , i.e., the sum of incoming flows equals the sum of the outgoing flows.

Let  $p_{e,i} + \mathbf{i}q_{e,i}$  be the rectangular representation of  $s_{e,i}$ , where  $p_{e,i} = (p_{e,i}^k)_{k \in \mathcal{P}_i}$  and  $q_{e,i} = (q_{e,i}^k)_{k \in \mathcal{P}_i}$  denote the real and reactive power at the  $i$ -end of line  $e$ . Constraints (2.2d) and (2.2e) specify the thermal limits on lines and the voltage bounds on buses.

In some disaster scenarios when some of the lines are broken, power flows of different phases on the same line can have opposite directions, which is very undesirable operationally. Constraints (2.2f) and (2.2g) prevent this behavior from happening.

The real and reactive power on different phase must stay within a certain limit. Let  $\hat{p}_{e,i} = \sum_{\bar{k} \in \mathcal{P}_e} p_{e,i}^{\bar{k}}$  and  $\hat{q}_{e,i} = \sum_{\bar{k} \in \mathcal{P}_e} q_{e,i}^{\bar{k}}$ . Then, these limits are formulated as follows:

$$\left( \underline{\beta}_e (1 - b_e) + \bar{\beta}_e b_e \right) \frac{\hat{p}_{e,i}}{|\mathcal{P}_e|} \leq p_{e,i}^k \leq \left( \underline{\beta}_e b_e + \bar{\beta}_e (1 - b_e) \right) \frac{\hat{p}_{e,i}}{|\mathcal{P}_e|}, \forall e \in E_V, k \in \mathcal{P}_e, \quad (2.4a)$$

$$\left( \underline{\beta}_e (1 - b'_e) + \bar{\beta}_e b'_e \right) \frac{\hat{q}_{e,i}}{|\mathcal{P}_e|} \leq q_{e,i}^k \leq \left( \underline{\beta}_e b'_e + \bar{\beta}_e (1 - b'_e) \right) \frac{\hat{q}_{e,i}}{|\mathcal{P}_e|}, \forall e \in E_V, k \in \mathcal{P}_e, \quad (2.4b)$$

where  $\underline{\beta}_e = 1 - \beta_e$  and  $\bar{\beta}_e = 1 + \beta_2$ .

**Generator/resiliency Constraints.** Moreover, each generator  $l \in \mathcal{U}$  has its own capacity and at least some percentage of critical and total loads must be satisfied as specified by the resiliency criteria  $\eta_c$  and  $\eta_t$ .

$$0 \leq g_{l,p}^k \leq \bar{g}_{l,p}^k u_l, \quad g_{l,q}^k \leq \bar{g}_{l,q}^k u_l, \quad \forall l \in \mathcal{U}, k \in \mathcal{P}_l, \quad (2.5a)$$

$$0 \leq d_{i,p}^k \leq D_{i,p}^k, \quad 0 \leq d_{i,q}^k \leq D_{i,q}^k, \quad \forall i \in N, k \in \mathcal{P}_i \quad (2.5b)$$

$$\sum_{i \in \mathcal{L}} d_{i,p}^k \geq \eta_c \sum_{i \in \mathcal{L}} D_{i,p}^k, \quad \sum_{i \in \mathcal{L}} d_{i,q}^k \geq \eta_c \sum_{i \in \mathcal{L}} D_{i,q}^k, \quad \forall k \in \mathcal{P}, \quad (2.5c)$$

$$\sum_{i \in N} d_{i,p}^k \geq \eta_t \sum_{i \in N} D_{i,p}^k, \quad \sum_{i \in N} d_{i,q}^k \geq \eta_t \sum_{i \in N} D_{i,q}^k, \quad \forall k \in \mathcal{P}. \quad (2.5d)$$

Constraint (2.5a) captures the power generation capacity constraints. Constraint (2.5b) states that the delivered power at each bus  $i$  should not exceed the load. Constraints (2.5c)-

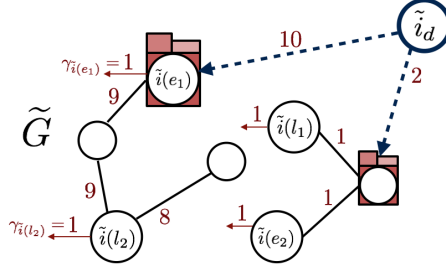


Figure 2.3: The Single-Commodity Flow Model for  $\tilde{G}$  (red-colored squares denote control centers).

(2.5d) enforce the resiliency constraints.

**Communication Constraints.** The operation of generators and RCSs depend on the communication network: A generator  $l \in \mathcal{U}$  and a RCS on line  $e \in \mathcal{E}_t$  is operable only if their associated control points  $\tilde{i}(l) \in \tilde{N}$  and  $\tilde{i}(e) \in \tilde{N}$  can receive a control signal from some control centers through  $\tilde{G}$ . To capture the connectivity of a vertex to some control centers, the formulation uses a single-commodity flow model summarized in Constraints (2.6) and Figure 2.3. The formulation uses a dummy node  $\tilde{i}_d$  to  $\tilde{N}$  and connect  $\tilde{i}_d$  to all control centers with additional links. The flow  $f \in \mathbb{R}^{|\tilde{E}|}$  originating from the dummy node  $\tilde{i}_d$  then is used to check the connectivity of every node. By Constraint (2.6c), the flow passes only through available links during disaster  $s$  (the big-M value is set to  $|\tilde{N}_c|$  in the implementation). If a control point  $i \in \tilde{N}_c$  is connected with some control center through some path, it can borrow a unit of flow from  $f$  to make  $\gamma_i$  1, as specified in Equations (2.6a) and (2.6b). In other words,  $\gamma_i$  indicates whether control point  $i \in \tilde{N}_c$  can receive a control signal. If  $\gamma_i$  is 1, the associated device in  $G$  is operable by Constraints (2.6d) and (2.6e).

$$\sum_{e:e_t=i} f_e - \sum_{e:e_h=i} f_e = \gamma_i, \quad \forall i \in \tilde{N}_c, \quad (2.6a)$$

$$\sum_{e:e_t=i} f_e - \sum_{e:e_h=i} f_e = 0, \quad \forall i \in \tilde{N} \setminus (\tilde{N}_c \cup \{\tilde{i}_d\}), \quad (2.6b)$$

$$-Mx_e \leq f_e \leq Mx_e, \quad \forall e \in \tilde{E}, \quad (2.6c)$$

$$0 \leq g_l^k \leq \bar{g}_l^k \gamma_{\tilde{i}(l)}, \quad g_l^k \leq \bar{g}_l^k \gamma_{\tilde{i}(l)}, \quad \forall l \in \mathcal{U}, \forall k \in \mathcal{P}_l, \quad (2.6d)$$

$$t_e \leq \gamma_{\tilde{i}(e)}, \quad \forall e \in \mathcal{E}_t, \quad (2.6e)$$

$$0 \leq \gamma_i \leq 1, \quad \forall i \in \tilde{N}_c. \quad (2.6f)$$

Some communication network may be affected by a failure in distribution grid, e.g., when the grid fails to supply power to communication centers. This kind of dependencies is not considered in this chapter but it can be easily captured if needed. Indeed, first assign a small critical load to each communication center and add constraints that restrict the auxiliary arcs between the dummy node and each communication center to have positive flow only when the associated communication center has a positive power supply. The constraints can be expressed in terms of an extra binary variable for each bus at which a communication center is located. The extra binary variable determines if there is a positive power supply to the communication center.

**Topological constraints.** The final set of constraints captures the topology restrictions in distribution systems:

$$x_e \geq t_e, \quad \forall e \in \mathcal{E}, \quad (2.8a)$$

$$z_e = x_e - t_e, \quad \forall e \in \mathcal{E}, \quad (2.8b)$$

$$x_e = h_e, \quad \forall e \in \mathcal{D}_s, \quad (2.8c)$$

$$\sum_{e \in C} y_e \leq |C| - 1, \quad \forall C \in \mathcal{C}, \quad (2.8d)$$

$$z_{\hat{e}} \leq y_e, \quad \forall \hat{e} \in E : \delta(\hat{e}) = \delta(e), e \in C, C \in \mathcal{C}. \quad (2.8e)$$

Constraint (2.8a) restrict switches to be operable only on existing lines. In Equation (2.8b),  $z_e$  represents whether line  $e \in \mathcal{E}$  is active under scenario  $s$ . A line is active when it exists and its switch is off. Equation (2.8c) states that a damaged line during scenario  $s \in \mathcal{S}$  is inoperable unless it is hardened. Constraints (2.8d) and (2.8e) ensures that the distribution grid should operate in a radial manner. Accordingly, Constraint (2.8d) eliminates the sub-tours within  $\mathcal{C}$ . Since  $G$  is usually sparse, the implementation enumerates all the sub-tours  $\mathcal{C}$  and variable  $y_e$  indicates whether  $i, j \in \delta(e)$  are disconnected. If they are disconnected, then all the lines between  $i$  and  $j$  are inactive by Constraint (2.8e).

Note also that, for existing lines not damaged under scenario  $s$ ,  $x_e$  is fixed as one. For each line  $e \in E \setminus \mathcal{E}_t$ ,  $t_e$  is set to zero. Second, for each line  $e \in \mathcal{E} \setminus \mathcal{E}_h$ ,  $h_e$  is fixed as 0 and all the existing generators have  $u_l = 1$ . Finally, for each line  $e = (i, j) \in E$  with strictly decreasing or increasing phases (i.e.,  $|\mathcal{P}_i| > |\mathcal{P}_j|$  or  $|\mathcal{P}_i| < |\mathcal{P}_j|$ ), the direction of power flow must be from a bus with more phases. Let  $E_>$  and  $E_<$  denote the set of lines with strictly decreasing and increasing phases, respectively. We add bound constraints  $p_{e,i}^k \geq 0$

for  $e \in E_>$ ,  $k \in \mathcal{P}_e$  and  $p_{e,i}^k \leq 0$  for  $e \in E_<$ ,  $k \in \mathcal{P}_e$ . This chapter assumes perfect hardening, i.e., a hardened line survives all disaster scenarios. This assumption can be naturally generalized to imperfect hardening [44].

### 2.3.1 Linearization of the ORDPDC

The formulation of the ORDPDC is nonlinear. This section discusses how to obtain a sufficiently accurate linearization.

#### 2.3.1.1 Linear Approximation of the AC Power Flow Equations for Radial Networks

The main difficulty lies in linearizing constraints (2a–2b) for which the formulation uses the tight linearization from [21]. The linearization is based on two assumptions: (A1) line losses are small, i.e.,  $Z_e I_e I_e^H \approx 0$  for  $e = (i, j) \in E$  and (A2) voltages are nearly balanced, i.e., if  $\mathcal{P}_i = \{a, b, c\}$ , then  $V_i^a/V_i^b \approx V_i^b/V_i^c \approx V_i^c/V_i^a \approx e^{i2\pi/3}$ . Informally speaking, the approximation generalizes the distflow equations to 3 phases, drops the quadratic terms, and eliminates the current variables using the balance assumption. The derivation assumes that all phases are well-defined for simplicity. Moreover, if  $A$  is an  $n \times n$  matrix, then  $\text{diag}(A)$  denotes the  $n$ -dimensional vector that represents its diagonal entries. If  $a$  is an  $n$ -dimensional vector, then  $\text{diag}(a)$  denotes the  $n \times n$  matrix with  $a$  in its diagonal entries and zero for the off-diagonal entries.

Let  $s_i = \sum_{l \in \mathcal{U}_i} g_l - d_i$  denote the power injection at bus  $i$ . By (A1),  $s_{e,i} = s_{e,j}$  for all  $e = (i, j) \in E$  and therefore, given  $s_i$ ,  $s_{e,i}$  ( $i \in \delta(e)$ ) is uniquely determined by Equation (2c).

Now define  $S_{e,i} := V_i I_e^H$ , whose diagonal entries are  $s_{e,i}$ . Multiplying both sides of  $V_j = V_i - Z_e I_e$  with their conjugate transposes gives

$$V_j V_j^H = V_i V_i^H - S_{e,i} Z_e^H - Z_e S_{e,i}^H + Z_e I_e I_e^H Z_e^H. \quad (2.9)$$

By assumption (A1), this becomes

$$V_j V_j^H = V_i V_i^H - S_{e,i} Z_e^H - Z_e S_{e,i}^H \quad (2.10)$$

and, by restricting attention to diagonal elements only,

$$v_j = v_i - \text{diag}(S_{e,i} Z_e^H - Z_e S_{e,i}^H). \quad (2.11)$$

where  $(v_i^k)_{k \in \mathcal{P}_i} = \text{diag}(V_i V_i^H)$  represents the squared voltage magnitude at bus  $i \in N$ .

By (A2), we have  $S_{e,i} \approx \gamma^{\mathcal{P}_e} \text{diag}(s_{e,i})$ , where

$$\gamma = \begin{bmatrix} 1 & \alpha^2 & \alpha \\ \alpha & 1 & \alpha^2 \\ \alpha^2 & \alpha & 1 \end{bmatrix} \text{ and } \alpha = e^{-i2\pi/3}.$$

As a result, Equation (2.11) can now be simplified as follows: for each line  $e = (i, j) \in E$  and  $k \in \mathcal{P}_e$ ,

$$v_j^k = v_i^k - \sum_{k' \in \mathcal{P}_e} 2 [ \text{Re}\{\alpha^{n_k - n_{k'}} Z_e^{kk'}\} p_{e,i}^{k'} + \text{Im}\{\alpha^{n_k - n_{k'}} Z_e^{kk'}\} q_{e,i}^{k'} ], \quad (2.12)$$

where  $n_a = 2, n_b = 1, n_c = 0$ ,  $R_e + \mathbf{i}X_e = Z_e$ , and superscript  $kk'$  of a matrix denotes its  $(k, k')$ -entry.

In summary, Ohm's law and the power flow equation in Constraints (2a) and (2b) are approximated by Eq. (2.12) for all  $e = (i, j) \in E$  and  $k \in \mathcal{P}_e$  and the big- $M$  is set to  $\max_{j'=i,j} (\bar{V}_{j',k})^2 - \min_{j'=i,j} (\underline{V}_{j',k})^2$ , along with Equation (2c). Accordingly, Constraint (2e) is replaced by the following constraint:

$$(\underline{V}_i^k)^2 \leq v_i^k \leq (\bar{V}_i^k)^2, \quad \forall i \in N, k \in \mathcal{P}_i.$$

### 2.3.1.2 Linearization of (2.4a)-(2.4b)

Constraints (2.4a) and (2.4b) contain products of a binary variable and a bounded real variable. These constraints are linearized without loss of accuracy using McCormick inequalities [77].

### 2.3.1.3 Piecewise-Linear Inner Approximation of Thermal Limits

The quadratic thermal limit constraint (Constraint (2d)) can be approximated with  $K$  linear inequalities as shown in Figure 2.4. The resulting inequalities are as follows: for all  $e \in E$ ,  $i \in \delta(e)$ ,  $k \in \mathcal{P}_e$ :

$$\begin{aligned} & \left( \sin\left(\frac{2n\pi}{K}\right) - \sin\left(\frac{2(n-1)\pi}{K}\right) \right) p_{e,i}^k \\ & - \left( \cos\left(\frac{2n\pi}{K}\right) - \cos\left(\frac{2(n-1)\pi}{K}\right) \right) q_{e,i}^k \leq \sin\left(\frac{2\pi}{K}\right) T_{e,k}, \quad \forall n = 1, \dots, K, \end{aligned} \quad (2.13a)$$

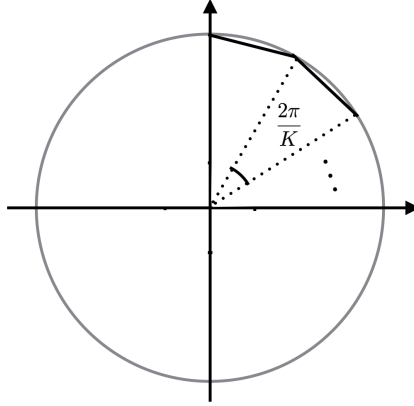


Figure 2.4: The Piecewise-Linear Inner Approximation of a Circle.

$$-Mz_e^s \leq p_{e,i}^k \leq Mz_e^s, \quad -Mz_e^s \leq q_{e,i}^k \leq Mz_e^s, \quad \forall e \in E, k \in \mathcal{P}_e. \quad (2.13b)$$

where the big-M is set to  $\sum_{i \in N} D_{i,k}^p$ . Our implementation uses  $K = 28$ .

## 2.4 Case Study

This section analyzes the behavior of the optimization model on a variety of test cases. In particular, it studies how the topology of the distribution grid and the dispersion level of its communication network affect the optimal design. For each network described in Section 2.4.1, this section analyzes the optimal design under different settings of damage probability, the resiliency level, and the number of communication centers. The default value of  $\eta_c$  and  $\eta_t$  are 98% and 50% respectively, the default number of communication centers is 4, and the phase variation parameter  $\beta$  is set to 15% for  $E_V$  and  $\infty$  otherwise. Unless specified otherwise, the comparisons are based on these default values.

### 2.4.1 Data Description

This section describes the distribution test systems. The data set is available from <https://github.com/lanl-ansi/micot/> in the `application_data/lpnorm` directory. Details of the data format are available from <https://github.com/lanl-ansi/micot/wiki/Resilient-Design-Executable>.

The first two sets, the *Rural* and *Urban* systems, is from [44]. They are based on the IEEE 34 bus system [78] (see Figure 2.5) and replicate the 34-bus distribution feeder three times. All three feeders are connected to a single transmission bus and candidate new

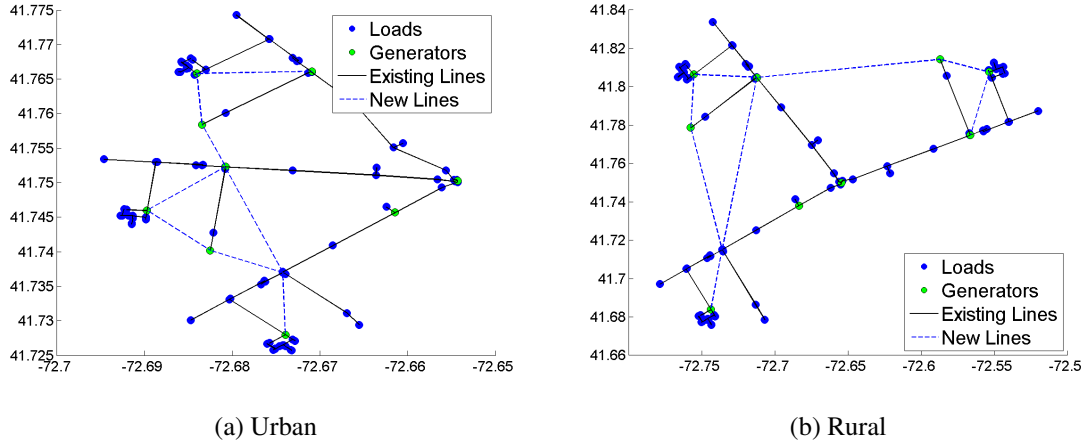


Figure 2.5: The urban and rural distribution systems which contain three copies of the IEEE 34 system to mimic situations where there are three normally independent distribution circuits that support each other during extreme events. These test cases include 109 nodes, 118 generators, 204 loads, and 148 edges.

lines were added to the network to allow back-feeds. In the rural model, the distribution feeder was geolocated to model feeders with long distances between nodes. Similarly, the urban network was geolocated to model compact feeders typical of urban environments. Geolocation of these networks has the net effect of adjusting the lengths of the power lines and their associated impedance values. Spreading the network out also increases the hardening and new line costs. As a result, the rural system is expected to favor solutions with distributed generation and the urban system solutions with new lines and switches (in addition to hardening lines). The fixed cost of installing a new distributed generator is set at \$500k. The cost of a distributed generator is set at \$1,500k per MW based on the 2025 projections from [79]. The cost of installing new switches for 3-phase lines is set between 10k and 50k [80]. The cost of new underground 3-phase lines is set at about \$500k per mile and the cost of new underground single phase lines is set at about \$100k per mile. The hardening cost is set at roughly \$50k and \$10k per mile for multi-phase and single-phase lines [81]. The third network, NETWORK123, is based on the 123-node network of [78]. This network is unaltered except for adding new line candidates and labeling large loads as critical.

The communication network  $\tilde{G}$  is built to conform to  $G$ . Let  $G' = (N', E')$  be the duplicate of  $G$ . For each generator  $l \in \mathcal{U}$ , its duplicate  $i(l)$  represents its control point. Consider  $\mathcal{E}'_t \subseteq E'$ , the duplicate of  $\mathcal{E}_t$ . To represent the control point for a switch,  $e \in \mathcal{E}'_t$  is divided in the middle and a new vertex  $v_e$  is added to represent the control point for the switch. In other words, the edge  $e = (e_h, e_t) \in \mathcal{E}'_t$  is replaced by a new vertex  $v_e$

and two new edges  $e_1 = (e_h, v_e), e_2 = (v_e, e_t)$ . The test cases assume that the damage, installation, and hardening of a line in  $G$  are also incurred for the corresponding line in  $\tilde{G}$ . These assumptions can be easily generalized without changing the nature of the model.

The experimental evaluation considers 100 scenarios per damage intensity for all three networks and the damage intensities are taken in the set  $\{1\%, 2\%, 3\%, 4\%, 5\%, 10\%, 15\%, 20\%, 25\%, 30\%, 35\%, 40\%, 45\%, 50\%, 55\%, 60\%, 65\%, 70\%, 75\%, 80\%, 85\%, 90\%, 95\%, 100\%\}$ . The scenario generation procedure is based on damage caused by ice storms. The intensity tends to be homogeneous on the scale of distribution systems [82]. Ice storm intensity is modeled as a per-mile damage probability, i.e. the probability at least one pole fails in a one mile segment of power line. Each line is segmented into 1-mile segments and a scenario is generated by randomly failing each segment with the specified probability. This probability is normalized for any line segment shorter than 1 mile. A line is “damaged” if any segment fails.

## 2.4.2 Impact of Grid Topology

Let  $n_h, n_x, n_t$ , and  $n_u$  be the number of hardened lines, new lines, new switches, and new generators in the optimal design. Figure 2.6 reports these values for various damage levels and the three networks. The red line indicates the optimal upgrade costs, and the counts of the upgrade options are represented as a bar. The results show that hardening lines is the major component of each optimal design and that its share increases with the disaster intensity. The results also show that DGs are used in significant numbers in the rural network, while new lines and switches complement hardening in the urban model. This was expected given the length of the lines in these two networks. The third network only needs line hardenings.

## 2.4.3 Impact of the Communication Network

First note that ignoring the communication network is equivalent to assuming that every bus has its own communication center. In the following,  $\tilde{G}(k)$  denotes a communication network with  $k$  centers and  $\tilde{G}(\infty)$  the case where each bus has a center.

Figure 2.9 and Table 2.3 report the impact of the communication system: They report optimal objective values and solution statistics under various numbers of communication centers. Fewer communication centers lead to significant cost increases in the rural network, but have limited effect on the urban network and NETWORK123. In the rural network, resiliency comes from forming microgrids with DGs, which require their own communication centers. When these are not available, optimal designs harden existing lines

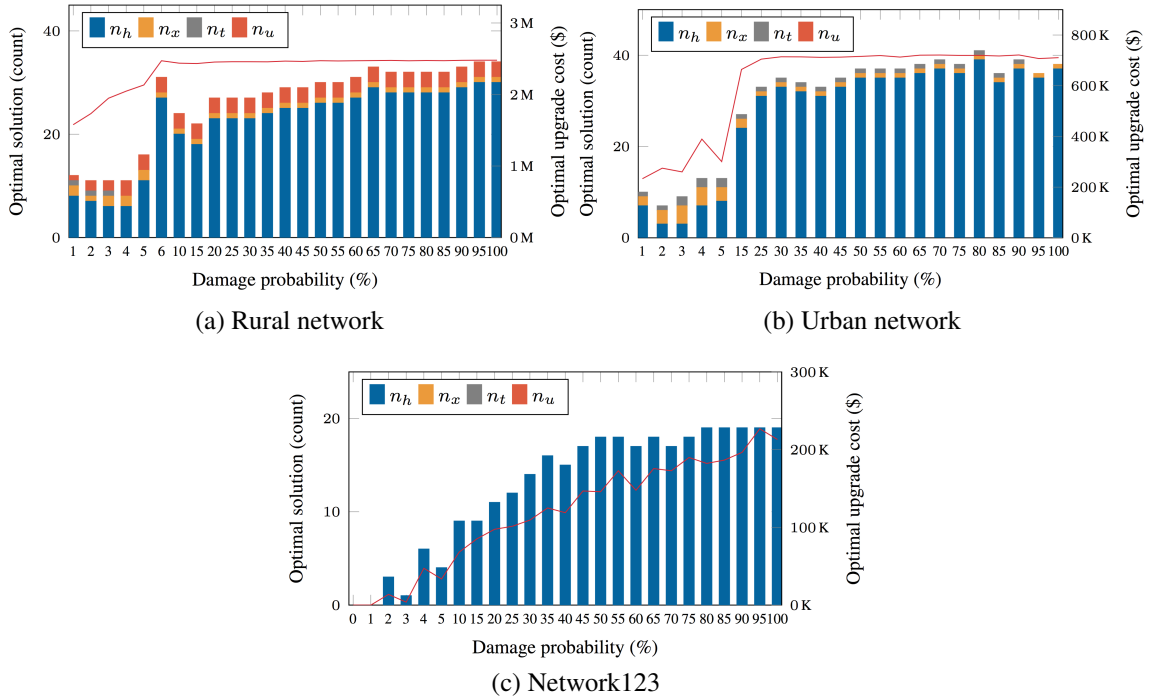


Figure 2.6: Statistics on the Optimal Grid Designs.

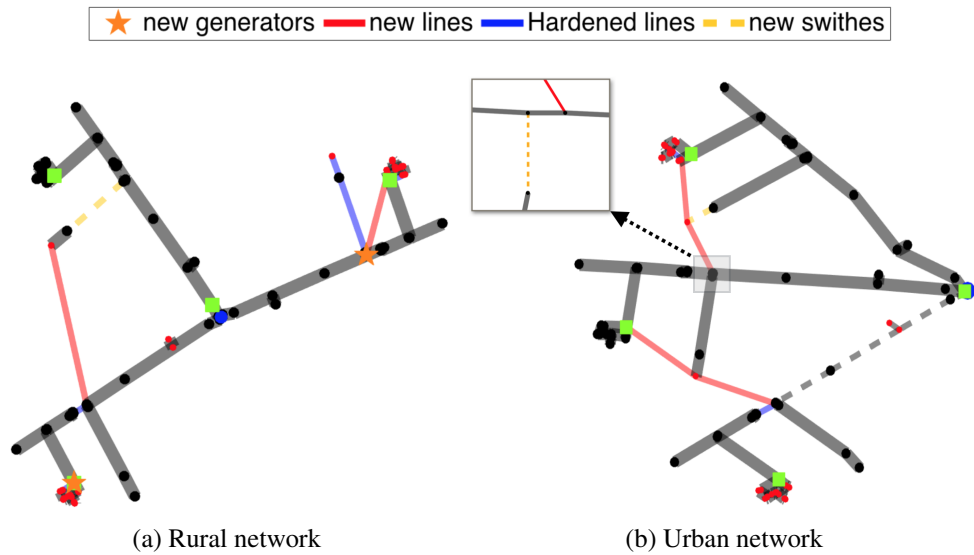


Figure 2.7: Optimal Designs of the Rural and Urban Networks (3% damage level).

and build new lines and switches, which are more costly as substantiated in Table 2.3.

Figure 2.10 illustrates the resulting designs on the rural network for scenarios with a damage level of 3%. The top row depicts some of the scenarios and shows the affected lines. The bottom row depicts the optimal designs for various configurations of the communication network. For  $\tilde{G}(\infty)$ , the optimal design features three new DGs in the west-,

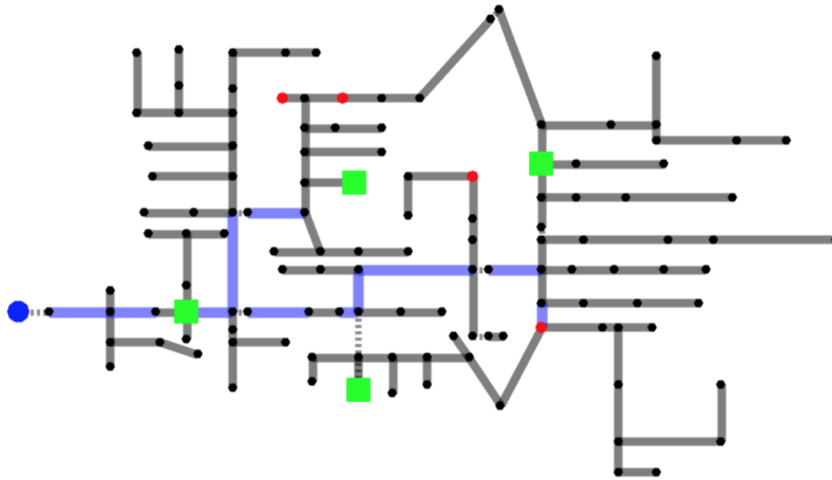


Figure 2.8: Optimal Design of Network NETWORK123 (20% damage level).

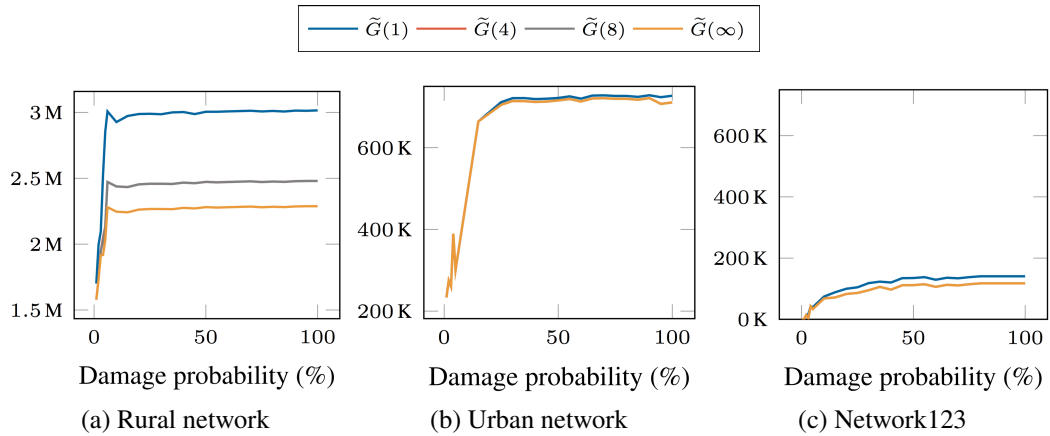


Figure 2.9: Cost Analysis For the Number of Communication Centers

north-, and east-end of the network to meet the critical loads of each region. These regions are then islanded under various scenarios. For  $\tilde{G}(4)$ , the optimal design installs a new line linking critical loads in the north side to the west side of the network, instead of using DG in the north side. This stems from Scenario 100 where a DG in the bus with critical loads cannot be operated since it has no communication center. For  $\tilde{G}(1)$ , scenario 1 prevents the operation of an east-end DG and scenario 100 the operation of a west-end DG. Hence, the optimal design only considers hardening and new lines and switches. On the other hand, the urban network and NETWORK123 achieve resiliency by increasing grid connectivity for all communication networks.

Table 2.3: Impact of the Communication Network on Optimal Grid Designs.

|                        | Comm. Network       | Obj.    | $n_h$ | $n_x$ | $n_t$ | $n_u$ |
|------------------------|---------------------|---------|-------|-------|-------|-------|
| Rural,<br>3%<br>damage | $\tilde{G}(1)$      | 2095.74 | 12    | 3     | 1     | 0     |
|                        | $\tilde{G}(4)$      | 1948.09 | 6     | 1     | 2     |       |
|                        | $\tilde{G}(8)$      | 1948.09 | 6     | 2     | 1     | 2     |
|                        | $\tilde{G}(\infty)$ | 1914.99 | 5     | 1     | 0     | 3     |

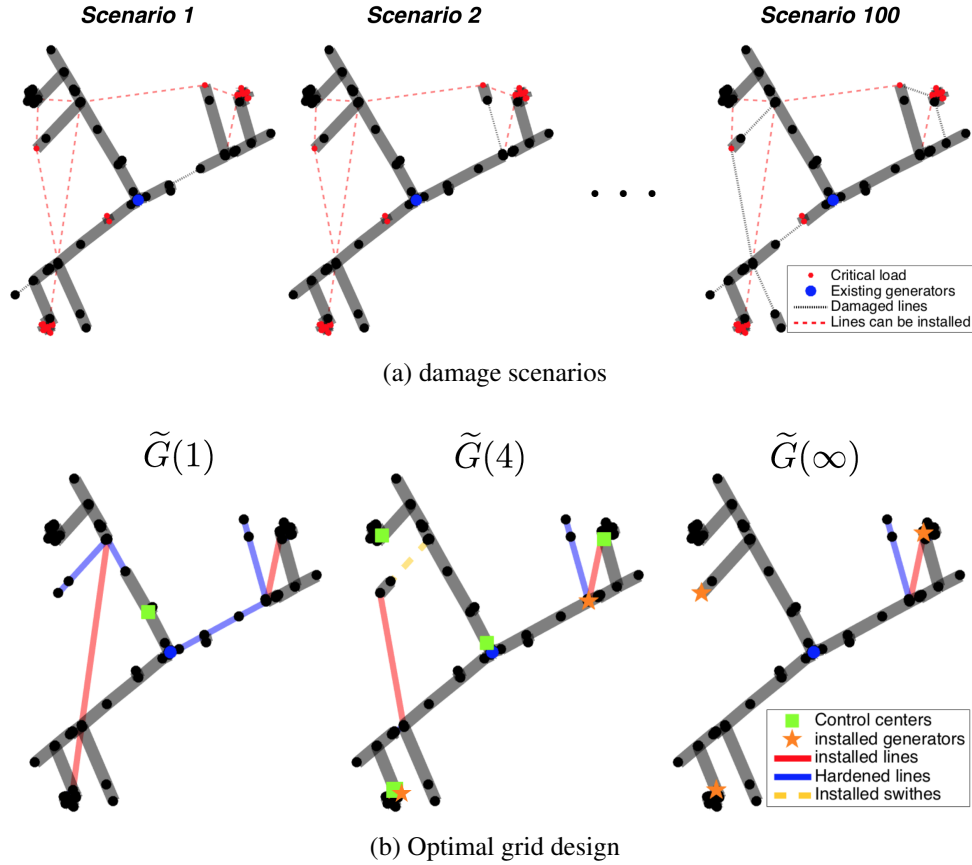


Figure 2.10: Optimal Designs of the Rural Network under 3% Damage and Various Communication Network Configurations.

#### 2.4.4 Load Flow Analysis of the Linearization of the ORDPDC

This section analyzes the accuracy of the linearization explained in Section 2.3.1. To simulate the actual load flow of the solution obtained by the linearized ORDPDC, we use the OpenDSS software, a comprehensive electrical power system simulation tool for distribution systems. The experiments consider a random set of 108 instances (approximately 10% of total instances) by setting  $\eta_t = 0.5$  and  $0.8$ , and the damage level to 5%, 25%, 45%, 65%, 85%, 100% for the three networks  $\tilde{G}(0)$ ,  $\tilde{G}(1)$ , and  $\tilde{G}(4)$ . Each instance has approximately 100 scenarios, which means that the results report the load flow analysis for about 10,800

scenarios.

In our initial experiments, OpenDSS reported that some solutions did not satisfy power flow physics. After analyzing these results, we found a single cause for these infeasibilities—zero flow on lines. In some situations, instead of using switches to remove flow from a line, the solutions based on the linearized model allowed zero flow on a line by letting both end-buses of the line have the same voltage magnitude. In practice, this effect is highly undesirable since it can reverse flows and allow flow from single phase buses to three phase buses. In such cases, even small voltage variation can result in significant voltage drops. Hence, we prevent these situations by adding the following set of constraints:

$$\sum_{e \in P} (x_e - \tau_e) \leq |P| - u_l, \forall P \in \mathcal{P}_l, l \in \mathcal{U}^n$$

$$\sum_{e' \in P} (x_{e'} - \tau_{e'}) \leq |P| - x_e, \forall P \in \mathcal{P}_e, e \in \mathcal{E}_x^n$$

where  $\mathcal{P}_l$  and  $\mathcal{P}_e$  denotes the set of paths that start from bus  $l$  with an edge  $e$  that has an increasing number of phases (e.g., a line from single phase bus to three phase bus), respectively. These constraints force a switch to be added along such a path, hence preventing the undesirable situation.

Once these constraints were added, the OpenDSS software reported that optimal solutions of the linearized ORDPDC for all 10,800 cases were feasible for the three phase AC power flow physics and satisfy all load and bound constraints.

## 2.5 Solution Approaches

### 2.5.1 Benchmark Approaches: Scenario-Based and Scenario Decomposition

In Section 2.6, the branch and price algorithm presented in the next section is compared to the Scenario-Based Decomposition (SBD) and the Scenario Decomposition (SD) algorithms proposed by [44] and [45] respectively.

The SBD algorithm iteratively solves a master problem  $P(\mathcal{S}')$  which only includes the constraints of a subset of scenarios  $\mathcal{S}' \subseteq \mathcal{S}$ . The algorithm terminates when the optimal solution to  $P(\mathcal{S}')$  is feasible (and hence optimal) for the remaining scenarios  $\mathcal{S} \setminus \mathcal{S}'$ . Otherwise, at least one scenario  $s \in \mathcal{S} \setminus \mathcal{S}'$  is infeasible. Scenario  $s$  is added to  $\mathcal{S}'$  and the process is repeated.

To apply the SD algorithm, consider the following equivalent problem:

$$(P') \quad \min \quad \sum_{s \in \mathcal{S}} \frac{1}{|\mathcal{S}|} c^T w^s \quad (2.14a)$$

$$\text{s.t.} \quad w^1 = \dots = w^{|\mathcal{S}|}, \quad (2.14b)$$

$$(2.1c), (2.1d).$$

The equivalence follows from the assumption that all new and hardened lines come with switches (i.e., a solution that dominates a feasible solution to a subproblem can be made feasible for the subproblem by switching). Let  $\sum_{s \in \mathcal{S}} A_s w^s = 0$  represent Equation (2.14b).

The SD algorithm explores solutions to each subproblem  $P'(s)$ ,  $\forall s \in \mathcal{S}$ , by minimizing the objective function  $\frac{1}{|\mathcal{S}|} c^T w^s + \lambda^T A_s w^s$  to find primal feasible solutions to Problem  $(P')$ , where  $\lambda$  is the dual vector of Equation (2.14b). The explored solutions are then cut off in all subproblems to leave them out of future consideration and improve the lower bound. The algorithm proceeds until it closes the gap between lower and upper bounds.

## 2.5.2 Proposed Approach: Branch-and-Price Algorithm

This chapter proposes a branch-and-price (BnP) algorithm for the ORDPDC. The BnP exploits the special structure of the ORDPDC in several ways. First, it uses a compact reformulation that yields a better lower bound than the LP relaxation. The reformulation also makes it possible to use column generation and solve independent pricing problems associated with each scenario in parallel. Finally, several additional techniques are used to accelerate the column generation significantly. Section 2.5.2.1 presents the problem reformulation and Section 2.5.2.2 briefly reviews the basic column generation of the BnP algorithm. Section 2.5.2.3 introduces several acceleration schemes. The implementation of the BnP algorithm is presented in Section 2.5.2.4.

### 2.5.2.1 The Problem Reformulation

Letting  $\tilde{Q}(s)$  be the linearization of  $Q(s)$ , the problem  $(P)$  is rewritten as

$$(P) \quad \min \quad c^T w \quad (2.15a)$$

$$\text{s.t.} \quad w - w^s \geq 0, \forall s \in \mathcal{S}, \quad (2.15a)$$

$$w^s \in \tilde{Q}(s), \forall s \in \mathcal{S}, \quad (2.15b)$$

$$w^s \in \{0, 1\}^m, \forall s \in \mathcal{S}. \quad (2.15c)$$

Without the linking constraint (2.15a),  $(P)$  can be decomposed into  $|\mathcal{S}|$  independent problems, each of which has a feasible region defined by

$$\mathcal{P}^s = \{w^s \in \mathbb{R}^m : (2.15b) \text{ and } (2.15c)\}, \forall s \in \mathcal{S}.$$

Observe that  $\mathcal{P}^s$  is bounded and let  $\mathcal{J}^s = \{\hat{w}_j^s \in \mathbb{R}^m : \hat{w}_j^s \text{ is a vertex of } \text{conv}(\mathcal{P}^s)\}$  be the set of all vertices of  $\text{conv}(\mathcal{P}^s)$ . Letting  $\mathcal{J} = \cup_s \mathcal{J}_s$ , consider the following problem:

$$\begin{aligned} (\tilde{P}) \quad & \min \quad c^T w \\ \text{s.t.} \quad & w - \sum_{j \in \mathcal{J}^s} \lambda_j^s \hat{w}_j^s \geq 0, \quad \forall s \in \mathcal{S}, \end{aligned} \quad (2.16a)$$

$$\sum_{j \in \mathcal{J}^s} \lambda_j^s = 1, \quad \forall s \in \mathcal{S}, \quad (2.16b)$$

$$w \in \{0, 1\}^m, \quad (2.16c)$$

$$\lambda_j^s \geq 0, \quad \forall j \in \mathcal{J}^s, s \in \mathcal{S}, \quad (2.16d)$$

and the following proposition, the proof of which is given in Appendix ??:

**Proposition 2.5.1.**  *$(P)$  and  $(\tilde{P})$  are equivalent.*

Now let  $(\tilde{w}, \{\tilde{\lambda}_j^s\}_{j \in \mathcal{J}^s} \text{ for } s \in \mathcal{S})$  be an optimal solution to  $(\tilde{P})$  and note that, by (2.16a), if  $\tilde{\lambda}_j^s > 0$  then  $\hat{w}_j^s$  is dominated by  $\tilde{w}$ . Therefore, we can construct another optimal solution to  $(\tilde{P})$  by choosing a single  $j^*$  for which  $\tilde{\lambda}_{j^*}^s > 0$  for each  $s \in \mathcal{S}$  and setting  $\tilde{\lambda}_{j^*}^s$  to one and the other  $\tilde{\lambda}_j^s$ 's to zero. Define  $\tilde{w}^s = \hat{w}_{j^*}^s$  for  $s \in \mathcal{S}$ , then  $(\tilde{w}, \{\tilde{w}^s\}_{s \in \mathcal{S}})$  is feasible to  $(P)$ .  $\square$

This chapter uses a branch-and-price algorithm to solve  $(\tilde{P})$ . Let  $LP_{\tilde{P}}$  denote the LP relaxation of  $(\tilde{P})$ . Since the feasible region of  $(\tilde{P})$  is the intersection of the convex hulls of each subproblem,  $LP_{\tilde{P}}$  yields a stronger lower bound than the LP relaxation of  $(P)$ .

### 2.5.2.2 The Basic Branch and Price

The BnP algorithm uses a restricted master problem  $(M)$  with a subset of columns of  $(\tilde{P})$  and  $|\mathcal{S}|$  independent subproblems  $(P_s)$  for  $s \in \mathcal{S}$ , instead of handling  $LP_{\tilde{P}}$  globally. The column generation starts with an initial basis that consists of the first-stage variables  $w$ , a column associated with a feasible solution for each subproblem, and some slack variables. Let  $\tilde{\mathcal{J}}^s$  be the corresponding subset of  $\mathcal{J}^s$ . The restricted master problem  $(M)$  is as follows:

$$(M) \quad \min c^T w$$

$$\text{s.t.} \quad w - \sum_{j \in \tilde{\mathcal{J}}^s} \lambda_j^s \hat{w}_j^s \geq 0, \quad \forall s \in \mathcal{S}, \quad (2.17a)$$

$$\sum_{j \in \tilde{\mathcal{J}}^s} \lambda_j^s = 1, \quad \forall s \in \mathcal{S}, \quad (2.17b)$$

$$w \geq 0, \quad (2.17c)$$

$$\lambda_j^s \geq 0, \quad \forall j \in \tilde{\mathcal{J}}^s, \forall s \in \mathcal{S}. \quad (2.17d)$$

and the pricing problem for scenario  $s$  is specified as follows:

$$(P_s) \quad \min \quad -\bar{\sigma}^s + \bar{y}^{sT} w^s$$

$$\text{s.t.} \quad w^s \in \tilde{\mathcal{Q}}(s),$$

$$w^s \in \{0, 1\}^m,$$

where, for scenario  $s$ ,  $\bar{y}^s$  is the dual solution for constraints (2.17a) and  $\bar{\sigma}^s$  is the dual solution of the convexity constraint (2.17b).

### 2.5.2.3 Acceleration Schemes

The performance of column generation deteriorates when the master problem exhibits degeneracy, leading to multiple dual solutions which may significantly influence the quality of columns generated by the pricing problem. The master problem  $(M)$  suffers from degeneracy, especially early in the column-generation process. Initially,  $(M)$  has  $(m + 1)|\mathcal{S}|$  constraints,  $m$  columns corresponding to the first-stage variables  $w$ , and  $|\mathcal{S}|$  columns for the second-stage variables  $\{\lambda^s\}_{s \in \mathcal{S}}$ . Therefore, in early iterations, linear solvers have a natural tendency to select  $m(|\mathcal{S}| - 1)$  columns from the slack variables in Constraints (2.17a). For example, assume that the slack variable is in basis for the constraint involving a non-basic first-stage variable  $w_k$  and a scenario  $s$  in Constraints (2.17a). By complementary slackness, this implies that the dual variable is zero. Consider a vertex  $\hat{w}^s$  whose  $k$ -th entry is non-zero. The value  $\bar{y}_k^s w_k^s$  is zero in the pricing problem. However, for this vertex to enter the basis, it must incur the cost  $c_k$  of  $w_k$ , which is ignored in the pricing subproblem. As a result, subproblem  $(P_s)$  prices many columns too optimistically and generates columns that do not improve the current objective value, resulting in a large number of iterations.

**Pessimistic Reduced Cost.** In order to overcome the poor pricing of columns, this section first proposes a pessimistic pricing scheme that selects more meaningful columns in early iterations. Consider a solution  $w^s$  to the pricing problem. If  $w_k^s = 1$  but the first-stage variable  $w_k$  is not in basis, then by the relevant constraint from (2.17a), the variable  $\lambda_j^s$  corresponding to  $w^s$  can only enter in the basis at 1 if  $w_k$  is also in the basis at 1. As a result, the pessimistic pricing scheme adds the reduced cost  $c_k - \sum_{s \in \mathcal{S}} \bar{y}_k^s$  to the pricing objective, which becomes

$$-\bar{\sigma}^s + (\bar{y}^s)^T w^s + \sum_{k \in \eta} (c_k - \sum_{s \in \mathcal{S}} \bar{y}_k^s) w_k^s$$

where  $\eta$  is the set of indices for non-basic first-stage variables, i.e.,  $\eta = \{k \mid w_k \text{ is non-basic}\}$ . Note that column generation with this pessimistic pricing subproblem is not guaranteed to converge to the optimal linear relaxation. Hence, the implementation switches to the standard pricing problem in later iterations.

**Optimality Cut.** A solution to the master problem ( $M$ ) where the first-stage variables take integer value gives an upper bound to the optimal solution. The BnP algorithm periodically solves the integer version of ( $M$ ) to obtain its objective value  $\bar{v}(M)$ . The constraint

$$c^T w^s \leq \bar{v}(M)$$

can then be added to the pricing subproblem for scenario  $s$  since any solution violating this constraint is necessarily suboptimal. As shown later on, this optimal cut is critical to link the two phases of the column generation, preventing many potential columns to be generated in the second phase.

**A Lexicographic Objective for Pricing Subproblems.** In general, sparse columns are more likely to enter the basis in the master problem ( $M$ ). As a result, the BnP algorithm uses a lexicographic objective in the pricing subproblem. First, it minimizes the (pessimistic or standard) reduced cost. Then it maximizes sparsity by minimizing  $1^T w^s$  subject to the constraint that the reduced cost must be equal to the optimal objective value of the first stage.

#### 2.5.2.4 The Final Branch and Price Implementation

**Column Generation.** The column generation starts with an initial basis built from the optimal solutions of each subproblems under the objective function of  $c^T w^s$ . It then pro-

ceeds with two phases of column generation, first using the pessimistic reduced cost and then switching to the standard one.

The second phase terminates when the optimality gap becomes lower than the predetermined tolerance, e.g., 0.1%. The lower bound is based on Lagrangian relaxation. Given a pair  $\bar{w}$  and  $(\bar{y}, \bar{\sigma})$  of optimal primal and dual solutions for  $(M)$ , the Lagrangian relaxation is given by

$$L(\bar{w}, \bar{y}, \bar{\sigma}) = c^T \bar{w} + \sum_{s \in \mathcal{S}} \mathcal{O}_s(\bar{y}, \bar{\sigma})$$

where  $\mathcal{O}_s(\bar{y}, \bar{\sigma})$  is the optimal solution of the pricing problem for scenario  $s$  under dual variables  $(\bar{y}, \bar{\sigma})$ . The first phase uses the same technique for termination, although the resulting formula is no longer guaranteed to be a lower bound. Once the gap between the upper bound and the “approximate” lower bound is smaller than the tolerance, the column generation process moves to the second phase.

The column generation also avoids generating dominated columns. Assume that  $[w_1^s = 1, w_2^s = 1]$  is a feasible solution of  $(P_s)$  and the corresponding column has been added to the master problem  $(M)$ . Then, there is no need to consider a solution  $[w_1^s = 1, w_2^s = 1, w_3^s = 1]$ . The column generation adds the constraint of  $w_1^s + w_2^s \leq 1$  to  $(P_s)$  when such a dominated solution is produced and does not include it in the master problem.

**The Branch and Bound.** After convergence of the column generation to  $LP_{\bar{P}}$ , the branch and bound algorithm solves the restricted master problem  $(M)$  with the integral condition  $w \in \{0, 1\}^m$  to obtain a strong primal bound. In general, this incumbent solution is of very high quality and the average optimality gap is 0.19%. Therefore, the branch and price algorithm uses a depth-first branch and bound. Moreover, at each branching node, it selects the variable that minimizes the optimality gap.

## 2.6 Performance Analysis of the Branch and Price Algorithm

This section studies the performance of the BnP algorithm. All computations were implemented with the C++/Gurobi 6.5.2 interface and OpenMPI. They use a Haswell architecture compute node configured with 24 cores (two twelve-core 2.5 GHz Intel Xeon E5-2680v3 processors) and 128 GB RAM.

### 2.6.1 Computational Performance

We compare the computational performance of the BnP algorithm with that of the SD and SBD algorithms in this section. In the implementation of the SD algorithm, we do not update the dual vector, i.e.,  $\lambda = 0$  for all iterations, as done in the original paper. For all instances, the SD algorithm exhibits a slow convergence rate and could not solve any of them within the wall time limit of 4 hours. That is because the ORDPDC does not satisfy the condition under which the SD algorithm is guaranteed to perform effectively. Indeed, the probability that a solution to a scenario becomes a global solution is very small since quite different scenarios have the same probability in the ORDPDC. Moreover, since there are many combinations of binary variables with similar objective values in the ORDPDC, cutting off already explored solutions improves the lower bound only by a small amount, which leads to a very slow convergence rate.

Figure 2.11a reports the computation time of the BnP and SBD algorithms for all the instances described in Section 2.4.1, where the reference line (in red) serves to delineate when an algorithm is faster than the other. Their statistics are displayed in Figure 2.11b. In average, the BnP algorithm is faster than the SBD algorithm by a factor of 3.25. These figures also indicate that the SBD algorithm has a high degree of performance variance. This comes from the nature of the scenario set  $\mathcal{S}$ . If  $S$  contains a dominating scenario and the scenario has low index in  $\mathcal{S}$ , then the SBD algorithm solves the problem quickly. Otherwise, the SBD may need a large number of iterations and the MIP model keeps growing in size with each iteration. For 2 out of 1120 instances, the SBD algorithm times out (wallclock time limit of 4 hours). On the other hand, the BnP algorithm is stable across all instances. The BnP algorithm also has the additional benefit that it produces improving feasible solutions continuously. In contrast, the SBD algorithm only produces a feasible solution at optimality. Finally, the BnP algorithm appears more stable numerically than the SBD algorithm. For 5 out of 1120 instances, the BnP algorithm yields a better optimal solution than the SBD algorithm as shown in Table 2.4. Each such solution was validated for feasibility.

### 2.6.2 Solution Quality at the Root Node.

The problem reformulation produces a strong lower bound and the majority of the instances are proven optimal at the root node. Table 2.5 summarizes the average number of branching nodes and the average optimality gap at the root node.

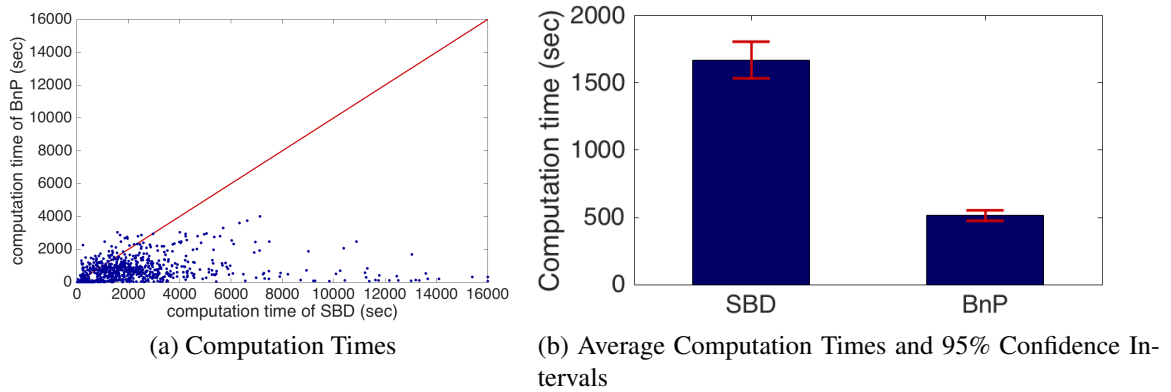


Figure 2.11: Comparison of Computation Times: SBD versus BnP.

Table 2.4: Numerical Stability of the BnP Algorithm.

| Instance   | Opt. obj.val |         | Gap     |
|--|--------------|---------|---------|
|  | SBD          | BnP     |         |
| Rural, 30% damage, $\eta_t = 0.5, \tilde{G}(4)$      | 2458.49      | 2453.79 | -0.19 % |
| Rural, 30% damage, $\eta_t = 0.6, \tilde{G}(4)$      | 2458.49      | 2453.79 | -0.19 % |
| Rural, 30% damage, $\eta_t = 0.7, \tilde{G}(4)$      | 2524.68      | 2519.98 | -0.19 % |
| Rural, 30% damage, $\eta_t = 0.8, \tilde{G}(4)$      | 2572.31      | 2567.60 | -0.19 % |
| Network123, 55% damage, $\eta_t = 0.8, \tilde{G}(8)$ | 232.48       | 227.27  | -2.24 % |

Table 2.5: Branching Tree Statistics.

| Avg. # of branching nodes | Avg. opt. gap at the root node |
|---------------------------|--------------------------------|
| 1.8                       | 0.19 %                         |

### 2.6.3 Benefits of the Accelerating Schemes

To highlight its design choices, the BnP algorithm is compared to a column generation with dual stabilization [46]. In addition, the benefit of each of the accelerating schemes is investigated independently by running the BnP algorithm without the considered extension. We sample 90 instances by setting  $\eta_t = 0.5$  and  $0.8$ , and the damage level to 5%, 30%, 65%, 85%, 100% for the three networks  $\tilde{G}(0)$ ,  $\tilde{G}(1)$ , and  $\tilde{G}(4)$ . Dual stabilization prevents dual variables from fluctuating too much, which is often the case in column generation. It tries to confine dual variables in a box that contains the current best estimate of the optimal dual solution and penalizes solutions that deviate from the box. See, for instance, [46, 5] for details about stabilized column generation. Our implementation updates the box whenever the Lagrangian lower bound is updated.

Table 2.6 summarizes the computational performance of the stabilized column generation in comparison with the BnP algorithm.  $\text{BnP}_B$  denotes the branch-and-price algorithm

Table 2.6: Comparison to a Column Generation with Dual Stabilization.

|                  | Avg. computation time (sec) | Avg. number of iterations |
|------------------|-----------------------------|---------------------------|
| BnP <sub>B</sub> | 12857.97 <sup>†</sup>       | 3122.57 <sup>†</sup>      |
| BnP <sub>S</sub> | 11563.44 <sup>†</sup>       | 1514.58 <sup>†</sup>      |
| BnP              | 488.03                      | 96.12                     |

Table 2.7: Benefits of the Accelerating Schemes.

|                   | Avg. computation time (sec) | Avg. number of iterations |
|-------------------|-----------------------------|---------------------------|
| BnP               | 488.03                      | 96.12                     |
| BnP <sub>\R</sub> | 844.24                      | 96.39                     |
| BnP <sub>\C</sub> | 2589.55 <sup>†</sup>        | 215.94 <sup>†</sup>       |
| BnP <sub>\O</sub> | 2979.84 <sup>†</sup>        | 544.65 <sup>†</sup>       |

with the basic scheme only (Section 2.5.2.2) and BnP<sub>S</sub> stands for the branch and price algorithm with dual stabilization. The symbol <sup>†</sup> is used to denote that the algorithm reaches the wallclock time limit for some instances. For more than one third of the sampled instances, BnP<sub>B</sub> and BnP<sub>S</sub> exceed the wallclock time limit. For instances where both algorithms terminate within the time limit, BnP<sub>S</sub> is faster than BnP<sub>B</sub> by a factor of around 4. Although the dual stabilization does improve the computation time of the basic algorithm, it is still not adequate to solve the ORDPDC practically. The BnP algorithm, on the other hand, shortens computation times by a factor of 26.35.

The next results investigate the performance gain of each accelerating scheme by removing them one at a time from the BnP algorithm. Table 2.7 describes the computational performance and Figure 2.12 illustrates the impact of each accelerating schemes on the convergence rate of the rural network under 6% damage level. In the table and figure, *R* denotes the revised reduced cost, *C* the optimality cut, *O* the lexicographic objective pricing problem, BnP<sub>\k</sub> the BnP algorithm without scheme *k*, with  $k \in \{R, C, O\}$ , and CG<sub>\k</sub> the column generation of BnP without scheme *k*.

The results in Table 2.7 indicate that all the accelerating schemes contribute to the computational performance of the BnP algorithm. Figure 2.12a illustrates the key role of the optimality cut. Without this cut, the second stage of the column generation which uses the traditional pricing objective does not take advantage of the columns generated in the first stage and its lower bound drastically drops. Figure 2.12b compares the convergence behavior of CG and CG<sub>\R</sub>, showing that CG reaches the optimal objective value faster than CG<sub>\R</sub>. Figure 2.12c highlights the impact of the lexicographic objective function and shows that it significantly contributes to the fast convergence of the algorithm.

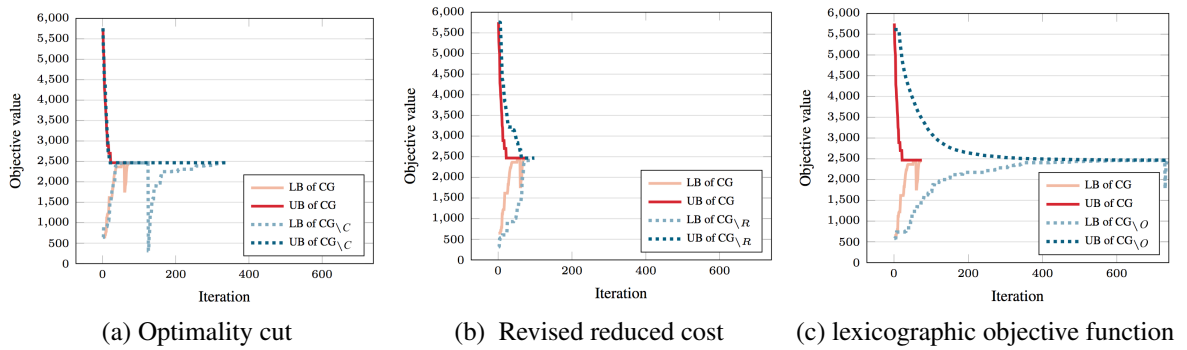


Figure 2.12: Comparison of Convergence Rates (rural network, 6% level of damage).

## 2.7 Concluding Remarks

This chapter proposed an expansion planning model to improve the resiliency of distribution systems facing natural disasters. The planning model considers the hardening of existing lines and the addition of new lines, switches, and distributed generators that would allow a subpart of the system to operate as a microgrid. The expansion model uses a 3-phase model of the distribution system. In addition, it also considers damages to the communication system which may prevent generators and switches to be controlled remotely. The input of the expansion model contains a set of damage scenarios, each of which specifying how the disaster affects the distribution system.

The chapter proposed a branch and price algorithm for this model where the pricing subproblem generates new expansions for each damage scenario. The branch and price uses a number of acceleration schemes to address significant degeneracy in the model. They include a new pricing objective, an optimality cut, and a multi-objective function to encourage sparsity in the generated expansions. The resulting branch and price algorithm significantly improves the performance of scenario-based and scenario decomposition algorithms and a branch and price with a stabilized column generation. The case studies show that optimal solutions strongly depend on the grid topology and the sophistication of the communication network. In particular, the results highlight the importance of distributed generation for rural networks, which necessitates a resilient communication system.

The acceleration techniques presented in this chapter are not limited to the electricity distribution grid planning problem; They can be used on problems with similar structure, i.e, two-stage stochastic problems with feasibility recourse.

Future work will be devoted to applying and scaling these techniques to instances with thousands of components.

## CHAPTER 3

# Unit Commitment with Gas Awareness

### 3.1 Introductory Remarks

Gas-Fueled Power Plants (GFPPs) have become a significant part of the energy mix in the last decades, primarily because of their operational flexibility and lower environmental impacts. Although GFPPs have introduced interdependencies between the natural gas and electrical power systems, these networks are still operated independently, with asynchronous market mechanisms. In particular, the unit commitment decisions in the electrical power system take place before the realization of natural gas spot prices, introducing reliability risks and economic inefficiencies in congested environments. Indeed, the GFPPs may not be able to secure gas at reasonable prices, introducing either reliability issues or electricity price spikes.

This undesirable outcome occurred in the Northeastern United States during the early winter of 2014. Extremely low temperatures induced an unusual coincident peak in electricity and natural gas demand. On the one hand, it produced record-high natural gas spot prices due to congestion. On the other hand, high electricity loads led the electrical power system operator to call for some emergency actions, which resulted in higher electricity prices [83]. Moreover, the power system operator, valuing reliability the most, encouraged committed GFPPs to buy natural gas at all costs without assurance of cost recovery, further aggravating the economic cost [84]. It is important to mention that the critical issue in this case was not the gas supply, but rather congestion in the gas transmission network. Moreover, a recent study [47] has shown that the cost of expanding the gas and electricity network infrastructures to avoid such events would be prohibitive.

To address these interdependencies, a number of researchers have studied how to incorporate the natural gas transmission capabilities into the operational decisions of electrical power systems. See, for instance, [85, 86, 87, 88, 89, 90, 91, 92, 93, 94]. Other researchers have also studied how to incorporate the economic coupling between these two infrastruc-

tures using new market mechanisms. A new market framework with a joint ISO, using price- or volume-based approaches, was investigated in [95, 96]. Instead of introducing one joint ISO, other researchers have proposed a new market framework that assumes centralized independent gas markets, synchronizes the electricity and gas market days, and allows some information exchange between some parties in the electricity and gas markets (e.g., market operators or GFPPs) [97, 98, 99, 100, 101, 102].

This chapter takes a different approach that stays within the current operating practices and does not introduce a new market mechanism. Instead, the approach generalizes the unit commitment model to capture the physical and economic couplings and strive to ensure both physical feasibility and economic viability. More precisely, the chapter introduces the Unit Commitment problem with Gas Network Awareness (UCGNA) to schedule a set of generating units for the next day while taking account the fuel delivery and the natural gas prices that are propagated back by the natural gas system. The UCGNA imposes bid-validity constraints on the GFPPs to ensure their profitability and estimates the natural gas prices for these constraints with the dual solutions associated with the flux conservation constraints of the gas market.

The UCGNA is formulated as a tri-level mathematical program and assumes that the power system operator has partial (or full) knowledge on gas demand forecast and gas network. When the power system is modeled with its DC approximation and the gas network with the second-order cone program from [103] to model its steady-state physics, the tri-level mathematical program can be reformulated as a single-level Mixed-Integer Second-Order Cone Program (MISOCP) through strong duality of the innermost problem. The resulting MISOCP can then be solved using a dedicated Benders decomposition recently proposed in [54].

The key contributions of this chapter are threefold. First, it proposes the first unit commitment model that incorporates both the physical and economic couplings of electrical power and natural gas transmission systems and can be used within current operating practices. Second, it proposes a MISOCP that captures the UCGNA and can be solved through Benders decomposition. Finally, it demonstrates the potential and practicality of the approach on a detailed case study that replicates the behavior of the 2014 polar vortex event on the Northeastern United States. In particular, the chapter shows that, on the case study, the UCGNA obtains a functional unit commitment decision, which avoids the electricity price peaks and keeps the total gas costs reasonable, contrary to current practice, even for highly congested electrical and gas networks.

The rest of this chapter is organized as follows. Section 3.2 formalizes the UCGNA and Section 3.3 briefly reviews the solution methods for solving the UCGNA. Section 3.4 ana-

lyzes the behavior of the model on a case study. Lastly, Section 3.5 discusses applicability and implications of the UCGNA and Section 3.6 concludes the chapter.

## 3.2 Mathematical Modeling: the UCGNA

This section specifies the UCGNA, including its electricity system, its natural gas network, and their physical and economic couplings. The electricity transmission grid is represented by an undirected graph  $\mathcal{G}^e = (\mathcal{N}, \mathcal{E})$  and the natural gas transmission system by a directed graph  $\mathcal{G}^g = (\mathcal{V}, \mathcal{A})^1$ . Boldface letters represent vectors of variables,  $[a, b]_{\mathbb{Z}}$  denotes the set of integers in interval  $[a, b]$ , and  $[n]$  denotes the set  $\{1, \dots, n\}$  for some integer  $n \geq 1$ . The letter  $\mathcal{T}$  denotes the set of time periods  $\{0, 1, \dots, T\}$ .

### 3.2.1 The Electricity Transmission System

In the United States, UC and ED problems are solved daily to determine the hourly operating schedule of generating units for the next day from bids submitted by market participants. Tables 3.1 and 3.2 summarize the parameters and variables of the UC/ED problems. With these notations, the UC model is specified in Problem (3.1).

$$\min \sum_{t \in [T]} \sum_{u \in \mathcal{U}} (c_u o_{u,t} + r_{u,t} + \sum_{b \in \mathcal{B}_u} \beta_b s_{b,t}^e) \quad (3.1a)$$

$$\begin{aligned} \text{s.t. } r_{u,t} &\geq C_{u,h} (o_{u,t} - \sum_{n \in [h]} o_{u,t-n}), \\ &\forall h \in \Psi_s, u \in \mathcal{U}, t \in [T], \end{aligned} \quad (3.1b)$$

$$r_{u,t} \geq 0, \forall u \in \mathcal{U}, t \in [T], \quad (3.1c)$$

$$o_{u,t} = \bar{o}_{u,0}, \forall u \in \mathcal{U}, t \in [0, \bar{\tau}_{u,0} + \underline{\tau}_{u,0}]_{\mathbb{Z}}, \quad (3.1d)$$

$$\begin{aligned} \sum_{t' \in [t - \bar{\tau}_u + 1, t]_{\mathbb{Z}}} v_{u,t'}^+ &\leq o_{u,t}, \\ &\forall u \in \mathcal{U}, t \in [\max\{\bar{\tau}_u, \bar{\tau}_{u,0} + 1\}, T]_{\mathbb{Z}}, \end{aligned} \quad (3.1e)$$

$$\sum_{t' \in [t - \underline{\tau}_u + 1, t]_{\mathbb{Z}}} v_{u,t'}^+ \leq 1 - o_{u,t - \underline{\tau}_u},$$

<sup>1</sup> In this chapter, the gas flux direction is assumed to be fixed, since many modern gas networks are not as loopy as the power transmission systems, and they are nearly tree like [104]. Therefore, for most of the pipelines, the flow directions remain unchanged. In addition, since the changes in natural gas flux are in a much slower pace, the directions do not vary too much from day to another. For a non-tree like network, we can generalize the model by including binary variables that represent the flux direction [103]

Table 3.1: Parameters of the Electricity System.

|  |  |
|--|--|
| $G^e = (\mathcal{N}, \mathcal{E})$         | Undirected graph where $\mathcal{N}$ is a set of buses indexed by $i = 1, \dots, N$ and $\mathcal{E}$ is a set of lines indexed with $l = 1, \dots, E$ |
| $\mathcal{U}$                              | Set of generators, indexed by $u = 1, \dots, U$  |
| $\mathcal{U}^g \subseteq \mathcal{U}$      | Set of GFPPs   |
| $\mathcal{U}(i) \subseteq \mathcal{U}$     | Set of generators located at $i \in \mathcal{N}$   |
| $\mathcal{B}_u$                            | Set of supply bids submitted by $u \in \mathcal{U}$ , indexed by $b = 1, \dots, B_u$   |
| $\beta_b$                                  | Bid price of $b \in \mathcal{B}_u$   |
| $\bar{s}_b$                                | Amount of real power generation of $b \in \mathcal{B}_u$   |
| $\underline{p}_u, \bar{p}_u$               | Minimum/maximum real power generation of $u \in \mathcal{U}$   |
| $\underline{R}_u, \bar{R}_u$               | Ramp-down/up rate of $u \in \mathcal{U}$   |
| $c_u$                                      | No-load cost of $u \in \mathcal{U}$  |
| $\Psi_u$                                   | Set of counts of time periods with distinct start-up costs of $u$ indexed by $h$   |
| $C_{u,h}$                                  | Start-up cost of $u \in \mathcal{U}$ when $u$ is turned on after it has been offline for some time $\in [\Psi_{u,h}, \Psi_{u,h+1}]$                    |
| $\bar{o}_{u,0}, \bar{p}_{u,0}$             | Initial on-off status/real power generation of $u \in \mathcal{U}$   |
| $\underline{\tau}_u, \bar{\tau}_u$         | Minimum-down/up time of $u \in \mathcal{U}$  |
| $\underline{\tau}_{u,0}, \bar{\tau}_{u,0}$ | The time that generator $u \in \mathcal{U}$ has to be inactive/active from $t = 0$   |
| $b_l$                                      | Line susceptance of $l \in \mathcal{E}$  |
| $\bar{f}_l$                                | Real power limit of $l \in \mathcal{E}$  |
| $(d_{i,t}^e)_{i \in \mathcal{N}}$          | Electricity load profile during $t \in \mathcal{T}$  |
| $\Delta_l$                                 | Maximum voltage angle difference between two end-points of $l \in \mathcal{E}$   |
| $\underline{\theta}_i, \bar{\theta}_i$     | Minimum/maximum voltage angle at $i \in \mathcal{N}$   |

Table 3.2: Variables of the Electricity System.

|                             |  |
|-----------------------------|--|
| <b>Binary variables</b>     |  |
| $o_{u,t}$                   | 1 if $u \in \mathcal{U}$ is on during $t \in \mathcal{T}$ , 0 otherwise                            |
| $v_{u,t}^+$                 | 1 if $u \in \mathcal{U}$ becomes online during $t \in \mathcal{T}$ , 0 otherwise                   |
| $v_{u,t}^-$                 | 1 if $u \in \mathcal{U}$ becomes offline during $t \in \mathcal{T}$ , 0 otherwise                  |
| <b>Continuous variables</b> |  |
| $s_{b,t}^e$                 | Real power generation from $b \in \mathcal{B}_u$ of $u \in \mathcal{U}$ during $t \in \mathcal{T}$ |
| $p_{u,t}$                   | Real power generation of $u \in \mathcal{U}$ during $t \in \mathcal{T}$                            |
| $f_{l,t}$                   | Real power flow on $l \in \mathcal{E}$ during $t \in \mathcal{T}$                                  |
| $r_{u,t}$                   | Start-up cost of $u \in \mathcal{U}$ during $t \in \mathcal{T}$                                    |
| $\theta_{i,t}$              | Voltage angle on $i \in \mathcal{N}$ during $t \in \mathcal{T}$                                    |

$$\forall u \in \mathcal{U}, t \in [\max\{\underline{\tau}_u, \underline{\tau}_{u,0} + 1\}, T]_{\mathbb{Z}}, \quad (3.1f)$$

$$v_{u,t}^+ - v_{u,t}^- = o_{u,t} - o_{u,t-1}, \forall u \in \mathcal{U}, t \in [T], \quad (3.1g)$$

$$v_{u,t}^+, v_{u,t}^-, o_{u,t} \in \{0, 1\}, \forall u \in \mathcal{U}, t \in [T], \quad (3.1h)$$

$$\mathbf{s}^e = \operatorname{argmin} \mathcal{Q}(\mathbf{o}, \mathbf{v}^+, \mathbf{v}^-), \quad (3.1i)$$

where  $\mathcal{Q}(\mathbf{u}, \mathbf{v}^+, \mathbf{v}^-)$  denotes the ED problem specified as follows:

$$\min \sum_{t \in [T]} \sum_{u \in \mathcal{U}} \left( \sum_{b \in \mathcal{B}_u} \beta_b s_{b,t}^e \right) \quad (3.1j)$$

$$\text{s.t.} \quad \sum_{u \in \mathcal{U}(i)} p_{u,t} - d_{i,t}^e = \sum_{l \in \mathcal{E}: l_t = i} f_{l,t} - \sum_{l \in \mathcal{E}: l_h = i} f_{l,t}, \quad \forall i \in \mathcal{N}, t \in [T], \quad (3.1k)$$

$$p_{u,t} = \sum_{b \in \mathcal{B}_u} s_{b,t}^e \quad \forall u \in \mathcal{U}, t \in [T], \quad (3.1l)$$

$$0 \leq s_{b,t}^e \leq \bar{s}_b, \quad \forall b \in \mathcal{B}_u, u \in \mathcal{U}, t \in [T], \quad (3.1m)$$

$$\underline{p}_u o_{u,t} \leq p_{u,t} \leq \bar{p}_u o_{u,t}, \quad \forall u \in \mathcal{U}, t \in [T], \quad (3.1n)$$

$$p_{u,0} = \bar{p}_{u,0}, \quad \forall u \in \mathcal{U}, \quad (3.1o)$$

$$p_{u,t} - p_{u,t-1} \leq \bar{R}_u o_{u,t-1} + \bar{p}_u v_{u,t}^+, \quad \forall u \in \mathcal{U}, t \in [T], \quad (3.1p)$$

$$p_{u,t-1} - p_{u,t} \leq \underline{R}_u o_{u,t-1} + \underline{p}_u v_{u,t}^-, \quad \forall u \in \mathcal{U}, t \in [T], \quad (3.1q)$$

$$f_{l,t} = -b_l (\theta_{l_h,t} - \theta_{l_t,t}), \quad \forall l \in \mathcal{E}, t \in [T], \quad (3.1r)$$

$$-\bar{f}_l \leq f_{l,t} \leq \bar{f}_l, \quad \forall l \in \mathcal{E}, t \in [T], \quad (3.1s)$$

$$\underline{\theta}_i \leq \theta_{i,t} \leq \bar{\theta}_i, \quad \forall i \in \mathcal{N}, t \in [T], \quad (3.1t)$$

$$-\Delta_l \leq \theta_{l_h,t} - \theta_{l_t,t} \leq \Delta_l \quad \forall l \in \mathcal{E}, t \in [T]. \quad (3.1u)$$

The objective function of the upper level problem (Equations (3.1a) - (3.1h)) includes the no-load costs, the start-up costs, and the costs of the selected supply bids of each electrical power generating units. Equation (3.1b) computes the start-up cost  $r_{u,t}$  of a generator  $u$  for time period  $t$  based on how long  $u$  has been offline [105]. The expression  $o_{u,t} - \sum_{n=1}^h o_{u,t-n}$  is one when generator  $u$  becomes online after it has been turned off for  $h$  time periods. Equation (3.1c) states the nonnegativity requirement on  $r_{u,t}$ . Equation (3.1d) specifies the initial on-off status of each generator. The minimum-up and -down constraints are specified in Equations (3.1e) and (3.1f) respectively. The relationship between the variables for the on-off, start-up, and shut-down statuses of each generator is stated in Equation (3.1g). The binary requirements for logical variables  $v_{u,t}^+, v_{u,t}^-, o_{u,t}$  are specified in Equation (3.1h).

Based on the commitment decisions, the lower-level problem (i.e., Equations (3.1j) - (3.1u)) decides the hourly operating schedule of each committed generators in order to minimize the system production costs. Equation (3.1k) states the flow conservation constraints for real power at each bus, using  $l_h$  and  $l_t$  to represent the head and tail of  $l \in \mathcal{E}$ . Equation (3.1l) states that the total real power generation of a generator  $u$  is equal to the

Table 3.3: Parameters of the gas system

|  |  |
|--|--|
| $\mathcal{G}^g = (\mathcal{V}, \mathcal{A})$ | Directed graph representing a natural gas transmission network, where $\mathcal{V}$ is a set of junctions, indexed with $j = 1, \dots, V$ , and $\mathcal{A} \subseteq \mathcal{V} \times \mathcal{V}$ is a set of connections, indexed with $a = 1, \dots, A$ |
| $\mathcal{A}_c \subseteq \mathcal{A}$        | Set of compressors   |
| $\mathcal{A}_v \subseteq \mathcal{A}$        | Set of control valves  |
| $\kappa_j$                                   | Cost of demand shedding at $j \in \mathcal{V}$   |
| $(d_{j,t}^g)_{j \in \mathcal{V}}$            | Gas demand profile during $t \in \mathcal{T}$  |
| $\underline{s}_j^g, \bar{s}_j^g$             | Lower/Upper limit on natural gas supply at $j \in \mathcal{V}$   |
| $c_j(\cdot)$                                 | Cost function for gas supply at $j \in \mathcal{V}$  |
| $W_a$  | Pipeline resistance (Weymouth) factor of $a \in \mathcal{A}$   |
| $\underline{\pi}_j, \bar{\pi}_j$             | Minimum/maximum squared pressure at $j \in \mathcal{V}$  |
| $\underline{\alpha}_a^c, \bar{\alpha}_a^c$   | Lower/upper compression ratio of $a \in \mathcal{A}_c$   |
| $\underline{\alpha}_a^v, \bar{\alpha}_a^v$   | Lower/upper control ratio of $a \in \mathcal{A}_v$   |

Table 3.4: Variables of the gas system

|                |   |
|----------------|---|
| $s_{k,t}^g$    | Amount of gas supplied by $k \in \mathcal{K}$ during $t \in \mathcal{T}$  |
| $\pi_{j,t}$    | Pressure squared at $j \in \mathcal{V}$ during $t \in \mathcal{T}$  |
| $\phi_{a,t}$   | Gas flow on $a \in \mathcal{A}$ during $t \in \mathcal{T}$  |
| $l_{j,t}$      | Satisfied gas demand at $j \in \mathcal{V}$ during $t \in \mathcal{T}$  |
| $q_{j,t}$      | Shedded gas demand at $j \in \mathcal{V}$ during $t \in \mathcal{T}$  |
| $\gamma_{j,t}$ | Total amount of gas consumed by the GFPP located at $j \in \mathcal{N} \cap \mathcal{V}$ during $t \in \mathcal{T}$ |

production of its selected bids. Equation (3.1m) constrains the power generation  $s_{b,t}^e$  from bid  $b \in \mathcal{B}_u$  to be no more than the submitted amount  $\bar{s}_b$ . Equation (3.1n) enforces the bound on the real power generation of each generator. Equation (3.1o) specifies the initial generation amount of each generator, and Equations (3.1p) and (3.1q) state the ramp-up and -down constraints of each generator. Equation (3.1r) captures the DC approximation of the power flow equations and Equation (3.1s) specifies the thermal limit on each line. Equations (3.1t) and (3.1u) state the voltage angle bounds on each bus and the bounds on the angle difference of two adjacent buses respectively.

### 3.2.2 The Natural Gas Transmission System

$$\min \sum_{t \in [T]} \sum_{j \in \mathcal{V}} \left( \sum_{s \in \mathcal{S}_j} c_{j,s} s_{s,t}^g + \kappa_j q_{j,t} \right) \quad (3.2a)$$

$$\text{s.t. } s_{j,t}^g - l_{j,t} - \gamma_{j,t} = \sum_{a \in \mathcal{A}: a_t=j} \phi_{a,t} - \sum_{a \in \mathcal{A}: a_h=j} \phi_{a,t},$$

$$\forall j \in \mathcal{V}, t \in [T], \quad (3.2b)$$

$$l_{j,t} = d_{j,t}^g - q_{j,t}, \forall j \in \mathcal{V}, t \in [T], \quad (3.2c)$$

$$0 \leq q_{j,t} \leq d_{j,t}^g, \forall j \in \mathcal{V}, t \in [T], \quad (3.2d)$$

$$\phi_{a,t} \geq 0, \forall a \in \mathcal{A}, t \in [T], \quad (3.2e)$$

$$\underline{s}_j^g \leq s_{j,t}^g \leq \bar{s}_j^g, \forall j \in \mathcal{V}, t \in [T], \quad (3.2f)$$

$$\underline{\alpha}_a^c \pi_{a_h,t} \leq \pi_{a_t,t} \leq \bar{\alpha}_a^c \pi_{a_h,t}, \forall a \in \mathcal{A}_c, t \in [T], \quad (3.2g)$$

$$\underline{\alpha}_a^v \pi_{a_h,t} \leq \pi_{a_t,t} \leq \bar{\alpha}_a^v \pi_{a_h,t}, \forall a \in \mathcal{A}_v, t \in [T], \quad (3.2h)$$

$$\pi_{a_h,t} - \pi_{a_t,t} = W_a \phi_{a,t}^2, \forall a \in \mathcal{A} \setminus (\mathcal{A}_v \cup \mathcal{A}_c), t \in [T], \quad (3.2i)$$

$$\underline{\pi}_j \leq \pi_{j,t} \leq \bar{\pi}_j, \forall j \in \mathcal{V}, t \in [T] \quad (3.2j)$$

$$s_{j,t}^g = \sum_{s \in \mathcal{S}_j} s_{s,t}^g \quad (3.2k)$$

Tables 3.3 and 3.4 specify the parameters and variables of the steady-state natural gas model, which is given in Problem (3.2). The modeling is similar to those in [47, 103, 35] and uses the Weymouth equation to capture the relationship between pressures and flux. The flux conservation constraint is given in Equation (3.2b), where  $a_h$  and  $a_t$  represent the head and tail of  $a \in \mathcal{A}$ . Equation (3.2c) determines the demand served at each junction: It captures the amount of gas load shedding which must be nonnegative and cannot exceed the demand at the corresponding junction (Equation (3.2d)). The model assumes that gas flow directions are predetermined and Equation (3.2e) enforces the sign of gas flow variables, i.e., it constrains  $\phi_{a,t}$  to be nonnegative. Equation (3.2f) specifies the upper and lower limits of natural gas supplies. The change in pressure through compressors and control valves are formulated in Equations (3.2g) and (3.2h) and the model use a single compressor machine approximation as in prior work. The steady-state physics of gas flows is formulated with the Weymouth equation in Equation (3.2i). Equation (3.2j) states the bounds on nodal pressures. Equation (3.2i) can be convexified using the second-order cone relaxation from [35]:  $\pi_{a_h,t} - \pi_{a_t,t} \geq W_a \phi_{a,t}^2$ . This relaxation is very tight [35].

When the gas system is not congested, the price of natural gas is relatively stable. However, during congestion and when some loads are being shedded, natural gas prices increase sharply. The cost of gas in the objective function captures this behavior: For a junction  $j$ , it is specified with an almost-linear piecewise linear function for production and a high penalty cost  $\kappa_j$  for gas shedding. To be specific, let  $\mathcal{S}_j$  be a set of non-overlapping intervals covering  $[0, \bar{s}_j^g]$ , each with a distinct slope  $c_{j,s}$  satisfying  $c_{j,s} \leq c_{j,s+1}$  for all consecutive intervals  $s, s+1 \in \mathcal{S}_j$ . Define an auxiliary nonnegative variable  $s_{s,t}^g$  that represents the amount of gas supply from  $s \in \mathcal{S}_j$  at time  $t$ . The objective function is then stated as Equation (3.2a). The model also includes constraint (3.2k) to link the gas variable at junction  $j$  with the auxiliary variables.

Table 3.5: Parameters for the Electricity and Gas Coupling.

|                         |  |
|-------------------------|--|
| $\{H_{u,i}\}_{i=0,1,2}$ | Coefficients of the heat rate curve of $u \in \mathcal{U}^g$   |
| $\alpha_u$              | Maximum allowable percentage of the expense on natural gas over its marginal bid price for $u \in \mathcal{U}^g$ |
| $\mathcal{K}$           | Set of pricing zones, indexed with $k = 1, \dots, K$   |
| $\mathcal{V}(k)$        | Set of junctions that belong to $k \in \mathcal{K}$  |

Table 3.6: Variables for the Electricity and Gas Coupling.

|              |  |
|--------------|--|
| $w_{b,t}$    | 1 if $b \in \mathcal{B}_u$ of $u \in \mathcal{U}$ is selected during $t \in \mathcal{T}$ , 0 otherwise |
| $\rho_{u,t}$ | Price of marginally selected bid of $u \in \mathcal{U}^g$ during $t \in \mathcal{T}$                   |
| $\psi_{k,t}$ | Zonal price of natural gas in $k \in \mathcal{K}$ during $t \in \mathcal{T}$                           |

### 3.2.3 Physical and Economic Couplings

GFPPs are the physical and economic interface between the electrical power and gas networks. This section first describes the resulting coupling constraints before describing how the natural gas zonal prices are computed. Tables 3.5 and 3.6 describe the parameters for the coupling.

The physical couplings between  $\mathcal{G}^e$  and  $\mathcal{G}^g$  can be formulated as follows ( $t \in [T], j \in \mathcal{N} \cap \mathcal{V}$ ):

$$\gamma_{j,t} = \sum_{u \in \mathcal{U}(j) \cap \mathcal{U}^g} H_{u,2} p_{u,t}^2 + H_{u,1} p_{u,t} + H_{u,0}. \quad (3.3)$$

The real power generation  $\mathbf{p}$  of a GFPP induces a demand  $\gamma$  in the natural gas system. Equation (3.3) specifies the relationship between the real power generation of a GFPP and the amount of natural gas needed for the generation. In the equation, this relationship is approximated by a quadratic heat-rate curve, whose coefficients are given as  $H_u$ . The equation can be convexified like the Weymouth equation.

Since the level of power generation of the GFPPs determines the load in the gas system, the physical coupling also affects the natural gas prices. The price formation of natural gas, in turn, governs the profitability of GFPPs, which submit bids before the realization of gas prices. To capture these economic realities, the model introduces binary variables of the form  $w_{b,t} \in \{0, 1\}$  for each bid  $b$  of a GFPP to Problem (3.1): Variable  $w_{b,t}$  indicates whether bid  $b$  is selected during time period  $t$ . Equation (3.1m) is then replaced by the following constraints (for all  $t \in [T]$ ):

$$\rho_{u,t} = \sum_{b \in [B_u - 1]} \beta_b (w_{b,t} - w_{b+1,t}) + \beta_{B_u} w_{B_u,t}, \forall u \in \mathcal{U}^g, \quad (3.4a)$$

$$0 \leq s_{b,t}^e \leq \bar{s}_b, \forall b \in \mathcal{B}_u, u \in \mathcal{U} \setminus \mathcal{U}^g, \quad (3.4b)$$

$$0 \leq s_{b,t}^e \leq \bar{s}_b w_{b,t}, \forall b \in \mathcal{B}_u, u \in \mathcal{U}^g, \quad (3.4c)$$

$$w_{b,t} \leq o_{u,t}, \forall b \in \mathcal{B}_u, u \in \mathcal{U}^g, \quad (3.4d)$$

$$\bar{s}_b w_{b+1,t} \leq s_{b,t}, \forall b \in [1, B_u - 1]_{\mathbb{Z}}, u \in \mathcal{U}^g. \quad (3.4e)$$

Equations (3.4b) and (3.4c) are bound constraints for the bids submitted by the non-GFPPs and GFPPs respectively. Equation (3.4c) ensures that the indicator variable  $w_{b,t}$  is one whenever bid  $b$  is used for time period  $t$  (i.e.,  $s_{b,t}^e > 0$ ). Equation (3.4d) states that the bid of a generator can be selected only when it is committed and Equation (3.4e) ensures that the  $(b+1)^{\text{th}}$  bid is selected only if the bid  $b$  is fully used. Accordingly, Equation (3.4a) states that  $\rho_{u,t}$  is the maximum/marginal bid price of GFPP  $u \in \mathcal{U}^g$  among its currently selected bids.

The economic coupling between the electricity and gas networks is enforced by *bid-Validity constraints* that ensure that the marginal costs of producing electricity by GFPPs are lower than their marginal bid prices. Although the natural gas system is operated in a decentralized manner, the zonal price of natural gas  $\psi$  can be modeled as a function  $g$  of the market supply and demand, i.e., as a function of the binary and continuous variables of Problems (3.1) and (3.2), which are denoted by  $\mathbf{z}$  and  $\mathbf{x}$ . Under this assumption, the bid validity constraints can be expressed as follows (for all  $t \in [T]$ ):

$$\psi = g(\mathbf{z}, \mathbf{x}), \quad (3.5a)$$

$$\begin{aligned} \alpha_u \rho_{u,t} &\geq [2p_{u,t} H_{u,2} + H_{u,1}] \psi_{k,t} o_{u,t}, \\ &\forall k \in \mathcal{K}, i \in \mathcal{V}(k), u \in \mathcal{U}(i) \cap \mathcal{U}^g, \end{aligned} \quad (3.5b)$$

where

$$2p_{u,t} H_{u,2} + H_{u,1}$$

is the derivative of the heat rate curve (i.e., Equation (3.3)) that represents the amount of natural gas needed for generating one additional unit of real power by GFPP  $u$ . The nonlinear term in the right-hand side of Equation (3.5b) is linearized by employing an exact McCormick relaxation. Accordingly, when a GFPP  $u$  is online, the right-hand side of Equation (3.5b) represents the realized natural gas price for generating one additional unit of real power by the GFPP  $u$ , hence Equation (3.5b) captures the fact that, when the realized natural gas price for generating one additional unit of real power by GFPP  $u$  is greater than its marginal bid price  $\rho_{u,t}$ , GFPP  $u$  is not profitable. This situation arises

because GFPP  $u$  submits its bids before the realization of  $\psi$ . The bid validity constraint is expressed in Equation (3.5b) and ensures that only profitable GFPPs are committed. Note that, as discussed at length subsequently,  $\alpha_u$  is best viewed as a part of the bid for GFPP  $u$  that reflects its risk aversion level; The larger  $\alpha_u$  is (possibly greater than 100%), the less likely GFPP  $u$  is of being de-committed due to the bid validity constraint and the larger the risk  $u$  is willing to take in terms of natural gas prices. The bid validity constraints use the realized zonal gas prices from Equation (3.5a) and the maximum natural gas price (e.g., \$200 per mmBtu) multiplied by  $[2\bar{p}_u H_{u,2} + H_{u,1}]$  as the upper bound of the continuous term in its right-hand side for the McCormick relaxation.

It remains to specify how to compute the zonal gas prices, i.e., the function  $g$  in Equation (3.5a). The UCGNA assumes that the nodal natural gas price at each junction  $j$  is given by the marginal cost of supplying natural gas at  $j$ . This marginal cost is the dual solution associated with the corresponding flux conservation constraint in Problem (3.2). The zonal natural gas prices  $\psi$  are then computed by averaging the nodal natural gas prices of a subset of junctions in the zone. Therefore, the zonal natural gas price  $\psi$  are given by linear functions of the dual solution to Problem (3.2).

Note that, by construction, the natural gas zonal prices  $\psi$  under normal operating conditions are given by the almost linear part of objective (3.2a). However, when the gas network is congested and load needs to be shed, the zonal prices increase sharply due to the high penalty cost  $\kappa_j$ . As a result, the resulting model closely captures the behavior of the market during the 2014 polar vortex. Note also that the model does not shed the demand of the GFPPs. The model assumes that GFPPs buy natural gas at any cost to meet its commitment obligation. Once again, this captures the 2014 Polar Vortex situation where GFPPs were encouraged to buy the natural gas from the spot market at any cost for the sake of the power system reliability [84].

### 3.2.4 Bilevel Formulation

This section shows how the UCGNA can be expressed as a bilevel program. Let variable subscripts  $e$  and  $g$  respectively denote the electricity and the gas systems. Let  $z_e$  and  $x_e$  respectively denote the vector of binary and continuous variables of the power system (i.e., Problem (3.1)) and let  $x_g$  be the vector of continuous variables of the gas system (i.e.,

Problem (3.2)). The UCGNA can be stated as a trilevel program<sup>2</sup>:

$$\min_{\substack{\mathbf{x}_e \geq 0, \mathbf{y}_g \\ \mathbf{z}_e \in \{0,1\}^m}} c_e^T \mathbf{x}_e + h^T \mathbf{z}_e \quad (3.6a)$$

$$\text{s.t. } \mathbf{z}_e \in \mathcal{Z}, \quad (3.6b)$$

$$(\mathbf{x}_e, \mathbf{y}_g) = \underset{\mathbf{x}_e \geq 0, \mathbf{y}_g}{\operatorname{argmin}} c_e^T \mathbf{x}_e \quad (3.6c)$$

$$\text{s.t. } A\mathbf{x}_e + B\mathbf{z}_e \geq b, \quad (3.6d)$$

$$\mathbf{y}_g \in \text{Dual sol. of (3.7)}, \quad (3.6e)$$

$$E\mathbf{y}_g + M\mathbf{z}_e \geq h \quad (3.6f)$$

where  $\mathcal{Z}$  denotes the feasible region of the unit commitment problem (i.e., Equations (3.1b)-(3.1h)), the third level problem is defined as

$$\min_{\mathbf{x}_g \in \mathcal{K}} c_g^T \mathbf{x}_g : D_e \mathbf{x}_e + D_g \mathbf{x}_g \geq d, \quad (3.7)$$

and  $\mathcal{K}$  is the proper cone denoting the domain of  $\mathbf{x}_g$ .

The first-level problem (i.e., Equations (3.6a) and (3.6b)) formulates the unit-commitment problem (i.e., Equations (3.1a)-(3.1h) and Equation (3.4)). The unit-commitment decisions  $\mathbf{z}_e$  from the first-level problem are then plugged into the second-level problem (i.e., Equation (3.6c)-(3.6d)), which formulates the economic dispatch problem (i.e., Equations (3.1j)-(3.1u)) and decides the hourly operating schedule of committed generating units. The economic dispatch decisions  $\mathbf{x}_e$  determine natural gas demand of committed GFPPs and are plugged into the third-level problem (i.e., Problem (3.6e)), which formulates the natural gas problem (i.e., Problem (3.2) and Equation (3.3)). Then, the third level problem determines the resulting nodal prices for natural gas based on the dual solution  $\mathbf{y}_g$  of the gas flux conservation constraints (i.e., Equation (3.2b)).

Equations (3.6a)-(3.6e) capture the current operating practice of the power system. Without Equation (3.6f), the first level captures the commitment decisions that are taken first without consideration of the gas network. The second and third levels implement a Stackelberg game, where the dispatch decisions of the electricity system are followed by those of the natural gas network. *The novelty in the UCGNA is the bid-validity constraint*

---

<sup>2</sup>From a game theoretic perspective, the problem at hand is a two-level problem (See Appendix B.1). However, for ease of deriving a bilevel formulation that allows some efficient solution method, presented in Chapter 4, the problem is posed as a tri-level

(3.6f), which corresponds to Equation (3.5b): It ensures that only profitable GFPPs are selected in the first level and uses the dual variables of the third-level problem to do so, allowing the unit-commitment problem to anticipate the zonal prices of natural gas.

The following proposition, whose proof is in Appendix B.2, shows that the tri-level problem can be reformulated as a bilevel mathematical program. The proof uses strong duality on the third-level problem and a lexicographic optimization to merge the second and third levels.

**Proposition 3.2.1.** *Problem (3.6) can be asymptotically approximated by the following bilevel optimization program:*

$$\min \delta h^T \mathbf{z}_e + \delta c_e^T \mathbf{x}_e + (1 - \delta) c_g^T \mathbf{x}_g \quad (3.8a)$$

$$\text{s.t. } \mathbf{z}_e \in \mathcal{Z}, \quad (3.8b)$$

$$(\mathbf{x}_e, \mathbf{x}_g, \mathbf{y}_g) = \text{An optimal primal \& dual solution pair of (3.9)}, \quad (3.8c)$$

$$\frac{1}{1 - \delta} E \mathbf{y}_g + M \mathbf{z}_e \geq h, \quad (3.8d)$$

$$\mathbf{x}_e \geq 0, \mathbf{x}_g \in \mathcal{K}, \mathbf{y}_g \geq 0, \quad (3.8e)$$

$$\mathbf{z}_e \in \{0, 1\}^m. \quad (3.8f)$$

for some  $\delta \in (0, 1)$  and

$$\min_{\mathbf{x}_e \geq 0, \mathbf{x}_g \in \mathcal{K}} \delta c_e^T \mathbf{x}_e + (1 - \delta) c_g^T \mathbf{x}_g \quad (3.9a)$$

$$\text{s.t. } A \mathbf{x}_e + B \mathbf{z}_e \geq b, \quad (3.9b)$$

$$D_e \mathbf{x}_e + D_g \mathbf{x}_g \geq d. \quad (3.9c)$$

Moreover, when  $\delta \rightarrow 1$ , the optimal solution of Problem (3.8) converges to the optimal solution of Problem (3.6).

*Remark 3.2.2.* Note that Problem (3.8) has some properties. First, the lower level problem (i.e., Problem (3.9)) is a SOCP and the lower level problem depends on the upper level problem only through the upper level binary variables (i.e.,  $\mathbf{z}_e$ ).

### 3.3 Solution Approach

This section briefly sketches how the bilivel formulation, given in Section 3.2.4, is solved. Using the strong duality of Problem (3.9), Problem (3.8) can be reformulated as

$$\min_{\mathbf{z}_e \in \mathbb{B}^n} \delta h^T \mathbf{z}_e + f(\mathbf{z}_e) \quad (3.10a)$$

$$\text{s.t. } \mathbf{z}_e \in \mathcal{Z}. \quad (3.10b)$$

where

$$f(\mathbf{z}_e) = \min \delta c_e^T \mathbf{x}_e + (1 - \delta) c_g^T \mathbf{x}_g \quad (3.11a)$$

$$\text{s.t. } A \mathbf{x}_e + B \mathbf{z}_e \geq b, \quad (3.11b)$$

$$D_e \mathbf{x}_e + D_g \mathbf{x}_g \geq d, \quad (3.11c)$$

$$\mathbf{y}_e^T (b - B \mathbf{z}_e) + \mathbf{y}_g^T d \geq \delta c_e^T \mathbf{x}_e + (1 - \delta) c_g^T \mathbf{x}_g, \quad (3.11d)$$

$$\mathbf{y}_g^T D_g \preceq_{\mathcal{K}^*} (1 - \delta) c_g^T, \quad (3.11e)$$

$$\mathbf{y}_e^T A + \mathbf{y}_g^T D_e \leq \delta c_e^T, \quad (3.11f)$$

$$\frac{1}{1 - \delta} E \mathbf{y}_g + M \mathbf{z}_e \geq h, \quad (3.11g)$$

$$\mathbf{x}_e \geq 0, \mathbf{x}_g \in \mathcal{K}, \mathbf{y}_e \geq 0, \mathbf{y}_g \geq 0. \quad (3.11h)$$

The implementation applies a Benders decomposition on this formulation to solve Problem (3.8). Moreover, the dual of Problem (3.11) has a special structure that can be exploited by the *dedicated Benders decomposition*, discussed in Chapter 4. The idea is to decompose the dual of Problem (3.11) into two more tractable problems. The extreme points and rays of these subproblems can be used to find the (feasibility and optimality) Benders cuts of Problem (3.11). The solution method also uses the acceleration schemes from [106, 107] which normalize the rays  $\hat{y}$  and perturb  $\hat{z}_e$ . The solution method also obtains feasible solutions periodically (e.g., every 30 iterations) heuristically by turning off violated generators. Finally, the solution method applies a preprocessing step to eliminate some invalid bids. It exploits the fact that the natural gas prices without the GFPP load gives a lower bound on the natural gas zonal prices. Therefore, the implementation solves Problem (3.2) with no GFPPs, i.e.,  $\gamma_{j,t} = 0$  for all  $j \in \mathcal{V}, t \in [1, T]_{\mathbb{Z}}$ . Those bids violating the bid-validity constraint with regard to these zonal prices are not considered further.

## 3.4 Case Study

This section analyzes, under various operating conditions, the behavior of the UCGNA on the realistic test system described in Section 3.4.1. The results are compared with current practices. The case study varies the level of stress on both the electrical power and gas systems. For the electrical power system, the load is uniformly increased by 30% and 60%. For the gas system, the load is uniformly increased by 10% up to 130%. Parameters  $\eta_e$  and  $\eta_g$  respectively represent the stress level imposed on the electrical power and gas systems. In the results, (A) denotes existing practices and (B) the UCGNA model. Solutions for (B) are obtained with a wall-clock time limit of 1 hour, while solutions for (A) is obtained by the following procedure:

- (i) Solve the power model (i.e., Problem (3.1));
- (ii) Retrieve the demand of GFPPs using Equation (3.3) and plug it into the gas model (i.e., Problem (3.2));
- (iii) Solve the gas model and compute the natural gas zonal prices using the dual values associated with the flux conservation constraints;
- (iv) Based on the zonal prices, determine the set of GFPPs violating the bid-validity constraint (i.e., Equation (3.5b)) and compute the loss of such GFPPs by multiplying the violation, i.e., the difference between the marginal gas price and the marginal bid price, with the scheduled amount of power generation.

### 3.4.1 Data Description

The UCGNA model is evaluated on the gas-grid test system from [47], which is representative of the natural gas and electric power systems in the Northeastern United States. This test system is composed of the IEEE 36-bus NPCC electric power system [108] and a multi-company gas transmission network covering the Pennsylvania-To-Northeast New England area in the United States [47]. The data for the test system can be found online at <https://github.com/lanl-ansi/GasGridModels.jl> and we only decrease nodal pressure bounds by a factor of 3 to get an interesting test case.

The test system consists of 91 generators of various types (e.g., hydro, gas-fueled, coal-fired, etc.). The unit-commitment data for these generators (e.g., generator offer curves including start-up and no-load costs and operational parameters such as minimum run time) was obtained from the RTO unit commitment test system [109]. Each generator in the gas-

grid test system is assigned the unit commitment data adapted to its fuel-type and megawatt capacity. To introduce more variety on bidding behaviors, we modify some offer curves.

The data sets account for the fact that prices in the gas spot market in the United States is zonal [110], and the gas-grid test case consists of two natural gas pricing zones: Transco Zone 6 non NY and Transco Leidy Line. The Transco Leidy Line represents the natural gas prices in the Marcellus Shale production area, which has a wealth of natural gas. On the other hand, the Transco Zone 6 non NY represents the natural gas prices near consumption points. Therefore, a large difference in prices between these two pricing zones implies a scarcity of transmission capacities between these two points. During normal operations, the average natural gas prices in the Transco Zone 6 non NY and the Leidy Line are around \$3/mmBtu and \$1.5/mmBtu respectively. The slopes  $c_{j,s}$  at junction  $j \in \mathcal{V}$  (see Section 3.2.2) are chosen to be around these numbers. The penalty cost for load shedding  $\kappa_{a,j}$  is set as \$130/mmBtu for all junctions. The results are given for a single time-period (i.e.,  $T = 1$ ).

### 3.4.2 Impact of the Gas-Awareness

The behaviors of (A) and (B) in the normal, stressed, and highly-stressed power systems are compared in Figures 3.1, 3.2, and 3.3 respectively. In each figure, (a) and (c) display the system costs and natural gas prices of (A), and (b) and (d) display those of (B). More precisely, (a) and (b) present the total cost breakdown in terms of the cost of electrical power system, the cost of the gas system, and the economic loss from invalid bids. (c) and (d) depict the natural gas zonal prices in each pricing zone.<sup>3</sup>

Figures 3.1a and 3.1c show that the gas system cost gradually increases as  $\eta_g$  increases up to 1.7, then it grows rapidly from  $\eta_g = 1.8$  on. The rapid increase is due to load shedding (see Section 3.2.2) and leads to natural gas price spikes in Transco Zone 6 non NY. The large difference between the prices in Zone 6 and Leidy Line indicates that the load shedding occurs due to the lack of transmission capacity between these two points, not because of a lack of gas supply. Due to the gas price spike in Transco Zone 6 non NY, some bids of GFPPs become invalid and incur some losses, which increases the total cost. On the other hand, for (B), the electrical power system cost is slightly higher than for (A), but it does not incur any economic loss from invalid bids and the overall cost is lower. Observe also that model (A) captures the same behavior as in the 2014 polar vortex. Additionally, observe that the gas price in the Zone 6 region is also exhibiting sharp increases in model

---

<sup>3</sup>Note that, as  $\eta_g$  increases, the total cost of (A) always increases, while the cost of (B) temporarily decreases sometimes. This is due to the presence of optimality gaps for some hard instances.

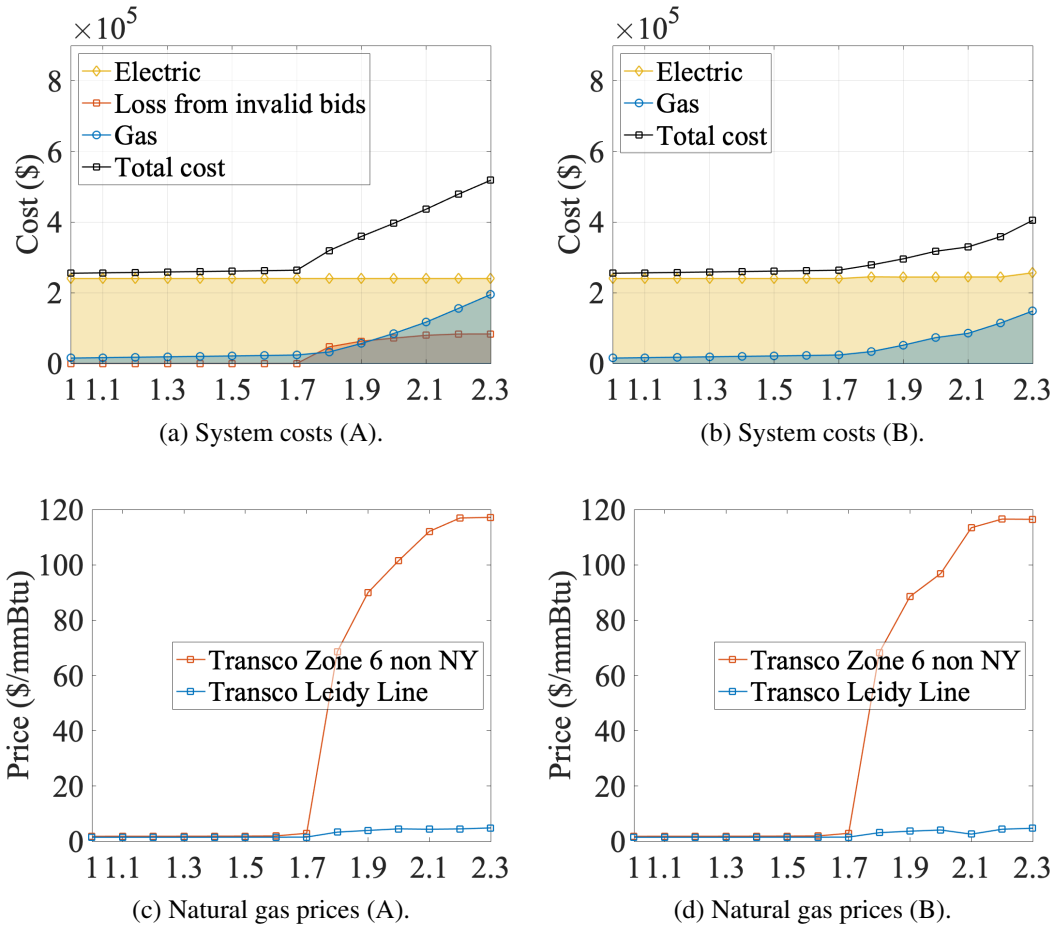


Figure 3.1: Results for the Normal Operating Conditions of the Electrical Power System ( $\eta_e = 1$ ), where  $x$ -axis represents  $\eta_g$

(B). However, this peak has significantly less impact for (B) given the different commitment decisions.

The differences in behavior between systems (A) and (B) become clearer as the load increases in the electrical power system. For the stressed power system, displayed in Figure 3.2, the difference between the total cost of (A) and (B) becomes very large: There are many invalid bids for (A), which puts the reliability of the power system at high risk and induces an electricity price peak. The price of gas and the economic losses both increase significantly in (A) and the increases start at stress level 1.5 for the gas network. In contrast, (B) maintains a reliable operation independently of the stress imposed on the natural gas system. The price of gas increases obviously but less than in (A) and the cost of the power system remains stable. The peak in gas price only starts at stress level 1.7, showing that (B) delays the impact of congestion in the gas networks by making better commitment

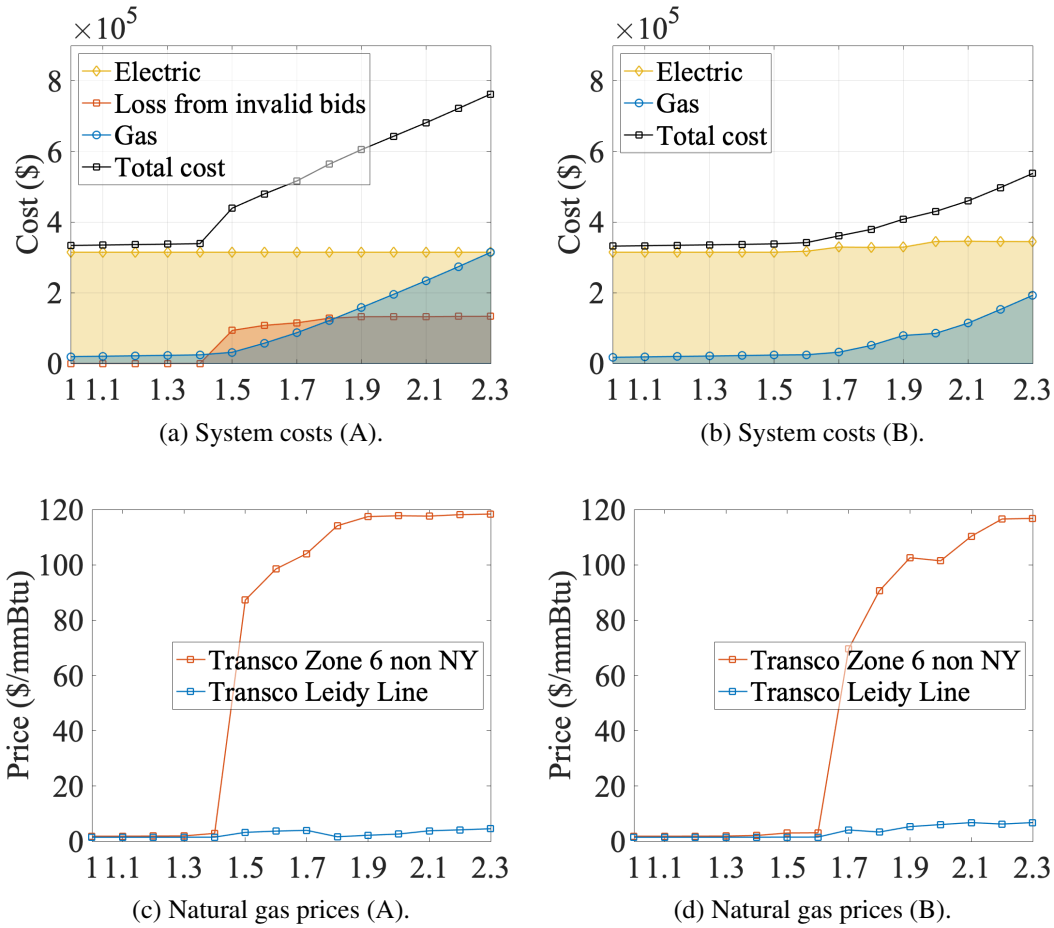


Figure 3.2: Results for the Stressed Electrical Power System ( $\eta_e = 1.3$ ), where  $x$ -axis represents  $\eta_g$

decisions.

Figure 3.3 shows the benefits of (B) over (A) become even more substantial when both systems are highly stressed. Observe that the cost of the electrical power system remains stable once again in (B) and that the cost of the gas network increases reasonably. In contrast, Model (A) exhibits significant increases in gas prices and economic cost from invalid bids. These results indicate that bringing gas awareness in unit commitment brings significant benefits in congested networks. By choosing commitment decisions that ensure bid validity, the UCGNA brings substantial cost and reliability benefits for congested situations like the 2014 polar vortex.

The great cost and reliability benefits of (B) are owing to better commitment decisions that anticipate the future state of the gas system. Table 3.7 summarizes some statistics on committed generators under the highly stressed power system. As the gas load increases, some of the GFPPs in (T) are no longer committed and the lost generation is replaced by

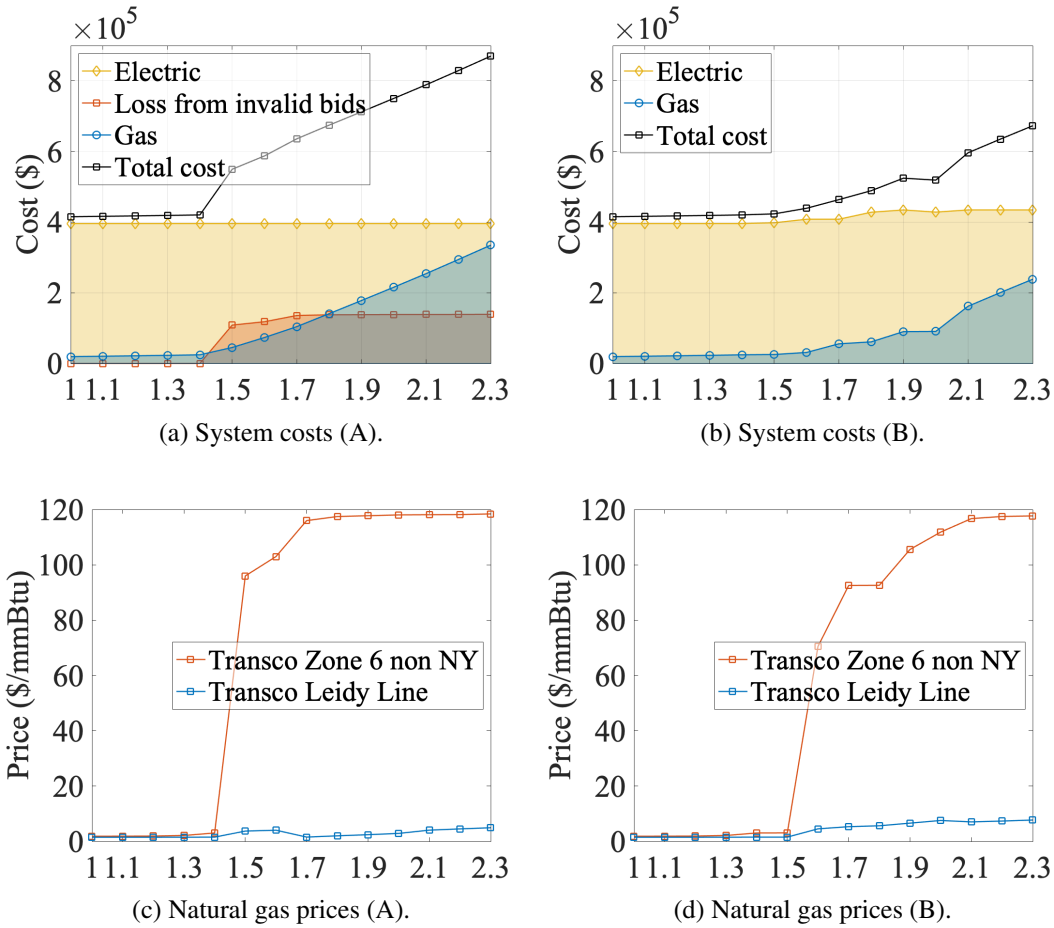


Figure 3.3: Results for the Highly-Stressed Electrical Power System ( $\eta_e = 1.6$ ), where  $x$ -axis represents  $\eta_g$

Table 3.7: Statistics on Committed Generators for the Stressed Electrical Power System ( $\eta_e = 1.6$ ): The first 7 columns display the number of committed generators with respect to its fuel type, where (O) Oil, (C) Coal, (G) Gas, (H) Hydro, (R) Refuse, (N) Nuclear, (E) Others, and the last two columns show the number of committed GFPPs in each pricing zone, where (T) Transco Zone 6 Non NY and (L) Transco Leidy Line.

| $\eta_g$ | (O) | (C) | (G) | (H) | (R) | (N) | (E) | (T) | (L) |
|----------|-----|-----|-----|-----|-----|-----|-----|-----|-----|
| 1.0      | 7   | 6   | 12  | 11  | 0   | 12  | 3   | 8   | 4   |
| 1.6      | 8   | 6   | 10  | 11  | 0   | 13  | 3   | 6   | 4   |
| 2.3      | 9   | 6   | 9   | 11  | 0   | 13  | 3   | 4   | 4   |

generators of different types or GFPPs with reasonable bid prices. More specifically, Figure 3.4 shows the commitment decision of (A) and (B) for  $(\eta_e, \eta_g) = (1.6, 2.3)$ . The numbers in black in Figures 3.4a and 3.4c report the number of committed GFPPs on the corresponding bus; Those in Figures 3.4b and 3.4d display the number of committed non-GFPPs. In

● Electricity system ● Gas system ▲ Pricing point (Zone 6) ■ Pricing point (Leidy Line)

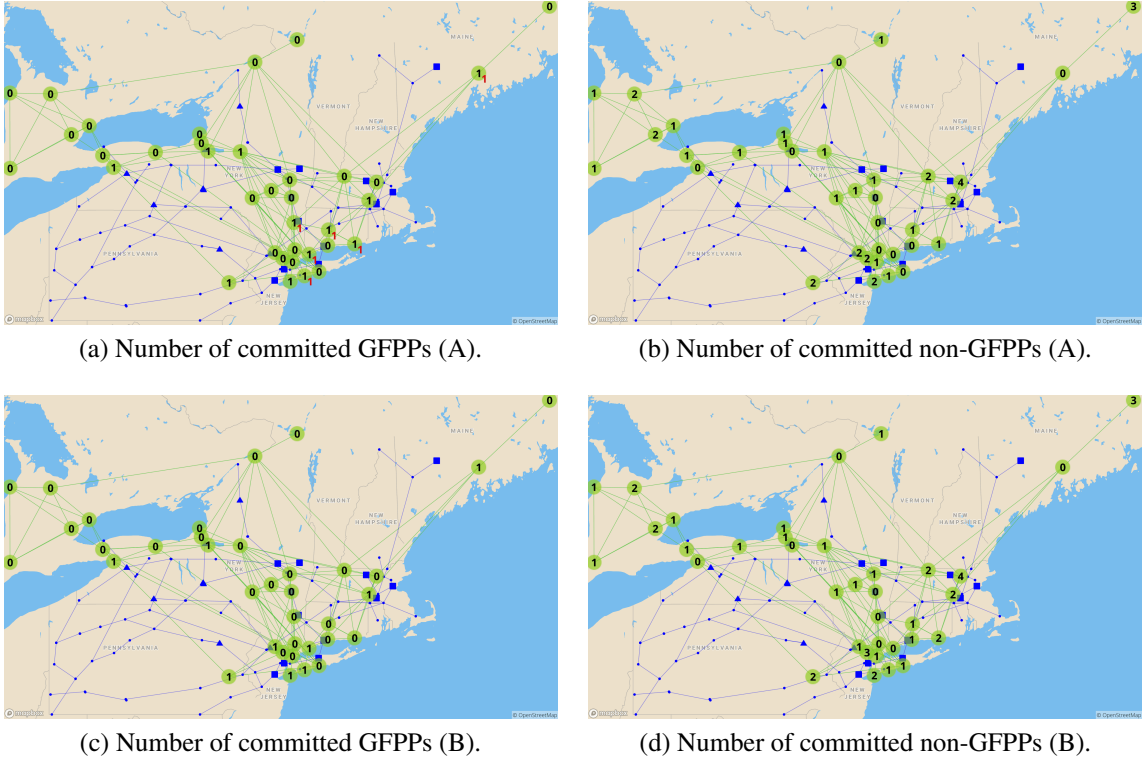


Figure 3.4: Results for the Highly-Stressed Condition  $(\eta_e, \eta_g) = (1.6, 2.3)$ .

Figure 3.4a, the numbers in red on the bottom right corner of some buses represent the number of committed GFPPs located at the bus without bid validity. Most invalid GFPPs in Figure 3.4a are turned off in Figure 3.4c and replaced by some non-GFPPs as Figure 3.4d indicates.

Finally, Table 3.8 summarizes the objective value and the optimality gap of (B) for each instance. For 16 out of 42 instances, the algorithm times out (wall-clock limit time of 1 hour) and it reports sub-optimal solutions whose optimality gaps are presented in columns denoted by (ii).

Suboptimal solutions are not desirable in market clearing, so future research should be devoted to improve these computational results further. Note however that these suboptimal results arise for highly congested situations in both networks. In such circumstances, operators are typically switching to an emergency reliability state, as was the case during the polar vortex events [84]. The results thus demonstrate that the UCGNA bring significant benefits for reliability of gas-grid networks.

Table 3.8: Solution Statistics for (B), where Column (i) denotes the final objective value of (B) for each instance and Column (ii) represents the optimality gap (time limit: one hour)

| $\eta_g \backslash \eta_e$ | 1        |      | 1.3      |      | 1.6      |      |
|----------------------------|----------|------|----------|------|----------|------|
|                            | (i)      | (ii) | (i)      | (ii) | (i)      | (ii) |
| 1                          | 255301.0 | 0.0  | 332123.0 | 0.0  | 415315.0 | 0.0  |
| 1.1                        | 256502.0 | 0.0  | 333333.0 | 0.0  | 416530.0 | 0.0  |
| 1.2                        | 257706.0 | 0.0  | 334548.0 | 0.0  | 417759.0 | 0.0  |
| 1.3                        | 258915.0 | 0.0  | 335776.0 | 0.0  | 419015.0 | 0.0  |
| 1.4                        | 260132.0 | 0.0  | 337036.0 | 0.0  | 420548.0 | 0.0  |
| 1.5                        | 261364.0 | 0.0  | 338564.0 | 0.0  | 423466.0 | 0.0  |
| 1.6                        | 262613.0 | 0.0  | 342066.0 | 0.3  | 439254.0 | 2.1  |
| 1.7                        | 264019.0 | 0.0  | 361089.0 | 3.5  | 463746.0 | 2.0  |
| 1.8                        | 278679.0 | 1.8  | 379532.0 | 3.2  | 489011.0 | 6.2  |
| 1.9                        | 296251.0 | 1.3  | 408407.0 | 3.3  | 524533.0 | 7.4  |
| 2                          | 317619.0 | 0.0  | 430415.0 | 4.2  | 519026.0 | 3.7  |
| 2.1                        | 329801.0 | 0.0  | 460127.0 | 4.3  | 596449.0 | 5.0  |
| 2.2                        | 358828.0 | 0.0  | 497952.0 | 4.0  | 635128.0 | 5.0  |
| 2.3                        | 405022.0 | 0.0  | 537874.0 | 0.0  | 672876.0 | 0.0  |

### 3.5 Discussion on the UCGNA

The contribution of this study is best viewed as two synergistic component: (1) a richer bid language for GFPPs allowing to express their risk aversion and (2) a market clearing mechanism, that use the more expressive bids to obtain the UCGNA, a gas-aware unit commitment for the electricity market. This section discusses the practical applicability and implication of the UCGNA as an alternative market clearing mechanism to the current practice.

A potential criticism of the UCGNA is the assumption that the power system operator has partial (or full) knowledge on the gas demand forecast and the gas network, which may require some level of cooperation of the natural gas system. It should be noted that both the electricity and natural gas markets have been wishing for measures that address the risks stemming from inter-dependencies between the two networks. Continuous development of regulations on these two systems reflects the market needs; For example, FERC Order 787 permits electricity and natural gas transmission operators to share, with each other, information that they deem necessary to promote the reliability and integrity of their systems [111]. When the natural gas demand forecast and the gas network data are shared, the UCGNA has the potential to enhance the reliability and efficiency of both systems, as demonstrated by the detailed case study in Section 3.4. Indeed, the results show that, in congested environments, the gas-aware unit commitment reduces the gas system cost and postpones the natural gas price spikes. This benefit would incentivize gas transmission operators to cooperate. Even without the cooperation of the natural gas system, the

proposed model can still be used with natural gas demand forecast that is obtained by the power system operator, as well as an incomplete description of the natural gas networks. The quality of the estimate, however, would improve as the power system operator acquire more accurate information about the gas system.

It is important to note that the UCGNA enables the GFPPs to hedge against risks induced by volatile natural gas prices. The main purpose of day-ahead markets is to produce a dispatch that anticipates and hedges against uncertainty that are observed in real time [112, 113]. In addition, the market should provide instruments that allow their participants to hedge risks so that a competitive equilibrium corresponds to the social optimum [114]. The current practice, however, neither anticipates uncertainty in the natural gas system nor has a market instrument for the GFPPs to hedge against their volatile operating costs. The GFPPs currently lack the ability to reflect changes to their operating costs after the reoffer period [84] and they have restrictive bidding language that cannot correctly incorporate their risk-appetite. Hence, the GFPPs may endure severe consequences when incorrectly forecasting natural gas prices. This makes the GFPPs less competitive and may eventually discourage them from staying in the market, which is highly undesirable, especially for power systems with a significant portion of renewable energy. The UCGNA, on the other hand, allows the GFPPs to make conditional bids: their bids are only valid as long as the realized natural gas prices are anticipated not to be much higher than their forecasts. It should be noted that, in the bid validity constraint, the system operator accepts different risk-aversion levels of each GFPP  $u$  through  $\alpha_u$ .

This study also advocates for *a richer bidding languages* so that GFPPs have more flexibility in the UCGNA. Indeed, ideally, a GFPP should be able to submit multiple bids, each of which is conditional on an anticipated range of realized natural gas prices and has an associated threshold  $\alpha_u$ . This enables the commitment decision to correctly reflect the “actual” price that the GFPP is willing to offer, which is conditional on natural gas prices. This can be naturally incorporated into the UCGNA by introducing additional binary variables in the first level that represent the expected price range of natural gas.

Another potential criticism of the UCGNA concerns the transparency of the natural gas price estimation that will be endogenously obtained and used in the UCGNA. One may question whether the GFPPs would be willing to accept the commitment decision when they are de-committed due to the bid validity constraints. In practice, the estimated natural gas prices in the UCGNA are largely dependent on natural gas demand forecast. The disclosure of natural gas demand forecast to GFPPs before the bid submission period closes thus gives GFPPs the opportunity to design their bidding strategy accurately.

Note also that the economic feedback from the natural gas system affects the commit-

ment and dispatch decisions *in a completely discrete manner*: Once the binary decisions are committed and ensure that the bid validity constraints are met, the second level clears the market in the same way as in the current practice. Thus, the current market properties (e.g., revenue adequacy of ISOs and cost recovery for committed generators achieved under some assumptions/market instruments) also applies to the UCGNA. Recently, several papers proposed stochastic energy-only market clearing mechanisms to address undesirable properties of the current market introduced by the increasing penetration of intermittent generators [115, 116, 112, 113]. The UCGNA can be adapted to embody a single-settlement stochastic dispatch (e.g., [113]) in the second level problem, which would result in a stochastic economic feedback from the gas system. In this case, the bid validity constraint should be formulated differently to accommodate the uncertainty (e.g., by using chance constraints). Future research will be devoted to incorporating a stochastic dispatch into the UCGNA.

### 3.6 Concluding Remark

The 2014 polar vortex showed how interdependencies between the electrical power and gas networks may induce significant economic and/or reliability risks under heavy congestion. This chapter has demonstrated that these risks can be effectively mitigated by making unit commitment decisions informed by the physical and economic couplings of the gas-grid network. The resulting Unit Commitment with Gas Network Awareness (UCGNA) model builds upon the standard unit commitment used in current practices but also reasons about the feasibility of gas transmission feasibility and the profitability of committed GFPPs. In particular, the UCGNA introduces bid-validity constraints that ensure the economic viability of committed GFPPs, whose marginal bid prices must be higher than the marginal natural gas prices by some percentage  $\alpha_u$ . Section 3.5 also advocated for a richer bidding language that the GFPPs can use to express more complex bids capturing different levels of natural gas prices.

The UCGNA is a three-level model whose bid validity constraints operate on the dual variables of flux conservation constraints in the gas network, which calculate the marginal cost of gas for producing a unit of electricity. It can be approximated as a bilevel optimization problem, in which the upper level problem is a mixed-integer linear program and the lower level program is a second-order cone program. The bilevel problem is then solved using a dedicated Benders decomposition approach discussed in Chapter 4. The case study, based on a modeling of the gas-grid network in the North-East of the United States, shows that the UCGNA has significant benefits compared to the existing operations: It is capable to ensure valid bids even at highly-stressed levels, while only increasing the cost of

gas and electricity in a reasonable way. In contrast, the existing operating practices induce significant economic losses and gas price increases.

In summary, the UCGNA allows GFPPs to hedge against their volatile operating costs by providing bids that are conditional to anticipated natural gas prices. The resulting bids effectively give them an opportunity to “withdraw” their bids when the gas prices are too high. The UCGNA also helps system operators to avoid the default of GFPPs and fuel supply issues that have plagued the gas network during the polar vortex events. The current market properties are maintained since the economic feedback only affects the first level solution. Future research will be devoted to adapting the second-level problem to a stochastic dispatch problem and further improving the solution techniques to solve the UCGNA, including the use of cut bundling and Pareto-optimal cuts.

## CHAPTER 4

# Benders Subproblem Decomposition for Discrete-Continuous Bilevel Problems

### 4.1 Introductory Remarks

A variety of real-world applications involves multiple decision-makers. These decision-makers (agents) may have an implicit *hierarchy* in the sense that each decision made by an agent at a certain level of the hierarchy precedes and affects the decisions of agents at lower levels that, in turn, affects the outcomes of the decisions at the higher levels. *Hierarchical optimization* models optimization problems that involve the hierarchical decision-making process of multiple agents.

In this chapter, we focus on *bilevel optimization* problems, a subclass of hierarchical optimization, with two decision-makers that are often referred to as a leader and a follower. In these problems, it is assumed that the leader can anticipate how the follower would respond to its decision. The objective of these problems is, thus, to optimize the leader's decision by solving a nested optimization problem that describes the followers response (see, e.g., [117] for more details). Bilevel problems are closely related to static Stackelberg games and can find many real-world applications across economics, energy infrastructure, and defense, to name a few. For instance, bilevel optimization models pricing mechanisms in transportation areas [48, 118], energy systems [119, 120], and IT industry [121]. Bilevel optimization is also an useful tool for making planning/design decisions for networks involving autonomous agents, such as transportation network planning [49] and supply chain design [122], and for defense planning against malicious attacks [50, 51, 123, 124].

Despite the wide applicability and increasing interest in bilevel optimization, research on computational aspects of bilevel optimization has been sparse. This is mainly due to the inherent complexity of bilevel optimization; Even the simplest subclass of bilevel optimization where leader and follower problems are Linear Programming (LP) problems is NP-hard [52]. In the present chapter, we propose a novel Benders decomposition method

for a family of bilevel problems in which the leader problem is modeled as a mixed-integer conic-linear program and the follower problem is modeled as a conic-linear program with strong duality. In this chapter, this problem class is called Mixed-Integer Bilevel Programming with Strong Duality in lower-level (MIBPSD) that is formally defined as follows:

$$\min_{x,y} \quad c_x^T x + c_y^T y \quad (4.1a)$$

$$\text{s.t.} \quad G_{xy}x + G_y y \geq h_y, \quad (4.1b)$$

$$x \in \mathcal{X} := \{x \in \mathcal{K}_x : x_i \text{ integer}, \forall i \in \mathcal{I}\}, \quad (4.1c)$$

$$y \in \arg \min_{y \in \mathcal{K}_y} \{d^T y : Ax + By \geq b\}, \quad (4.1d)$$

where  $x$  and  $y$  respectively represent  $n_1$ -dimensional leader variables and  $n_2$ -dimensional follower variables,  $\mathcal{I} \subseteq \{1, \dots, n_1\}$  denotes a set of indices of the leader's variables for which the corresponding variable is integer,  $\mathcal{K}_x$  and  $\mathcal{K}_y$  denote some proper cones in  $\mathbb{R}^{n_1}$  and  $\mathbb{R}^{n_2}$ , and  $c_x, c_y, G_{xy}, G_y, h_y, d, A, B, b$  are given rational matrices or vectors of appropriate dimension.

This chapter makes the following assumption on MIBPSD:

**Assumption 4.1.1.** *Strong duality holds for Problem (4.1d).*

**Assumption 4.1.2.** *Problem (4.1d) is not affected by continuous upper level variables, i.e.,  $i'$ -th column of  $A$  is  $\mathbf{0}_{m_2 \times 1}$  for  $i' \notin \mathcal{I}$  (4.1d).*

**Assumption 4.1.3.** *The bilevel problem (4.1) is optimistic, i.e., when there are multiple lower level optimal solutions for a given upper level decision  $\hat{x}$ , it chooses  $\hat{y}$  that benefits the upper level most, among the optimal solutions [125].*

For notational simplicity, this chapter focuses on the mixed-integer linear subclass of MIBPSD, i.e.,  $\mathcal{K}_x = \mathbb{R}_+^{n_1}$ ,  $\mathcal{K}_y = \mathbb{R}_+^{n_2}$ . The results however can be easily generalized to mixed-integer conic-linear bilevel problems that satisfies Assumption 4.1.1. In addition, using binary representation of general integer variables, we focus on the case where  $x_i \in \{0, 1\}$  for all  $i \in \mathcal{I}$ . Therefore, w.l.o.g, we assume  $\mathcal{X} = \{x \in \mathbb{R}_+^{n_1} : x_i \in \{0, 1\}, \forall i \in \mathcal{I}\}$ .

In this chapter, we also consider the following problem, which gives a lower bound to

Problem (4.1):

$$\min_{x \in \mathcal{X}, y \in \mathbb{R}_+^{n_2}} c_x^T x + c_y^T y \quad (4.2a)$$

$$\text{s.t.} \quad G_{xy}x + G_y y \geq h_y, \quad (4.2b)$$

$$Ax + By \geq b. \quad (4.2c)$$

In order to ensure that Problem (4.1) is well posed, we make the following additional assumptions:

**Assumption 4.1.4.** *Problem (4.2) is feasible and bounded.*

**Assumption 4.1.5.** *There exists  $\hat{x} \in \mathcal{X}$  for which the lower-level problem of Problem (4.1) (i.e., Problem (4.1d)) has a finite optimum at  $\hat{y}$  and  $(\hat{x}, \hat{y})$  satisfies Constraint (4.1b).*

Note that Assumption 4.1.4 guarantees a finite lower bound of Problem (4.1) and Assumption 4.1.5 ensures that Problem (4.1) has a feasible solution with a finite objective value (i.e., a finite upper bound of Problem (4.1)), hence they imply that Problem (4.1) has a finite optimum.

Using the strong duality at lower level, a MIBPSD problem is often reformulated as a single-level Mixed-Integer Programming (MIP) problem by replacing the lower level with its optimality condition. The resultant MIP problem, however, is complex since it intertwines the leader problem and the follower's primal and dual problems. For large instances, the complexity of the MIP formulation often challenges up-to-date commercial solvers and existing decomposition methods like the Benders decomposition method.

Accordingly, this chapter proposes a dedicated Benders decomposition for MIBPSD that deals with the complex MIP formulation effectively by decomposing the Benders subproblem into two more tractable, sequentially solvable problems that are closely related to the leader and the follower problems. The main contributions of this chapter can be summarized as follows:

- A new decomposition technique for MIBPSD is proposed, which allows easy implementation and intuitive interpretation of Benders cuts and several accelerating schemes are discussed.
- An interesting extension of MIBPSD is introduced, which formulates important real-world problems where the leader is affected by the follower's dual solution; It is shown that the decomposition technique also carries over the extension. In addition, a discussion on some special cases of MIBPSD that allow sequence-independent decomposition is given.

- A computational study is reported which demonstrates significant performance improvement of the proposed method and the accelerating schemes over an up-to-date commercial solver and the standard Benders method.

The rest of the chapter is organized as follows: Section 4.2 discusses previous literature and Section 4.3 presents the MIP formulation of MIBPSD. In Section 4.4, the dedicated Benders method for MIBPSD is proposed. Section 4.5 discusses some interesting extension of MIBPSD that incorporates additional constraints on follower’s dual variables in the leader problem and Section 4.6 shows some special cases of MIBPSD that allow stronger algorithmic results. Some accelerating schemes for the dedicated Benders method is presented in Section 4.7. Finally, the computational performance of the proposed method is demonstrated in Section 4.8, and Section 4.9 concludes the chapter.

## 4.2 Literature Review

MIBPSD can find many applications in network planning/design problems with autonomous agents; For instance, [126, 127] and [128] formulated the optimal zonal configuration problem in zonal-pricing electricity markets as MIBPSD, an urban traffic network design problem was formulated as MIBPSD by [49], and MIBPSD also arose in facility location problems for logistics distribution center [129] and the evasive flow capturing problem discussed by [130] which has many applications in transportation, revenue management, and security management.

In addition, unit scheduling problems under sequentially cleared markets can be modelled with MIBPSD in its extended form where an additional constraint stating the impact of the follower’s dual solution on the leader problem is added to the leader problem. Such constraints may be desirable in some sequential market environment where the follower’s dual solution settles the prices of commodities that are used by the leader; See, e.g., an unit-commitment problem for interdependent natural gas and electricity markets studied in Chapter 3. We discuss this extension in later section (Section 4.5).

Taking advantage of the strong duality in the lower level problem, the common solution approach for MIBPSD is to reformulate the bilevel problem into a single-level MIP problem and to solve the MIP problem via off-the-shelf solvers. There are two widely-used reformulation schemes: (1) A Karush-Kuhn-Tucker (KKT) condition approach (2) A strong duality approach. The former replaces the lower level problem by the KKT condition and linearizes the nonlinear complementary slackness condition by introducing additional binary variables and logic-based constraints (see, e.g., [48]). However, due to the large

number of binary variables and constraints that should be introduced for the linearization, this approach does not scale well and is not adequate for solving large-size instances. The later method, on the other hand, replaces the complementary slackness condition with the reversed weak duality inequality to ensure the primal and dual objective values of the lower level are the same. Then, the bilinear terms in the reversed weak duality are linearized using the McCormick relaxation [131, 132, 49] or some problem-specific properties [130]. Recently, [133] have compared these two schemes and computationally shown that the latter approach outperforms significantly the former approach for many classes of instances.

For large-scale problems, however, solving the resultant MIP is still challenging since it entangles the leader problem and the follower primal and dual problems. Accordingly, some problem-specific and generic decomposition/separation techniques for solving the associated MIP have been proposed. [126] proposed a generalized Benders algorithm that uses a special structure of the given tri-level problem (which has an equivalent MIBPSD counterpart) and [130] developed a Branch-and-Cut (BnC) approach for a certain class of MIBPSD, named the Evasive Flow Capturing Problem. For general approaches, [134] proposed a decomposition algorithm which, at every iteration, fixes the integer variables at some values, reformulates the resultant bilevel linear subproblem into a MIP problem using the KKT scheme, solves the MIP problem to construct the associated LP problem with its active constraint set, solves the LP problem to obtain the dual information, and adds a cut. Since this approach reformulates the bilevel linear subproblem as a MIP problem using the KKT scheme at every iteration, its application to large-scale problems would be computationally expensive. The most relevant work is by [49] who applied the Benders decomposition to the MIP formulation obtained by the strong duality scheme. It proposed an acceleration scheme for solving the Benders subproblem which sequentially solves the follower problem, the leader problem, and the follower dual-related problem to obtain optimality cut. However they did not discuss the case for unbounded Benders subproblem (i.e., feasibility cuts). This present chapter, on the other hand, accelerates the computation for the Benders cut generation (both optimality and feasibility cut) by decomposing the Benders subproblem into two more tractable subproblems that are closed related to the leader and the follower problems.

It is worth mentioning generic solution approaches for Mixed-Integer Bilevel Programming (MIBP) that involves integer leader and follower variables, which subsumes MIBPSD. [135] first proposed a Branch-and-Bound approach for solving MIBP, and building upon the approach of [135], [136] and [137] developed a BnC algorithm, which was further improved by [138]. Another BnC algorithm that works for integer leader and follower variables was proposed by [139], which solves a MIBPSD problem for generating

cuts. As a result, the method proposed in this chapter can be applied to such generic solver.

### 4.3 MIP reformulation

In this section, we reformulate Problem (4.1) as a single-level MIP problem using the strong duality approach. Note that, using Assumptions 4.1.1 and 4.1.3, Problem (4.1) can be expressed as follows:

$$\min_{x \in \mathcal{X}} c_x^T x + f(x) \quad (4.3)$$

where

$$f(x) := \min c_y^T y \quad (4.4a)$$

$$\text{s.t. } G_{xy}x + G_y y \geq h_y, \quad (4.4b)$$

$$Ax + By \geq b, y \geq 0, \quad (4.4c)$$

$$\psi^T B \leq d^T, \psi \geq 0, \quad (4.4d)$$

$$d^T y \leq \psi^T (b - Ax). \quad (4.4e)$$

Constraints (4.4c) and (4.4d) respectively ensure primal and dual feasibility of the lower level problem, Constraint (4.4e) captures strong duality in the lower level. Thus, for any  $x \in \mathbb{R}_+^{n_1}$ , a feasible  $y \in \mathbb{R}_+^{n_2}$  to Constraints (4.4c) and (4.4e) is an optimal solution of the lower level problem for the given  $x$ . Accordingly, Constraint (4.4b) models how the lower level reaction affects the upper level feasible region. Due to (4.4a), when there are multiple optimal solutions in the lower level problem, Problem (4.4) will choose the most beneficial  $y$  to the upper level problem among the optimal lower level solutions, which aligns with Assumption 4.1.3.

Problem (4.4) contains a bilinear term of  $\psi^T Ax$  in Constraint (4.4e). Note that, due to Assumption 4.1.2, each bilinear term is a multiplication of some continuous variable and a binary variable. Assuming that  $\psi$  has an upper bound of  $\bar{\psi}$ , this term can be linearized: First introduce an additional vector of variables  $s \in \mathbb{R}_+^{m|I|}$  and constraints

$$s_{(j-1) \times |I| + i} = A_{ji} \psi_j x_i, \quad \forall j = 1, \dots, m, i \in I \quad (4.5)$$

to represent  $\psi^T Ax$  as  $s^T \mathbf{1}$ , where  $m$  represents the number of rows of  $A$ . Then use a McCormick transformation to replace Equation (4.5) by a set of linear constraints of the

form

$$K_\psi \psi + K_s s \geq k + K_x x, \quad s \geq 0, \quad (4.6)$$

for some matrices  $K_\psi, K_s, K_x$ , and some vector  $k$ . Then,  $f(x)$  can be obtained by solving the following problem:

$$\min \quad c_y^T y \quad (4.7a)$$

$$\text{s.t.} \quad G_y y \geq h_y - G_{xy} x, \quad (4.7b)$$

$$B y \geq b - A x, \quad y \geq 0, \quad (4.7c)$$

$$- \psi^T B \geq -d^T, \quad \psi \geq 0, \quad (4.7d)$$

$$- d^T y + \psi^T b - s^T \mathbf{1} \geq 0, \quad (4.7e)$$

$$K_\psi \psi + K_s s \geq k + K_x x, \quad s \geq 0. \quad (4.7f)$$

In the following, Problem (MIP) denotes the resulting mixed-integer linear programming, i.e., Problem (4.3) where  $f(x)$  is defined by Problem (4.7).

## 4.4 A Dedicated Benders Decomposition Method for MIBPSD

This section proposes a novel decomposition method for the Benders subproblem arising in MIBPSD. Benders Decomposition (BD) is defined by a Relaxed Master Problem (RMP) and a Benders SubProblem (BSP). The RMP generates a guess  $\hat{x} \in \mathcal{X}$  and its initial version is simply

$$\begin{aligned} \min_{x \in \mathcal{X}} \quad & c_x^T x + t \\ \text{s.t.} \quad & t \in \mathbb{R}. \end{aligned} \quad (4.8)$$

For a guess  $\hat{x}$ , the BSP is defined by the dual of Problem (4.7). We slightly abuse notation and let  $u_y, \psi, y, w$ , and  $v$  represent the dual variable associated with Constraints (4.7b), (4.7c), (4.7d), (4.7e), and (4.7f) respectively. Then the dual of Problem (4.7) can be expressed as follows:

$$\max \quad \psi^T (b - A \hat{x}) + u_y^T (h_y - G_{xy} \hat{x}) - [d^T y - v^T (k + K_x \hat{x})] \quad (4.9a)$$

$$\text{s.t.} \quad B y - K_\psi^T v \geq b w, \quad (4.9b)$$

$$B^T \psi + G_y^T u_y \leq d w + c_y, \quad (4.9c)$$

$$K_s^T v \leq \mathbf{1}w, \quad (4.9d)$$

$$\psi, u_y, w, y, v \geq 0. \quad (4.9e)$$

Note that Problem (4.9) is feasible, since otherwise, Problem (4.7) is infeasible or unbounded for any  $\hat{x} \in \mathcal{X}$  and contradicts Assumptions 4.1.4 and 4.1.5. If Problem (4.9) is unbounded, then Problem (4.7) is infeasible and BD adds a feasibility cut to the RMP using an unbounded ray of Problem (4.9). If Problem (4.9) has a finite optimal value, which means  $\hat{x}$  is feasible to Problem (MIP), then BD adds an optimality cut to the RMP. BD iteratively solves the updated RMP (Problem (4.8)) and the BSP (Problem (4.9)) until the value of  $t$  in the optimal RMP solution and the optimal BSP solution agree.

Unfortunately, for large-scale bilevel problems, Problem (4.9) is highly complex since it has primal-related (e.g., (4.9b) and (4.9d)) and dual-related (e.g., (4.9c)) constraints for Problem (4.1d) which are linked by variable  $w$ . *The main contribution of this chapter is to show that Problem (4.9) does not need to be solved as a whole.* Rather, the Benders cuts of Problem (MIP) can be obtained by solving two more tractable problems, i.e., a problem associated with the lower-level problem (to be defined as Problem (4.10)) and a problem related to the upper level problem (to be defined as Problem (4.11)):

**Theorem 4.4.1.** *Problem (4.9) can be solved by solving two more tractable problems sequentially: Solve the following problem:*

$$\min d^T y - v^T(k + K_x \hat{x}) \quad (4.10a)$$

$$s.t. By - K_\psi^T v \geq b, \quad (4.10b)$$

$$K_s^T v \leq \mathbf{1}, \quad (4.10c)$$

$$y, v \geq 0, \quad (4.10d)$$

and then solve the following problem:

$$\max \psi^T(b - A\hat{x}) + u_y^T(h_y - G_{xy}\hat{x}) - \mathcal{O}w \quad (4.11a)$$

$$s.t. B^T \psi + G_y^T u_y \leq dw + c_y, \quad (4.11b)$$

$$\psi, u_y, w \geq 0, \quad (4.11c)$$

where  $\mathcal{O}$  denotes the optimal objective value of Problem (4.10) if it has a finite optimum,  $\infty$  otherwise.

*Remark 4.4.2.* Consider the dual of Problem (4.10):

$$\max_{\psi, s \geq 0} b^T \psi - s^T \mathbf{1} \quad (4.12a)$$

$$\text{s.t.} \quad B^T \psi \leq d, \quad (4.12b)$$

$$K_\psi \psi + K_s s \geq k + K_x \hat{x}, \quad (4.12c)$$

where  $\psi$  and  $s$  are dual variables associated with Constraints (4.10b) and (4.10c) respectively. For any  $\hat{x} \in \mathcal{X}$ , the McCormick relaxation (i.e., (4.12c)) is exact and the optimal objective value of Problem (4.12) becomes equivalent to

$$\max_{\psi \geq 0} \{\psi^T (b - A\hat{x}) : B^T \psi \leq d\} = \min_{y \geq 0} \{d^T y : By \geq b - A\hat{x}\}. \quad (4.13)$$

Therefore, the infeasibility of Problem (4.10) implies that Problem (4.1d) is infeasible or unbounded for any  $\hat{x} \in \mathcal{X}$ , which contradicts Assumption 4.1.5.

Likewise, Assumption 4.1.4 guarantees Problem (4.11) to be feasible. Consider the dual of Problem (4.11):

$$\min_{y \geq 0} \{c_y^T y : By \geq b - A\hat{x}, G_y^T y \geq h_y - G_{xy}\hat{x}, d^T y \leq \mathcal{O}\}. \quad (4.14)$$

Note that if Problem (4.11) is infeasible, Problem (4.14) is infeasible or unbounded for any  $\hat{x} \in \mathcal{X}$  and  $\mathcal{O} \in \mathbb{R} \cup \{\infty\}$ , which contradicts Assumption 4.1.4.

Theorem 4.4.1 implies that Benders cuts can be generated by solving Problem (4.10) (i.e. a lower level-related problem) and Problem (4.11) (i.e., an upper level-related problem) sequentially, and leads to the following corollary.

**Corollary 4.4.3.** *Let  $\mathcal{J}_1$  and  $\mathcal{R}_1$  be the set of all extreme points and rays of Problem (4.10) and  $\mathcal{J}_2$  and  $\mathcal{R}_2$  be the set of all extreme points and rays of Problem (4.11), respectively. With  $\mathcal{J}_1, \mathcal{J}_2, \mathcal{R}_1,$  and  $\mathcal{R}_2$ , Problem (MIP) is equivalent to the following problem:*

$$\begin{aligned} \min_{x \in \mathcal{X}} c_x^T x + t \\ \text{s.t. } t \geq \hat{\psi}^T (b - Ax) - \hat{u}_y (h_y - G_{xy}\hat{x}) - \hat{w} (d^T \hat{y} - \hat{v} (k + K_x x)), \\ \forall (\hat{\psi}, \hat{u}_y, \hat{w}, \hat{y}, \hat{v}) \in \mathcal{J}_2 \times \mathcal{J}_1, \end{aligned} \quad (4.15a)$$

$$d^T \tilde{y} - \tilde{v} (k + K_x x) \geq 0, \forall (\tilde{y}, \tilde{v}) \in \mathcal{R}_1, \quad (4.15b)$$

$$0 \geq \tilde{\psi}^T (b - Ax) - \tilde{u}_y (h_y - G_{xy}\hat{x}), \forall (\tilde{\psi}, \tilde{u}_y, 0) \in \mathcal{R}_2, \quad (4.15c)$$

$$\begin{aligned} 0 \geq \tilde{\psi}^T (b - Ax) - \tilde{u}_y (h_y - G_{xy}\hat{x}) - \tilde{w} (d^T \hat{y} - \hat{v} (k + K_x x)), \\ \forall (\hat{y}, \hat{v}) \in \mathcal{J}_1, \forall (\tilde{\psi}, \tilde{u}_y, \tilde{w}) \in \mathcal{R}_2 : \tilde{w} > 0. \end{aligned} \quad (4.15d)$$

---

**Algorithm 1:** The Benders Separation Algorithm.

---

```

1 begin
  Input:  $\hat{x} \in \mathbb{R}^{n_1}$ 
2  Solve Problem (4.10);
3  if Problem (4.10) is unbounded with an unbounded ray  $(\tilde{y}, \tilde{v}) \in \mathcal{R}_1$  then
4    Solve Problem (4.11) with  $\mathcal{O} = \infty$  (i.e., by fixing  $w = 0$ );
5    if Problem (4.11) is unbounded with an unbounded ray  $(\tilde{\psi}, \tilde{u}_y, 0) \in \mathcal{R}_2$  then
6      Add the feasibility cut  $d^T \tilde{y} - \tilde{v}(k + K_x x) \geq 0$  and
7       $0 \geq \tilde{\psi}^T (b - Ax) - \tilde{u}_y (h_y - G_{xy} \hat{x})$  to the RMP;
8    else
9      Add the feasibility cut  $d^T \tilde{y} - \tilde{v}(k + K_x x) \geq 0$  to the RMP;
10   else
11     Obtain its optimal solution  $(\hat{y}, \hat{v}) \in \mathcal{J}_1$  and let  $\mathcal{O}$  be its optimal objective
12     value;
13     Solve Problem (4.11) with  $\mathcal{O}$ ;
14     if Problem (4.11) is unbounded with an unbounded ray  $(\tilde{\psi}, \tilde{u}_y, \tilde{w}) \in \mathcal{R}_2$  then
15       Add the feasibility cut
16        $0 \geq \tilde{\psi}^T (b - Ax) - \tilde{u}_y (h_y - G_{xy} \hat{x}) - \tilde{w} (d^T \hat{y} - \hat{v}(k + K_x x))$  to the RMP;
17     else
18       Obtain its optimal solution  $(\hat{\psi}, \hat{u}_y, \hat{w}) \in \mathcal{J}_2$ ;
19       Add the optimality cut
20        $t \geq \hat{\psi}^T (b - Ax) - \hat{u}_y (h_y - G_{xy} \hat{x}) - \hat{w} (d^T \hat{y} - \hat{v}(k + K_x x))$  to the RMP;
21       Update the best primal bound with the obtained feasible solution;

```

---

Let  $\mathcal{C}_1, \mathcal{C}_2, \mathcal{C}_3, \mathcal{C}_4$  denote the set of all constraints in (4.15a), (4.15b), (4.15c), and (4.15d) respectively. At each iteration, the RMP is a relaxation of Problem (4.15) with a subset of the constraints, i.e.,  $\tilde{\mathcal{C}}_1 \subseteq \mathcal{C}_1$ ,  $\tilde{\mathcal{C}}_2 \subseteq \mathcal{C}_2$ ,  $\tilde{\mathcal{C}}_3 \subseteq \mathcal{C}_3$ , and  $\tilde{\mathcal{C}}_4 \subseteq \mathcal{C}_4$ . The Benders separation routine at each iteration for an optimal solution  $\hat{x}$  of the RMP is given by Algorithm 1 instead of by solving Problem (4.9) and produces a violated constraints in  $\mathcal{C}_i \setminus \tilde{\mathcal{C}}_i$ , for some  $i \in \{1, \dots, 4\}$ .

#### 4.4.1 Interpretation of Benders Cuts

While the Benders cuts (i.e., Equations (4.15a)-(4.15d)) are valid for any  $\hat{x}$  feasible to the linear relaxation of Problem (MIP), they allow for an intuitive interpretation when  $\hat{x} \in \mathcal{X}$  (i.e., when the integrality condition is met). Recall that Remark 4.4.2 indicates, for  $\hat{x} \in \mathcal{X}$ ,

$$\mathcal{O} = \min_{y \geq 0} \{d^T y : By \geq b - A\hat{x}\}, \quad (4.16a)$$

$$\mathcal{O}_{(4.11)} = \min_{y \geq 0} \{c_y^T y : By \geq b - A\hat{x}, G_y^T y \geq h_y - G_{xy}\hat{x}, d^T y \leq \mathcal{O}\}. \quad (4.16b)$$

Note that Equations (4.16) imply that, for  $\hat{x} \in \mathcal{X}$ , Problem (4.10) corresponds to the follower problem, while Problem (4.11) represents the leader's problem conditional on the follower optimal decision. Therefore, when both Problems (4.16a) and (4.16b) have a finite optimum  $\mathcal{O}$  and  $\mathcal{O}_{(4.11)}$  at  $\hat{x} \in \mathcal{X}$ , the optimality cut (i.e., Equation (4.15a)) correctly evaluates the cost incurred by the follower reaction  $y$  (i.e., equal to the value of  $c_y^T y$ ). The feasibility cuts (4.15b), (4.15c), and (4.15d) respectively represent the case where the follower problem is infeasible for  $\hat{x}$ , the situation in which there is no follower feasible solution that satisfies Equation (4.1b) for  $\hat{x}$ , and the case where none of the follower *optimal* solution meets Equation (4.1b) for  $\hat{x}$ .

## 4.5 MIBPSD with Additional Upper Level Constraints on Dual Variables of Lower Level

An interesting extension of MIBPSD is to add an additional constraint to the upper level problem which states the impact of the follower dual variables on the leader problem. Such constraints may be desirable in some sequential market environment where the follower dual variables settle the prices of commodities that are used by the leader; See, e.g., an unit-commitment problem for interdependent natural gas and electricity markets studied by [55]. This section discusses how the BSP decomposition technique carries over to this extension.

In order to formulate the situation where the follower's dual solution affects the leader problem, MIBPSD can be extended as follows:

$$\min_{x, y, \psi} \quad c_x^T x + c_y^T y \quad (4.17a)$$

$$\text{s.t.} \quad G_{xy}x + G_y y \geq h_y, \quad (4.17b)$$

$$G_{x\psi}x + G_\psi \psi \geq h_\psi, \quad (4.17c)$$

$$x \in \mathcal{X} := \{x \in \mathcal{K}_x : x_i \in \mathbb{B}, \forall i \in \mathcal{I}\}, \quad (4.17d)$$

$$(y, \psi) \in \mathcal{Q} \left( \min_{y \in \mathcal{K}_y} \{d^T y : Ax + By \geq b\} \right), \quad (4.17e)$$

where  $\psi$  denote dual variables of the follower,  $\mathcal{Q}(P)$  denotes the set of optimal primal and dual solution pairs of Problem  $P$ , and  $G_{x\psi}, G_\psi, h_\psi$  are given rational matrices or vectors of appropriate dimension.

We define the counterpart of Problem (4.2) as follows:

$$\min_{x \in \mathcal{X}, y \in \mathbb{R}_+^{n_2}, \psi \in \mathbb{R}_+^m} c_x^T x + c_y^T y \quad (4.18a)$$

$$\text{s.t.} \quad G_{xy}x + G_y y \geq h_y, \quad (4.18b)$$

$$G_{x\psi}x + G_\psi \psi \geq h_\psi, \quad (4.18c)$$

$$Ax + By \geq b, \quad (4.18d)$$

$$B^T \psi \leq d, \quad (4.18e)$$

and we assume Assumption 4.1.4 on Problem (4.18).

Let Problem (MIP)' denote the MIP reformulation of Problem (4.17). It is easy to see that Problem (MIP)' is equivalent to Problem (MIP) to which Constraint (4.17c) added. Let  $u_\psi$  denote the dual variable associated with Constraint (4.17c). Then, the dual of Problem (4.7) with Constraint (4.17c) is expressed as Problem (4.9) with additional terms  $u_\psi^T (h_y - G_{x\psi} \hat{x})$  on the objective and  $-G_\psi^T u_\psi$  on the left-hand side of Constraint (4.9b). One can easily see that Theorem 4.4.1 and Corollary 4.4.3 extend to Problem (MIP)' by replacing Problem (4.10) with

$$\min d^T y - u_\psi^T (h_y - G_{x\psi} \hat{x}) - v^T (k + K_x \hat{x}) \quad (4.19a)$$

$$\text{s.t.} \quad By - G_\psi^T u_\psi - K_\psi^T v \geq b, \quad (4.19b)$$

$$K_s^T v \leq \mathbf{1}, \quad (4.19c)$$

$$y, u_\psi, v \geq 0, \quad (4.19d)$$

and adding appropriate terms on  $u_\psi$  to Problem (4.15).

## 4.6 Sequence-Independent BSP Decomposition

Some special cases of MIBPSD allow for a stronger alternative to Theorem 4.4.1. In this section, we deal with the extended version of MIBPSD discussed in Section 4.5 (i.e., Problem (4.17)), so any result in this section also holds for Problem (4.1). As noted in Sections 4.5, the BSP of Problem (MIP)' is decomposed into two problems, i.e., Problems (4.19) and (4.11), which are solved in a sequential manner. A sequence-independent BSP decomposition is allowed in two special cases of MIBPSD: (i)  $d = c_y$  (ii)  $c_y = 0$ . Case (i)

subsumes a class of mixed-integer conic-linear optimization problems that involves additional constraints on the dual variables of its inner-continuous problem, which is the case of the model proposed in Chapter 3. The following corollaries are the stronger alternatives to Theorem 4.4.1 for the cases (i) and (ii) respectively:

**Corollary 4.6.1.** *Let Problem (4.11)' denote Problem (4.11) with  $w$  fixed at zero. Then, the BSP for Problem (MIP)' with  $d = c_y$  can be solved by solving Problem (4.19) and Problem (4.11)' independently.*

**Corollary 4.6.2.** *Let Problem (4.11)'' denote Problem (4.11) with  $w$  fixed at zero and the right-hand side of Equation (4.11b) replaced with  $d$ . Then, the BSP for Problem (MIP)' with  $c_y = 0$  can be solved by solving Problem (4.19) and Problem (4.11)'' independently.*

Corollary 4.6.1 (or 4.6.2) implies that the Benders cuts for MIBPSD with  $d = c_y$  (or  $c_y = 0$ ) can be obtained by solving Problems (4.10) and (4.11)' (or (4.11)'') independently and comparing their objective values; This simplifies the Benders cut generation algorithm as described in Algorithm 2.

## 4.7 Acceleration Schemes for the Dedicated Benders Method

This section presents some acceleration schemes for the standard Benders decomposition method discussed in previous literature (e.g., [106] and [140]) and shows that these schemes can be applied to the dedicated Benders method described in Section 4.4. All results in this section also hold for the extended version of MIBPSD (Section 4.5).

### 4.7.1 Normalizing Benders Feasibility Cuts

[106] have shown that normalizing the ray used in Benders feasibility cuts can improve the performance of Benders decomposition. *The main contribution of this section is to show that the Benders subproblem decomposition can be generalized to produce a normalized ray.*

When Problem (4.9) is unbounded, the problem at hand consists in solving (4.9) with

---

**Algorithm 2:** The Benders Separation Algorithm for MIBPSD with  $d = c_y$  (or  $c_y = 0$ ).

---

```

1 begin
  Input:  $\hat{x} \in \mathbb{R}^{n_1}$ 
2   Solve Problems (4.10) and (4.11)' (or (4.11)'' ) independently and let  $\mathcal{O}_1$  and  $\mathcal{O}_2$ 
   respectively denote their objective value;
3   if  $\mathcal{O}_2 = \infty$  with an unbounded ray of  $(\tilde{\psi}, \tilde{u}_y)$  then
4     Add the feasibility cut (4.15c) to the RMP;
5   else
6     Obtain the optimal solution of Problem (4.11)' (or (4.11)'' ),  $(\hat{\psi}, \hat{u}_y)$ ;
7     if  $\mathcal{O}_1 = -\infty$  with an unbounded ray  $(\tilde{y}, \tilde{u}_\psi, \tilde{v})$  then
8       Add the feasibility cut  $c_y^T \tilde{y} - \tilde{u}_\psi^T (h_\psi - G_{x\psi} x) - \tilde{v}^T (k + K_x x) \geq 0$  to the
       RMP;
9     else
10      Obtain the optimal solution  $(\hat{y}, \hat{u}_\psi, \hat{v})$  of Problem (4.10);
11      if  $\mathcal{O}_1 < \mathcal{O}_2$  then
12        Add the feasibility cut
13           $\hat{\psi}^T (b - Ax) + \hat{u}_y^T (h_y - G_{xy} \hat{x}) \leq c_y^T \hat{y} - \hat{u}_\psi^T (h_\psi - G_{x\psi} x) - \hat{v}^T (k + K_x x)$ 
          to the RMP;
14        else
          Add the optimality cut  $t \geq \hat{\psi}^T (b - Ax) + \hat{u}_y^T (h_y - G_{xy} \hat{x})$  (or  $t \geq 0$ )
          to the RMP; Update the best primal bound with the obtained
          feasible solution;

```

---

an additional normalization constraint, i.e.,

$$\max \quad \psi^T (b - A\hat{x}) + u_y^T (h_y - G_{xy}\hat{x}) - [d^T y - v^T (k + K_x \hat{x})] \quad (4.20a)$$

$$\text{s.t.} \quad By - K_\psi^T v \geq bw, \quad (4.20b)$$

$$B^T \psi + G_y^T u_y \leq dw, \quad (4.20c)$$

$$K_s^T v \leq \mathbf{1}w, \quad (4.20d)$$

$$\|(\psi, u_y, w, y, v)\|_1 = 1, \quad (4.20e)$$

$$\psi, u_y, w, y, v \geq 0. \quad (4.20f)$$

Note that, in Problem (4.20), the constants have been set to zero, since the goal is to find a ray. In particular, the right-hand side of Equation (4.20c) has become  $dw$  instead of  $dw + c_y$ . The proof of Theorem 4.4.1 showed that Problem (4.9) has three different types of extreme unbounded rays:

- (i)  $\tilde{\mu}_1 := (0, 0, 0, \tilde{y}, \tilde{v})$  for  $(\tilde{y}, \tilde{v}) \in \mathcal{R}_1$ .

(ii)  $\tilde{\mu}_2 := (\tilde{\psi}, \tilde{u}_y, 0, 0, 0)$  for  $(\tilde{\psi}, \tilde{u}_y, 0) \in \mathcal{R}_2$ .

(iii)  $\tilde{\mu}_3 := (\tilde{\psi}, \tilde{u}_y, \tilde{w}, \tilde{w}\hat{y}, \tilde{w}\hat{v})$  for  $(\hat{y}, \hat{v}) \in \mathcal{J}_1$  and  $(\tilde{\psi}, \tilde{u}_y, \tilde{w}) \in \mathcal{R}_2$  with  $\tilde{w} > 0$ .

Cases (i) and (ii) are simple: It suffices to solve Problem (4.10) and Problem (4.11) with the additional constraint of  $\|(y, v)\|_1 = 1$  and  $\|(\psi, u_y, w)\|_1 = 1$  respectively. Case of (iii) (i.e., when Problem (4.10) has a finite optimum  $\mathcal{O}$  at  $(\hat{y}, \hat{v}) \in \mathcal{J}_1$  and Problem (4.11) is unbounded with an unbounded ray of  $(\tilde{\psi}, \tilde{u}_y, \tilde{w}) \in \mathcal{R}_2$  with  $\tilde{w} > 0$  and  $\mathcal{U} := \tilde{\psi}^T(b - A\hat{x}) + \tilde{u}_y^T(h_y - G_{xy}\hat{x}) - \mathcal{O}\tilde{w} > 0$ ) is more difficult and requires to find a normalized ray  $\tilde{r}' = (\tilde{\psi}', \tilde{u}'_y, \tilde{w}', \tilde{y}', \tilde{v}')$  that maximizes Equation (4.20a) while satisfying  $\|\tilde{r}'\|_1 = 1$  and  $\tilde{w}' > 0$ . Note that  $\tilde{\mu}_3/\|\tilde{\mu}_3\|_1$  is a feasible solution to Problem (4.20). Hence, Problem (4.20) is feasible and bounded.

Consider the Lagrangian relaxation of Problem (4.20) with  $w > 0$  that penalizes the violation of Constraint (4.20e) with some  $\lambda \in \mathbb{R}$ :

$$\begin{aligned} & \lambda + \sup \psi^T(b - A\hat{x} - \lambda\mathbf{1}) + u_y^T(h_y - G_{xy}\hat{x} - \lambda\mathbf{1}) - [(d + \lambda\mathbf{1})^T y - \lambda\mathbf{1}] - v^T(k + K_x\hat{x} - \lambda\mathbf{1}) - \lambda w \\ & \text{s.t. } By - K_\psi^T v \geq bw, \\ & \quad B^T \psi + G_y^T u_y \leq dw, \\ & \quad K_s^T v \leq \mathbf{1}w, \\ & \quad \psi, u_y, w, y, v \geq 0. \end{aligned}$$

For  $w > 0$ , defining  $(\psi, u_y, w, y, v) = (\frac{\psi}{w}, \frac{u_y}{w}, 1, \frac{y}{w}, \frac{v}{w})$ , Problem (4.20) becomes

$$\min_{\lambda \in \mathbb{R}} \left\{ \lambda + \sup_{w > 0} \{w(t^1(\lambda) - t^2(\lambda) - \lambda)\} \right\}, \quad (4.21)$$

where

$$t^1(\lambda) = \max_{\psi, u_y \geq 0} \psi^T(b - A\hat{x} - \lambda\mathbf{1}) + u_y^T(h_y - G_{xy}\hat{x} - \lambda\mathbf{1}), \quad (4.22a)$$

$$\text{s.t. } B^T \psi + G_y^T u_y \leq d, \quad (4.22b)$$

and

$$t^2(\lambda) = \min_{y, v \geq 0} (d + \lambda\mathbf{1})^T y - \lambda\mathbf{1} - v^T(k + K_x\hat{x} - \lambda\mathbf{1}) \quad (4.23a)$$

$$\text{s.t. } By - K_\psi^T v \geq b, K_s^T v \leq \mathbf{1}. \quad (4.23b)$$

---

**Algorithm 3:** The Subgradient Newton's Method for Problem (4.24).

---

```

1 begin
   Input:  $\lambda^0 = 0, t(\lambda^0) = \frac{U}{\bar{w}}, k = 0;$ 
2   while  $t(\lambda^k) > \epsilon$  do
3     Calculate  $\delta t(\lambda^k)$  (a subgradient of  $t$  at  $\lambda = \lambda^k$ );
4      $\lambda^{k+1} = \lambda^k - \frac{t(\lambda^k)}{\delta t(\lambda^k)}$ ;
5     Solve  $t^1(\lambda^{k+1})$  and  $t^2(\lambda^{k+1})$  and calculate
        $t(\lambda^{k+1}) = t^1(\lambda^{k+1}) - t^2(\lambda^{k+1}) - \lambda^{k+1}$ ;
6      $k \leftarrow k + 1$ ;

```

---

Define  $t(\lambda) := t^1(\lambda) - t^2(\lambda) - \lambda$ . If  $t(\lambda) < 0$ , the optimal objective value of the inner optimization problem of Problem (4.21) approaches zero as  $w$  converges to 0. If  $t(\lambda) > 0$  then Problem (4.21) is unbounded. Therefore, Problem (4.20) becomes equivalent to the following problem:

$$\min_{\lambda \in \mathbb{R}} \{ \lambda : t(\lambda) \leq 0 \}. \quad (4.24)$$

Note that  $t(\lambda)$  is non-increasing in  $\lambda$  and  $t(0) = \frac{U}{\bar{w}} > 0$ . Therefore, the optimal solution  $\lambda^*$  of Problem (4.24) is the solution of  $t(\lambda) = 0$ . Since  $t(\lambda)$  is a convex piecewise linear function of  $\lambda$ , Problem (4.24) can be solved by Newton's method, using subgradients (instead of gradients) as shown in Algorithm 3. At each iteration  $k$ ,  $-(\hat{\psi}^k, \hat{u}_y^k, 1, \hat{y}_k, \hat{v}_k)^T \mathbf{1}$ , where  $(\hat{\psi}^k, \hat{u}_y^k)$  and  $(\hat{y}_k, \hat{v}_k)$  are the solutions of  $t^1(\lambda^k)$  and  $t^2(\lambda^k)$  respectively, is a subgradient of  $t$  at  $\lambda^k$  and is denoted by  $\delta t(\lambda^k)$ . *Observe that Problems (4.22) and (4.23) are the counterparts to Problem (4.10) and (4.11), demonstrating that the subproblem decomposition carries over to the decomposition.*

## 4.7.2 An In-Out Approach

[140] proposed an acceleration scheme (the in-out method) for general cutting-plane algorithms. The method carefully chooses the separation point, rather than using the solution obtained from the RMP. The method considers two points: a feasible point  $x_{in}$  to Problem (4.15) and the optimal solution  $x_{out}$  of the RMP. It uses a convex combination of these two points when generating the separating cut, i.e., it solves Problem (4.9) with  $\hat{x} = \lambda x_{in} + (1 - \lambda)x_{out}$  for some  $\lambda \in (0, 1)$ .

[141] applied the in-out approach with an additional perturbation to solve facility location problems:

$$\hat{x} = \lambda x_{in} + (1 - \lambda)x_{out} + \epsilon \mathbf{1}, \quad (4.25)$$

for some  $\lambda \in (0, 1)$  and  $\epsilon > 0$ , and showed a computational improvement.

This chapter also employs the in-out approach equipped with some perturbation as [141]. It periodically finds  $x_{in}$  in a heuristic manner and chooses the separation point according to Equation (4.25). The implementation starts with  $\lambda = 0.5$  and  $\epsilon = 10^{-6}$  and decrease  $\lambda$  by half if the BD halts (i.e., it does not improve the optimality gap for more than 3 consecutive iterations). If the algorithm halts and  $\lambda$  is smaller than  $10^{-5}$ ,  $\epsilon$  is set to 0. After 3 more consecutive iterations without a lower bound improvement, the algorithm returns to the original BD. Whenever a new best incumbent solution is found, the in-out approach is applied again with this new feasible point.

## 4.8 Performance Analysis of the Dedicated Benders Method

This section studies the performance of the decomposition approach (Section 4.4) and the benefits of the acceleration schemes explained in Sections 4.7.1 and 4.7.2. All algorithms were implemented with the C++/Gurobi 8.0.1 interface and executed on an Intel Core i5 PC at 2.7 GHz with 8 GB of RAM. Each run has a wall-time limit of 1 hour.

### 4.8.1 Test Instances

Chapter 3 introduced the unit commitment problem with Gas Network Awareness (UCGNA), a tri-level optimization problem where the first and second levels determine how to commit and dispatch electric power generating units; The third level decides how to operate the gas network given the natural gas demands of committed gas-fueled generators that are determined in the first and second levels. The economic feedback from the gas network, i.e., the natural gas zonal prices, is given by the dual solution  $\psi$  of the third-level optimization and the first-level optimization is subject to constraints over both  $\psi$  and commitment decisions  $x$  in order to ensure the robustness of the unit commitment decisions against the economic feedback from the gas system. In Section 3.2.4, it is showed that the tri-level problem can be reformulated as a special case of MIBPSD discussed in Section 4.6. The evaluation of the proposed method is performed on the instances of the UCGNA problem.

The instances are based on the gas-grid test system, which is representative of the natural gas and electric power systems in the Northeastern United States [47]. There are 42 different instances, each of which constructed by uniformly increasing the demand of each system by some percentage;  $\eta_p$  denotes the stress level imposed on the power system which

takes values from  $\{1, 1.3, 1.6\}$  and  $\eta_g$  denotes the stress level of the gas system that has values of  $\{1, 1.1, \dots, 2.2, 2.3\}$ . For example,  $(\eta_p, \eta_g) = (1.3, 2.3)$  means the demands of the power and natural gas systems are increased uniformly by 30% and 130% respectively. Before we experiment the solution approaches on the instances of the UCGNA problem, we apply some preprocessing step which eliminates invalid bids with regard to a lower bound on natural gas zonal prices. Detailed description of the instances and the preprocessing step can be found in Section 3.3.

## 4.8.2 Computational Performance

This section compares three different solution approaches for MIBPSD:

- D: our dedicated Benders method (Section 4.4) with the acceleration schemes (Section 4.7);
- G: a state-of-the-art solver (Gurobi 8.0.1);
- B: the standard Benders method with the acceleration schemes (Section 4.7).

The implementation of D is sequential, although Problems (4.11)' and (4.19) can be solved independently (See Corollary 4.6.1). All solution approaches use the same values for the Gurobi parameters, i.e., the default values except `NumericFocus` set at 3, `DualReductions` at 0, `ScaleFlag` at 0, `BarQCPConvTol` at  $1e-7$ , and `Aggregate` at 0 for more rigorous attempts to detect and manage numerical issues.

Tables 4.1-4.3 report the computation times and optimality gaps of the three solution methods. The symbol † indicates that a method reaches the time limit and the symbol ‡ that the method did not find any incumbent solution.

The results for  $\eta_p = 1$  are summarized in Table 4.1. D timed out for two instances, G reached the time limit for 5 instances, and B timed out for all the instances. For the two instances with  $\eta_g = 1.8, 1.9$ , where all methods time out, D found incumbent solutions within optimality gaps of 1.8% and 1.3% and B found solutions with gaps of 6.7% and 10.6%. On the other hand, G did not find any incumbent solution. For easy instances that both D and G found optimal solutions within two minutes, G is faster than D by a factor of 2 in average.

For instances with  $\eta_p = 1.3$ , reported in Table 4.2, D and G timed out for 7 instances and B reached the time limit for all the instances. For the 7 instances with  $\eta_g = 1.6, \dots, 2.2$ , where all methods reached the time limit, D found incumbent solutions within 4.3% of optimality and B found worse solutions. On the other hand, G did not find any incumbent

Table 4.1: Computational Performance Comparison ( $\eta_p = 1$ ).

| Instance |          | D        |         | G        |         | B        |         |
|----------|----------|----------|---------|----------|---------|----------|---------|
| $\eta_p$ | $\eta_g$ | Time (s) | Gap (%) | Time (s) | Gap (%) | Time (s) | Gap (%) |
| 1        | 1        | 25.42    | 0.0     | 15.28    | 0.0     | †        | 6.8     |
|          | 1.1      | 25.91    | 0.0     | 23.24    | 0.0     | †        | 4.3     |
|          | 1.2      | 25.86    | 0.0     | 14.78    | 0.0     | †        | 2.2     |
|          | 1.3      | 29.33    | 0.0     | 31.17    | 0.0     | †        | 4.4     |
|          | 1.4      | 26.60    | 0.0     | 6.76     | 0.0     | †        | 2.6     |
|          | 1.5      | 25.80    | 0.0     | 13.24    | 0.0     | †        | 6.2     |
|          | 1.6      | 27.01    | 0.0     | 33.56    | 0.0     | †        | 3.1     |
|          | 1.7      | 100.82   | 0.0     | 22.78    | 0.0     | †        | 4.5     |
|          | 1.8      | †        | 1.8     | †        | ‡       | †        | 6.7     |
|          | 1.9      | †        | 1.3     | †        | ‡       | †        | 10.6    |
|          | 2.0      | 67.13    | 0.0     | †        | 1.3     | †        | 10.8    |
|          | 2.1      | 1091.88  | 0.0     | †        | 3.2     | †        | 20.0    |
|          | 2.2      | 566.94   | 0.0     | †        | 3.6     | †        | 19.1    |
| 2.3      | 31.52    | 0.0      | 15.94   | 0.0      | †       | 8.4      |         |

Table 4.2: Computational Performance Comparison ( $\eta_p = 1.3$ ).

| Instance |          | D        |         | G        |         | B        |         |
|----------|----------|----------|---------|----------|---------|----------|---------|
| $\eta_p$ | $\eta_g$ | Time (s) | Gap (%) | Time (s) | Gap (%) | Time (s) | Gap (%) |
| 1.3      | 1        | 31.01    | 0.0     | 4.37     | 0.0     | †        | 1.9     |
|          | 1.1      | 28.93    | 0.0     | 3.20     | 0.0     | †        | 2.8     |
|          | 1.2      | 30.87    | 0.0     | 3.28     | 0.0     | †        | 2.9     |
|          | 1.3      | 48.22    | 0.0     | 2.93     | 0.0     | †        | 3.3     |
|          | 1.4      | 32.69    | 0.0     | 12.07    | 0.0     | †        | 3.8     |
|          | 1.5      | 44.13    | 0.0     | 23.89    | 0.0     | †        | 2.2     |
|          | 1.6      | †        | 0.3     | †        | 0.2     | †        | 4.1     |
|          | 1.7      | †        | 3.5     | †        | ‡       | †        | 11.0    |
|          | 1.8      | †        | 3.2     | †        | ‡       | †        | 10.9    |
|          | 1.9      | †        | 3.3     | †        | ‡       | †        | 17.4    |
|          | 2        | †        | 4.2     | †        | 19.9    | †        | 14.9    |
|          | 2.1      | †        | 4.3     | †        | ‡       | †        | 9.7     |
|          | 2.2      | †        | 4.0     | †        | ‡       | †        | 14.8    |
| 2.3      | 43.23    | 0.0      | 10.43   | 0.0      | †       | 5.7      |         |

Table 4.3: Computational Performance Comparison ( $\eta_p = 1.6$ ).

| Instance |          | D        |         | G        |         | B        |         |
|----------|----------|----------|---------|----------|---------|----------|---------|
| $\eta_p$ | $\eta_g$ | Time (s) | Gap (%) | Time (s) | Gap (%) | Time (s) | Gap (%) |
|          | 1        | 43.51    | 0.0     | 4.33     | 0.0     | †        | 5.8     |
|          | 1.1      | 27.88    | 0.0     | 5.46     | 0.0     | †        | 2.8     |
|          | 1.2      | 26.63    | 0.0     | 7.67     | 0.0     | †        | 3.9     |
|          | 1.3      | 22.19    | 0.0     | 6.25     | 0.0     | †        | 2.7     |
|          | 1.4      | 29.75    | 0.0     | 6.35     | 0.0     | †        | 4.7     |
|          | 1.5      | 330.88   | 0.0     | 21.08    | 0.0     | †        | 7.0     |
| 1.6      | 1.6      | †        | 2.1     | †        | ‡       | †        | 9.7     |
|          | 1.7      | †        | 2.0     | †        | ‡       | †        | 8.1     |
|          | 1.8      | †        | 6.2     | †        | ‡       | †        | 17.1    |
|          | 1.9      | †        | 7.4     | †        | ‡       | †        | 11.5    |
|          | 2        | †        | 3.7     | †        | ‡       | †        | 8.7     |
|          | 2.1      | †        | 5.0     | †        | ‡       | †        | 9.1     |
|          | 2.2      | †        | 5.0     | †        | ‡       | †        | 9.0     |
|          | 2.3      | 12.44    | 0.0     | 3.76     | 0.0     | †        | 3.9     |

solution except the two instances with  $\eta_g = 1.6$  and 2. For easy instances that both D and G found optimal solutions within two minutes, G is faster than D by a factor of around 7 in average.

Instances with  $\eta_p = 1.6$  display similar behaviors. While B failed to find optimal solutions for all the instances, D and G found optimal solutions for 7 instances. For the hard instances where all methods timed out, D found incumbent solutions with optimality gaps less than 7.5%, B found worse solutions, and G failed to find any incumbent solution. For the instances where both D and G found optimal solutions, G is faster than D.

To compare the computational performance of D and G more precisely, Figure 4.1 visualizes the performance of D and G for all the instances. Figure 4.1a reports the computation times of D and G, Figure 4.1b displays the optimality gaps of the two methods for all the instances, and the reference lines (in red) serve to delineate when a method is faster than the other. For Figure 4.1b, the axes are in logarithmic scale and a 100% optimality gap is assigned to instances with no incumbent. The figure indicates that, although D is slower than G for some easy instances (the points at the bottom left corner of Figure 4.1a), it has notable benefits for hard instances (the points in the upper left side of sections/bilevel/Figures 4.1a and 4.1b).

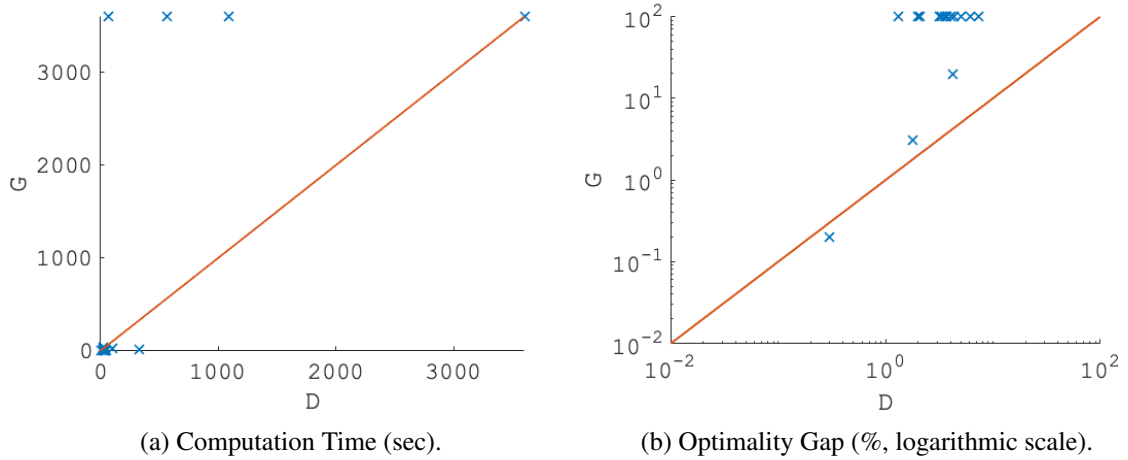


Figure 4.1: D vs G.

### 4.8.3 Benefits of the Acceleration Schemes

This section studies the benefits of the acceleration schemes by comparing the performance of the dedicated Benders method with different combinations of acceleration schemes applied. It uses  $D(n_k, i_k)$  to denote the dedicated Benders method with acceleration schemes  $(n_k, i_k)$  where

- $n_k$ :  $k = 1$  if the normalization scheme is applied;  $k = 0$  otherwise;
- $i_k$ :  $k = 1$  if the in-out approach is applied;  $k = 0$  otherwise.

Tables 4.4-4.6 summarize the computational performance of the dedicated Benders methods with the four combinations of acceleration schemes.

Table 4.4 displays the computation times and optimality gaps for instances with  $\eta_p = 1$ . Without the in-out approach,  $D(n_1, i_0)$  and  $D(n_0, i_0)$  timed out for all instances. Although both  $D(n_1, i_0)$  and  $D(n_0, i_0)$  reach the time limit for all instances, the normalization scheme does improve optimality gaps. On the other hand, with the in-out approach,  $D(n_0, i_1)$  solves 10 instances within 100 seconds. However,  $D(n_0, i_1)$  still cannot solve the two instances with  $\eta_g = 2.1, 2.2$ . The slight increase in computation time of  $D(n_1, i_1)$  for some instances, compared to  $D(n_0, i_1)$ , is due to the additional computation time required to find a normalized ray.

The results for instances with  $\eta_p = 1.3$  are reported in Table 4.5. Again, without the in-out approach,  $D(n_1, i_0)$  and  $D(n_0, i_0)$  timed out for all instances, but  $D(n_1, i_0)$  has significant improvement in optimality gaps for some instances. With the in-out approach,  $D(n_0, i_1)$  solved 7 instances within 150 seconds and so did  $D(n_1, i_1)$ . The normalization scheme does

Table 4.4: Benefits of the Acceleration Schemes ( $\eta_p = 1$ ).

| $\eta_g$ | D ( $n_1, i_1$ ) |         | D ( $n_0, i_1$ ) |         | D ( $n_1, i_0$ ) |         | D ( $n_0, i_0$ ) |         |
|----------|------------------|---------|------------------|---------|------------------|---------|------------------|---------|
|          | Time (s)         | Gap (%) |
| 1        | 25.42            | 0.00    | 30.61            | 0.00    | †                | 49.38   | †                | 52.65   |
| 1.1      | 25.91            | 0.00    | 25.39            | 0.00    | †                | 50.70   | †                | 52.53   |
| 1.2      | 25.86            | 0.00    | 25.35            | 0.00    | †                | 51.13   | †                | 53.59   |
| 1.3      | 29.33            | 0.00    | 28.19            | 0.00    | †                | 50.82   | †                | 52.67   |
| 1.4      | 26.60            | 0.00    | 26.74            | 0.00    | †                | 53.15   | †                | 53.20   |
| 1.5      | 25.80            | 0.00    | 27.51            | 0.00    | †                | 51.99   | †                | 52.63   |
| 1.6      | 27.01            | 0.00    | 25.90            | 0.00    | †                | 38.88   | †                | 53.36   |
| 1.7      | 100.82           | 0.00    | 98.52            | 0.00    | †                | 19.33   | †                | 53.30   |
| 1.8      | †                | 1.77    | †                | 1.42    | †                | 3.09    | †                | 52.81   |
| 1.9      | †                | 1.32    | †                | 1.47    | †                | 1.52    | †                | 53.36   |
| 2        | 67.13            | 0.00    | 58.85            | 0.00    | †                | 9.17    | †                | 52.96   |
| 2.1      | 1091.88          | 0.00    | †                | 4.80    | †                | 4.52    | †                | 52.56   |
| 2.2      | 566.94           | 0.00    | †                | 4.45    | †                | 5.23    | †                | 53.46   |
| 2.3      | 31.52            | 0.00    | 23.85            | 0.00    | †                | 38.59   | †                | 52.97   |

Table 4.5: Benefits of the Acceleration Schemes ( $\eta_p = 1.3$ ).

| $\eta_g$ | D ( $n_1, i_1$ ) |         | D ( $n_0, i_1$ ) |         | D ( $n_1, i_0$ ) |         | D ( $n_0, i_0$ ) |         |
|----------|------------------|---------|------------------|---------|------------------|---------|------------------|---------|
|          | Time (s)         | Gap (%) |
| 1        | 31.01            | 0.00    | 30.83            | 0.00    | †                | 63.96   | †                | 63.78   |
| 1.1      | 28.93            | 0.00    | 27.83            | 0.00    | †                | 54.30   | †                | 63.93   |
| 1.2      | 30.87            | 0.00    | 143.36           | 0.00    | †                | 60.95   | †                | 63.65   |
| 1.3      | 48.22            | 0.00    | 52.89            | 0.00    | †                | 56.01   | †                | 64.09   |
| 1.4      | 32.69            | 0.00    | 31.04            | 0.00    | †                | 51.67   | †                | 64.85   |
| 1.5      | 44.13            | 0.00    | 44.98            | 0.00    | †                | 53.98   | †                | 64.80   |
| 1.6      | †                | 0.31    | †                | 1.08    | †                | 1.94    | †                | 65.07   |
| 1.7      | †                | 3.53    | †                | 5.34    | †                | 3.42    | †                | 65.99   |
| 1.8      | †                | 3.15    | †                | 4.01    | †                | 3.73    | †                | 65.92   |
| 1.9      | †                | 3.26    | †                | 8.28    | †                | 7.97    | †                | 66.22   |
| 2        | †                | 4.24    | †                | 4.59    | †                | 4.51    | †                | 64.58   |
| 2.1      | †                | 4.27    | †                | 4.12    | †                | 4.29    | †                | 63.36   |
| 2.2      | †                | 4.03    | †                | 4.07    | †                | 4.08    | †                | 64.46   |
| 2.3      | 43.23            | 0.00    | 48.06            | 0.00    | †                | 14.51   | †                | 62.93   |

Table 4.6: Benefits of the Acceleration Schemes ( $\eta_p = 1.6$ ).

| $\eta_g$ | $D(n_1, i_1)$ |         | $D(n_0, i_1)$ |         | $D(n_1, i_0)$ |         | $D(n_0, i_0)$ |         |
|----------|---------------|---------|---------------|---------|---------------|---------|---------------|---------|
|          | Time (s)      | Gap (%) |
| 1        | 43.51         | 0.00    | 44.01         | 0.00    | †             | 45.17   | †             | 69.59   |
| 1.1      | 27.88         | 0.00    | 26.88         | 0.00    | †             | 59.44   | †             | 69.33   |
| 1.2      | 26.63         | 0.00    | 26.84         | 0.00    | †             | 14.54   | †             | 69.51   |
| 1.3      | 22.19         | 0.00    | 30.55         | 0.00    | †             | 34.22   | †             | 69.81   |
| 1.4      | 29.75         | 0.00    | 30.51         | 0.00    | †             | 6.91    | †             | 69.95   |
| 1.5      | 330.88        | 0.00    | 208.22        | 0.00    | †             | 2.58    | †             | 71.69   |
| 1.6      | †             | 2.10    | †             | 2.09    | †             | 2.13    | †             | 71.43   |
| 1.7      | †             | 2.05    | †             | 3.84    | †             | 2.11    | †             | 71.73   |
| 1.8      | †             | 6.16    | †             | 7.80    | †             | 6.68    | †             | 71.86   |
| 1.9      | †             | 7.43    | †             | 7.62    | †             | 7.49    | †             | 71.80   |
| 2        | †             | 3.75    | †             | 3.81    | †             | 3.77    | †             | 67.66   |
| 2.1      | †             | 5.04    | †             | 5.15    | †             | 5.05    | †             | 68.12   |
| 2.2      | †             | 5.01    | †             | 5.15    | †             | 5.01    | †             | 67.27   |
| 2.3      | 12.44         | 0.00    | 13.75         | 0.00    | 73.32         | 0.00    | †             | 67.84   |

have some computational benefits, as  $D(n_1, i_1)$  has smaller optimality gaps than  $D(n_0, i_1)$  for the remaining 7 instances except one instance with  $\eta_g = 2.2$ . Moreover, for some hard instances where  $D(n_0, i_1)$  reached the time limit,  $D(n_1, i_0)$  has smaller optimality gaps (i.e.,  $\eta_g = 1.7, \dots, 2$ ).

The acceleration schemes display similar behaviors for instances with  $\eta_p = 1.6$ . Without the in-out approach,  $D(n_0, i_0)$  timed out for all instances, while  $D(n_1, i_0)$  solves one instance to optimality and has significant improvements in optimality gaps. With the in-out approach, both  $D(n_0, i_1)$  and  $D(n_1, i_1)$  solve 7 instances within 350 seconds, and  $D(n_1, i_1)$  has smaller optimality gaps for the unsolved instances. Again, for some hard instances for which  $D(n_0, i_1)$  reached the time limit,  $D(n_1, i_0)$  has smaller optimality gaps (i.e.,  $\eta_g = 1.7, \dots, 2.2$ ).

#### 4.8.4 Benefits of the Decomposition Method

Section 4.8.2 indicated that the decomposition method has significant benefits for solving MIBPSD. The decomposition method not only shortens computation times required for solving the dual of the inner-continuous problem, but also allows us to address the numerical issues of MIBPSD.

Figure 4.2 displays the average computation time for generating a Benders cut, where

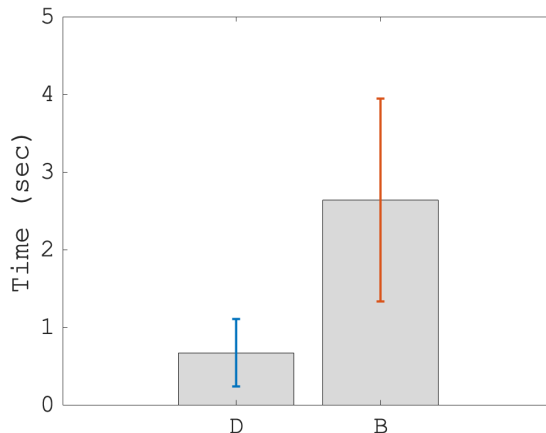


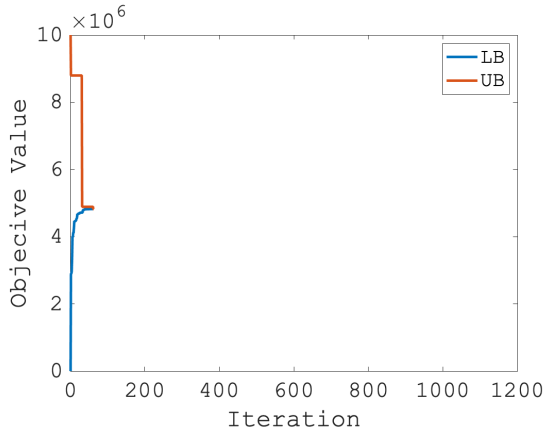
Figure 4.2: Statistics on Computation Times for Cut Generation.

the error bars represent the standard deviation. In average, the cut generation time of D is faster than B by a factor of 3.94. Since the subproblems that D solves to generate cuts (i.e., Problems (4.11)' and (4.10)) can be solved independently, an implementation in parallel computing would improve the computation time even further.

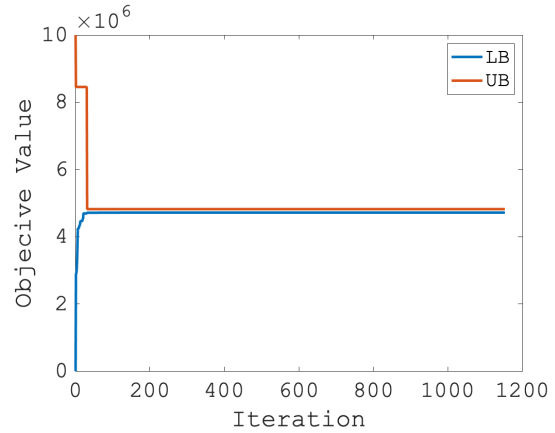
Moreover, the decomposition method deals better with numerical issues arising from the complex inner-continuous problem of MIBPSD. Figure 4.3 displays the convergence behavior of D and B for two instances,  $(\eta_p, \eta_g) = (1, 1.2), (1.6, 1.8)$ . For instance  $(\eta_p, \eta_g) = (1, 1.2)$  (i.e., Figure 4.3a and Figure 4.3b), D closes the gap in 30 seconds, but B does not improve its lower bound even if it finds a good incumbent solution early. For instance  $(\eta_p, \eta_g) = (1.6, 1.8)$  (i.e., Figure 4.3c and Figure 4.3d), although both D and B timed out, B improves its lower bound much slower than D. This behavior of B is explained by the fact that it suffers from numerical issues when solving Problem (4.9); it sometimes terminates with an optimal solution even if there exists an unbounded ray. This incorrect evaluation of the first-stage variable leads to ineffective cut generation and a slower convergence rate. On the other hand, the decomposition method effectively decomposes Problem (4.9) into two more stable and smaller problems, which addresses the numerical issues effectively.

## 4.9 Concluding Remarks

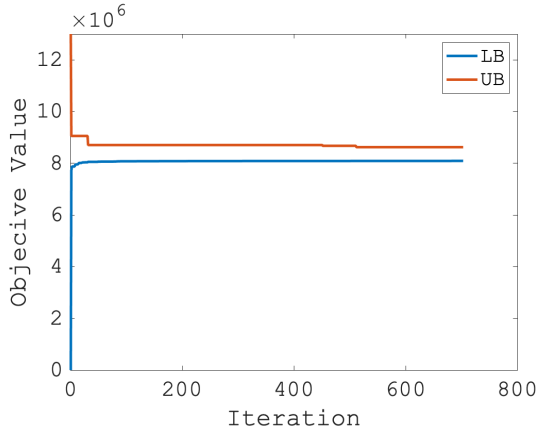
MIBPSD is an important class of hierarchical optimization model that arises in many practical contexts, including network planning/design problems in energy systems and transportation networks, facility location problems, and unit scheduling problems under interdependent markets.



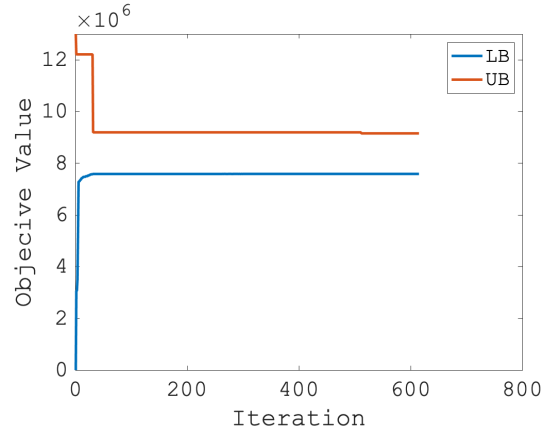
(a) D,  $(\eta_p, \eta_g) = (1, 1.2)$ .



(b) B,  $(\eta_p, \eta_g) = (1, 1.2)$ .



(c) D,  $(\eta_p, \eta_g) = (1.6, 1.8)$ .



(d) B,  $(\eta_p, \eta_g) = (1.6, 1.8)$ .

Figure 4.3: Convergence Behaviors of D and B.

This chapter proposed a dedicated Benders decomposition algorithm to solve MIBPSD models, recognizing that the Benders subproblem is not necessarily easy to solve for large MIBPSD problems. The dedicated approach decomposes the Benders subproblem into two more tractable, sequentially solvable problems that are closely related to the leader and the follower problems. It is shown that the Benders subproblem decomposition can also be applied to the extension of MIBPSD where the upper level problem has additional constraints on the leader variables and the follower dual variables. In this chapter, a couple of subclasses of MIBPSD were discussed, which allows for sequence-independent subproblem decomposition. In addition, the chapter showed how to adapt existing acceleration schemes to this decomposition. In particular, it showed how to normalize Benders feasibility cuts using a Newton's (subgradient) method and how to carefully choose the separation points using the in-out approach [140].

The resulting Benders method significantly improves the performance of a standard Benders method and outperforms a state-of-the-art mathematical-programming solvers for hard instances. The experimental results highlighted the benefits of acceleration schemes—normalizing feasibility rays and the in-out approach—and demonstrated that decomposing the Benders subproblem not only shortens the computation time for generating Benders cuts but also addresses the numerical issues arising when solving complex Benders subproblems.

## CHAPTER 5

# Conclusions

In this thesis, we study some challenges that current infrastructure systems—especially, electric power systems—face and develop both mathematical modeling and their solution approaches for coping with those challenges.

More specifically, we study (i) in Chapter 2 how to build resiliency in electricity distribution grids by leveraging microgrid technologies as well as traditional network hardening measures. To make such decisions, a two-stage mixed-integer linear optimization model with a feasibility recourse and nonanticipativity-type constraints in the first stage is proposed. We develop a branch-and-price algorithm equipped with several acceleration schemes for solving the model that tackles its large-scale and complexity using parallel computing. We then investigate (ii) in Chapters 3 and 4 how to operate electricity systems while effectively handling—both economic and physical—risks that could be propagated back by the natural gas networks. We model this decision-making problem as a bilevel optimization model where the first level makes binary operational decisions (i.e., the unit commitment decision) and the second level makes a continuous operational decision (i.e., dispatch decision for joint electricity and natural gas systems) in response to the leader’s binary decision. A Benders subproblem decomposition technique has been developed for solving this class of optimization models. The models proposed in this thesis show that taking account of risks from interdependencies plays an important role in building resiliency and enhancing the reliability of these systems. It has been also demonstrated that the developed solution methods have improved computational properties over existing methods.

Possible future directions include:

- Developing network decomposition technique for solving large-scale mixed-integer optimization problems defined on a huge network;
- Utilizing machine learning/cutting-plane techniques for accelerating the column generation and Benders decomposition methods;

- Incorporating uncertainties arising in power systems (e.g., renewable energy) into the proposed models and applying the proposed models for a wider range of applications (e.g., cyber-security and dynamic pricing).

## APPENDIX A

### Appendix for Chapter 2

#### A.1 Proof of Proposition 2.5.1

**Proof.** Since  $(P)$  and  $(\tilde{P})$  have the same objective function, it suffices to show that  $(P)$  has an optimal solution that is feasible to  $(\tilde{P})$  and vice versa. Let  $(\bar{w}, \{\bar{w}^s\}_{s \in \mathcal{S}})$  be the optimal solution of  $(P)$ . By the Farkas-Minkowski-Weyl theorem [142], for each  $s \in \mathcal{S}$ ,  $\bar{w}^s$  can be expressed as a convex combination of extreme points in  $\mathcal{J}^s$ , i.e.,  $\exists \{\bar{\lambda}_j^s\}_{j \in \mathcal{J}^s} : \bar{w}^s = \sum_{j \in \mathcal{J}^s} \bar{\lambda}_j^s \hat{w}_j^s, \sum_{j \in \mathcal{J}^s} \bar{\lambda}_j^s = 1$ . Hence,  $(\bar{w}, \{\bar{\lambda}_j^s\}_{j \in \mathcal{J}^s} \text{ for } s \in \mathcal{S})$  is feasible to  $(\tilde{P})$ .  $\square$

## APPENDIX B

### Appendix for Chapter 3

#### B.1 Equivalence of Problem (3.6) to a Two-Level Problem

Consider the following two-level problem:

$$\min_{\substack{\mathbf{x}_e \geq 0, \mathbf{y}_g \\ \mathbf{z}_e \in \{0,1\}^m}} c_e^T \mathbf{x}_e + h^T \mathbf{z}_e \quad (\text{B.1a})$$

$$\text{s.t. } \mathbf{z}_e \in \mathcal{Z}, \quad (\text{B.1b})$$

$$A\mathbf{x}_e + B\mathbf{z}_e \geq b, \quad (\text{B.1c})$$

$$\mathbf{y}_g \in \text{Dual sol. of } \min_{\mathbf{x}_g \in \mathcal{K}} c_g^T \mathbf{x}_g \quad (\text{B.1d})$$

$$\text{s.t. } D_e \mathbf{x}_e + D_g \mathbf{x}_g \geq d, \quad (\text{B.1e})$$

$$E\mathbf{y}_g + M\mathbf{z}_e \geq h, \quad (\text{B.1f})$$

where the first level (i.e. Equations (B.1a), (B.1b), and (B.1c)) represents the power system's action taken by UC/ED problem, and the second level problem represents the response of the natural gas system (i.e., natural gas price  $\mathbf{y}_g$ ). In addition, the bid validity constraint (i.e., Constraint (B.1f)) affects the power system's commitment decisions based on the response of the gas system. Hence the power system can be viewed as a “leader” and the gas system as a “follower” in the Stackelberg game.

Let  $(\hat{\mathbf{z}}_e, \hat{\mathbf{x}}_e, \hat{\mathbf{y}}_g)$  be a feasible solution of Problem (3.6). Then, it is easy to see that  $(\hat{\mathbf{z}}_e, \hat{\mathbf{x}}_e, \hat{\mathbf{y}}_g)$  is also a feasible solution to Problem (B.1) with the same objective function value.

Conversely, consider a feasible solution to Problem (B.1),  $(\tilde{\mathbf{z}}_e, \tilde{\mathbf{x}}_e, \tilde{\mathbf{y}}_g)$ . Note that, with  $\mathbf{z}_e$  fixed to  $\tilde{\mathbf{z}}_e \in \mathcal{Z}$ ,  $(\tilde{\mathbf{x}}_e, \tilde{\mathbf{y}}_g)$  is also an optimal solution of the lower level problem of

Problem (3.6). This is because the second level decision (i.e.,  $\mathbf{x}_e$ ) is not affected by the third level decision, thus  $\mathbf{x}_e = \tilde{\mathbf{x}}_e$  is an optimal solution of the second level problem. Then, when  $\mathbf{x}_e$  fixed to  $\tilde{\mathbf{x}}_e$ ,  $\mathbf{y}_g = \tilde{\mathbf{y}}_g$  is a valid response of the gas system. Accordingly, Constraint (B.1f) is satisfied and hence  $(\tilde{\mathbf{z}}_e, \tilde{\mathbf{x}}_e, \tilde{\mathbf{y}}_g)$  is feasible for Problem (3.6) with the same objective value. Therefore, the two problems are equivalent.

## B.2 Proof of Proposition 3.2.1

By strong duality of the third-level optimization in Problem (3.6), the lower-level problem (i.e., second- and third-level) of Problem (3.6) is equivalent to:

$$(\mathbf{x}_e, \mathbf{y}_g) \in \underset{\mathbf{x}_e \geq 0, \mathbf{y}_g}{\operatorname{argmin}} c_e^T \mathbf{x}_e \quad (\text{B.2a})$$

$$\text{s.t.} \quad A\mathbf{x}_e + B\mathbf{z}_e \geq b, \quad (\text{B.2b})$$

$$(\mathbf{x}_g, \mathbf{y}_g) \in \underset{\mathbf{x}_g \in \mathcal{K}, \mathbf{y}_g \geq 0}{\operatorname{argmin}} c_g^T \mathbf{x}_g$$

$$\text{s.t.} \quad D_e \mathbf{x}_e + D_g \mathbf{x}_g \geq d, \quad (\text{B.2c})$$

$$\mathbf{y}_g^T (d - D_e \mathbf{x}_e) \geq c_g^T \mathbf{x}_g,$$

$$\mathbf{y}_g^T D_g \preceq_{\mathcal{K}^*} c_g.$$

where  $\mathcal{K}^*$  denotes the dual cone of  $\mathcal{K}$ . The first and third constraints of Problem (B.2c) state the primal and dual feasibility of the third-level problem, while the second constraint ensures their optimality.

Equation (B.2b) (i.e., the constraint of the upper level problem of Problem (B.2)) does not involve the lower-level variables (i.e.,  $\mathbf{x}_g$  and  $\mathbf{y}_g$  of Problem (B.2c)), which means the upper-level solution is not affected by the solutions to the lower-level problem. Problem (B.2) can thus be solved in two steps: (i) solve the upper-level problem and obtain  $\bar{\mathbf{x}}_e$ , (ii) solve the lower-level problem with  $\mathbf{x}_e$  fixed as  $\bar{\mathbf{x}}_e$  and obtain  $\bar{\mathbf{y}}_g$ . Accordingly, Problem (B.2) can be expressed as a Lexicographic optimization [143] as follows:

$$(\mathbf{x}_e, \mathbf{x}_g, \mathbf{y}_g) \in \underset{\mathbf{x}_e \geq 0, \mathbf{x}_g \in \mathcal{K}, \mathbf{y}_g \geq 0}{\operatorname{argmin}} \langle c_e^T \mathbf{x}_e, c_g^T \mathbf{x}_g \rangle \quad (\text{B.3a})$$

$$\text{s.t.} \quad A\mathbf{x}_e + B\mathbf{z}_e \geq b, \quad (\text{B.3b})$$

$$D_e \mathbf{x}_e + D_g \mathbf{x}_g \geq d, \quad (\text{B.3c})$$

$$\mathbf{y}_g^T (d - D_e \mathbf{x}_e) \geq c_g^T \mathbf{x}_g, \quad (\text{B.3d})$$

$$\mathbf{y}_g^T D_g \preceq_{\mathcal{K}^*} c_g. \quad (\text{B.3e})$$

An optimal solution  $(\bar{x}_e, \bar{x}_g, \bar{y}_g)$  of Problem (B.3) satisfies the following conditions:

$$\bar{x}_e \in \underset{\mathbf{x}_e \geq 0}{\operatorname{argmin}} c_e^T \mathbf{x}_e \quad (\text{B.4a})$$

$$\text{s.t. } A\mathbf{x}_e \geq b - B\mathbf{z}_e, \quad (\text{B.4b})$$

$$D_e \mathbf{x}_e + D_g \mathbf{x}_g \geq d, \mathbf{x}_g \in \mathcal{K}. \quad (\text{B.4c})$$

$$(\bar{x}_g, \bar{y}_g) \in \underset{\mathbf{x}_g \in \mathcal{K}, \mathbf{y}_g \geq 0}{\operatorname{argmin}} c_g^T \mathbf{x}_g \quad (\text{B.5a})$$

$$\text{s.t. } D_g \mathbf{x}_g \geq d - D_e \bar{x}_e, \quad (\text{B.5b})$$

$$\mathbf{y}_g^T (d - D_e \bar{x}_e) \geq c_g^T \mathbf{x}_g, \quad (\text{B.5c})$$

$$\mathbf{y}_g^T D_g \preceq_{\mathcal{K}^*} c_g. \quad (\text{B.5d})$$

Observe that any feasible  $(\hat{x}_g, \hat{y}_g)$  of Problem (B.5) is optimal. That is because, by strong duality forced in Equation (B.5c),  $(\hat{x}_g, \hat{y}_g)$  satisfies the following conditions:

$$\hat{x}_g \in \underset{\mathbf{x}_g \in \mathcal{K}}{\operatorname{argmin}} c_g^T \mathbf{x}_g \quad (\text{B.6a})$$

$$\text{s.t. } D_g \mathbf{x}_g \geq d - D_e \bar{x}_e. \quad (\text{B.6b})$$

$$\hat{y}_g \in \underset{\mathbf{y}_g \geq 0}{\operatorname{argmax}} \mathbf{y}_g^T (d - D_e \bar{x}_e) \quad (\text{B.7a})$$

$$\text{s.t. } \mathbf{y}_g^T D_g \preceq_{\mathcal{K}^*} c_g. \quad (\text{B.7b})$$

Accordingly, using the weighted-sum method [143] for Lexicographic optimization problems and the optimality conditions of Problem (B.3), given in Problems (B.4) and (B.6)-(B.7), we approximate Problem (B.3) as Problem (3.9). As a result, Problem (3.6)

can be approximated by Problem (3.8). Note that the objective function and Equation (3.8d) in the first level need to be adjusted in terms of  $\alpha$ , since  $\alpha$  scales the dual solution.

It remains to show that Problem (3.8) is indeed an asymptotic approximation of Problem (3.6). By strong duality of Problem (3.9), it can be expressed as follows:

$$\min \delta h^T \mathbf{z}_e + \delta c_e^T \mathbf{x}_e + (1 - \delta) c_g^T \mathbf{x}_g \quad (\text{B.8a})$$

$$\text{s.t. } \mathbf{z}_e \in \mathcal{Z}, \mathbf{z}_e \in \{0, 1\}^m, \quad (\text{B.8b})$$

$$A \mathbf{x}_e + B \mathbf{z}_e \geq b, \quad (\text{B.8c})$$

$$D_e \mathbf{x}_e + D_g \mathbf{x}_g \geq d, \quad (\text{B.8d})$$

$$\mathbf{y}_e^T (b - B \mathbf{z}_e) + \mathbf{y}_g^T d \geq \delta c_e^T \mathbf{x}_e + (1 - \delta) c_g^T \mathbf{x}_g, \quad (\text{B.8e})$$

$$\mathbf{y}_g^T D_g \preceq_{\mathcal{K}^*} (1 - \delta) c_g^T, \quad (\text{B.8f})$$

$$\mathbf{y}_e^T A + \mathbf{y}_g^T D_e \leq \delta c_e^T, \quad (\text{B.8g})$$

$$\frac{1}{1 - \delta} E \mathbf{y}_g + M \mathbf{z}_e \geq h, \quad (\text{B.8h})$$

$$\mathbf{x}_e \geq 0, \mathbf{x}_g \in \mathcal{K}, \quad (\text{B.8i})$$

$$\mathbf{y}_e \geq 0, \mathbf{y}_g \geq 0, \quad (\text{B.8j})$$

Replacing  $y_e$  with  $y_e/\delta$  and  $y_g$  with  $y_g/(1 - \delta)$  in Problem (B.8) gives the following equivalent problem:

$$\min \delta h^T \mathbf{z}_e + \delta c_e^T \mathbf{x}_e + (1 - \delta) c_g^T \mathbf{x}_g \quad (\text{B.9a})$$

$$\text{s.t. } \mathbf{z}_e \in \mathcal{Z}, \quad (\text{B.9b})$$

$$A \mathbf{x}_e + B \mathbf{z}_e \geq b, \quad (\text{B.9c})$$

$$D_e \mathbf{x}_e + D_g \mathbf{x}_g \geq d, \quad (\text{B.9d})$$

$$\mathbf{y}_e^T (b - B \mathbf{z}_e) - c_e^T \mathbf{x}_e \geq \frac{1 - \delta}{\delta} [c_g^T \mathbf{x}_g - \mathbf{y}_g^T d], \quad (\text{B.9e})$$

$$\mathbf{y}_g^T D_g \preceq_{\mathcal{K}^*} c_g^T, \quad (\text{B.9f})$$

$$\mathbf{y}_e^T A + \frac{1 - \delta}{\delta} \mathbf{y}_g^T D_e \leq c_e^T, \quad (\text{B.9g})$$

$$E \mathbf{y}_g + M \mathbf{z}_e \geq h, \quad (\text{B.9h})$$

$$\mathbf{x}_e \geq 0, \mathbf{x}_g \in \mathcal{K}, \mathbf{y}_e \geq 0, \mathbf{y}_g \geq 0, \quad (\text{B.9i})$$

$$\mathbf{z}_e \in \{0, 1\}^m. \quad (\text{B.9j})$$

Let  $P(\hat{z}_e)$  and  $\hat{P}(\hat{z}_e)$  denote Problems (B.3) and (B.9) in which the binary variables  $\mathbf{z}_e$  are fixed to some  $\hat{z}_e \in \{0, 1\}^m$ . Let  $(\hat{x}_e, \hat{x}_g, \hat{y}_e, \hat{y}_g)$  be the optimal solution of  $\hat{P}(\hat{z}_e)$ . Note that, as  $\delta \rightarrow 1$ , Equations (B.9e) and (B.9g) become as follows:

$$\mathbf{y}_e^T (b - B\hat{z}_e) \geq c_e^T \mathbf{x}_e, \quad (\text{B.10a})$$

$$\mathbf{y}_e^T A \leq c_e^T, \quad (\text{B.10b})$$

which implies that  $\hat{x}_e$  and  $\hat{y}_e$  approximate the optimal primal and dual solutions of Problem (B.4) when  $\mathbf{z}_e$  is fixed as  $\hat{z}_e$ . This is because  $\hat{x}_e$  is feasible for (B.4) (by Equation (B.9c)),  $(\hat{y}_e, 0)$  becomes feasible to the dual of Problem (B.4) as  $\delta$  approaches 1 (by Equation (B.10b)), and together they satisfy the strong duality condition of Equation (B.10a) as  $\delta$  becomes closer to 1 (by Equation (B.10a)). Therefore, as  $\delta \rightarrow 1$ ,  $(\hat{x}_e, \hat{y}_e)$  becomes a feasible solutions of  $P(\hat{z}_e)$  and has the same optimal objective value.

Moreover, combining Equations (B.9e) and (B.9g) gives

$$\begin{aligned} & (\text{Equation (B.9e)}) - \hat{x}_e \times (\text{Equation (B.9g)}) \\ \rightarrow & \hat{y}_e^T (b - B\hat{z}_e - A\hat{x}_e) + \frac{1-\delta}{\delta} \hat{y}_g^T (d - D_e \hat{x}_e) \geq \frac{1-\delta}{\delta} c_g^T \hat{x}_g \\ \rightarrow & \hat{y}_g^T (d - D_e \hat{x}_e) \geq c_g^T \hat{x}_g, \end{aligned} \quad (\text{B.11a})$$

where the last derivation follows from Equation (B.9c) and  $y_g \geq 0$ . Therefore,  $\hat{x}_g$  and  $\hat{y}_g$  are the optimal solutions of Problem (B.5) when  $x_e$  is fixed as  $\hat{x}_e$  (since its feasibility is guaranteed by Equations (B.9d) and (B.9f), while the optimality is guaranteed by Equation (B.11a)).

In summary,  $\hat{x}_e$  is an approximate solution of  $P(\hat{z}_e)$  that becomes increasingly close to the optimal solution of Problem  $P(\hat{z}_e)$  as  $\delta \rightarrow 1$ , and  $\hat{y}_g$  is the exact response of the follower with respect to  $\hat{x}_e$  for any  $\delta \in (0, 1)$ . Therefore, the approximation may sacrifice the leader's optimality when  $\delta$  is not large enough, but it always gives a feasible solution.  $\square$

## APPENDIX C

### Appendix for Chapter 4

#### C.1 Proof of Theorem 4.4.1

The proof strategy is to show that there is a surjective mapping from the possible outcomes of Problems (4.10) and (4.11) to those of Problem (4.9), which implies that Problem (4.9) is completely determined by Problems (4.10) and (4.11).

Let  $U_{(i)}$  and  $F_{(i)}$  respectively denote the unbounded and finite outcome of Problem ( $i$ ) for  $i \in \{4.9, 4.10, 4.11\}$ . Due to Remark 4.4.2, the combination of all possible outcomes of Problems (4.10) and (4.11) are given by

$$\mathcal{A} = \{(U_{(4.10)}, U_{(4.11)}), (U_{(4.10)}, F_{(4.11)}), (F_{(4.10)}, U_{(4.11)}), (F_{(4.10)}, F_{(4.11)})\}.$$

Likewise, the possible outcomes of Problem (4.9) can be expressed as  $\mathcal{B} = \{U_{(4.9)}, F_{(4.9)}\}$ . The proof gives a surjective mapping  $g : \mathcal{A} \rightarrow \mathcal{B}$ , showing the solution of Problem (4.9) can be obtained from the solutions of Problems (4.10) and (4.11).

1. Outcome  $U_{(4.10)}$ : Let  $(\tilde{y}, \tilde{v})$  be the unbounded ray of Problem (4.10) and  $\mathcal{U} := d^T \tilde{y} - \tilde{v}(k + K_x \hat{x}) < 0$ . Note that, by construction,  $\mathcal{O} = \infty$  and thus, without loss of generality, we can assume  $w$  to be zero in Problem (4.11).
  - (a) Outcome  $U_{(4.11)}$ : Let  $(\tilde{\psi}, \tilde{u}_y, 0)$  be the unbounded ray of Problem (4.11). Then  $\tilde{\mu}_1 := (0, 0, 0, \tilde{y}, \tilde{v})$  and  $\tilde{\mu}_2 := (\tilde{\psi}, \tilde{u}_y, 0, 0, 0)$  are respectively an unbounded ray of Problem (4.9) and Problem (4.9) is unbounded.
  - (b) Outcome  $F_{(4.11)}$ : Let  $(\hat{\psi}, \hat{u}_y, 0)$  be the optimal solution of Problem (4.11) and let  $\mathcal{O}_{(4.11)}$  denote its optimal objective value. Then, for any  $\alpha > 0$ ,  $(\hat{\psi}, \hat{u}_y, 0, 0, 0) + \alpha(0, 0, 0, \tilde{y}, \tilde{v})$  is a feasible solution to Problem (4.9) and has an objective value of  $\mathcal{O}_{(4.11)} - \alpha\mathcal{U}$ , which increases as  $\alpha$  increases. Hence  $\tilde{\mu}_1$  is an unbounded ray of Problem (4.9) and Problem (4.9) is unbounded.

2. Outcome  $F_{(4.10)}$ : Let  $(\hat{y}, \hat{v})$  be the optimal solution of Problem (4.10) and, by construction,  $\mathcal{O}$  denotes its optimal objective value.

- (a) Outcome  $U_{(4.11)}$ : Let  $(\tilde{\psi}, \tilde{u}_y, \tilde{w})$  denote the unbounded ray of Problem (4.11). Note that  $\tilde{\mu}_3 := (\tilde{\psi}, \tilde{u}_y, \tilde{w}, \tilde{w}\hat{y}, \tilde{w}\hat{v})$  is a feasible ray to Problem (4.9) and has a positive objective value of  $\tilde{\psi}^T(b - A\hat{x}) + \tilde{u}_y^T(h_y - G_{xy}\hat{x}) - \mathcal{O}w > 0$ . Therefore  $\tilde{\mu}_3$  is an unbounded ray of Problem (4.9) and Problem (4.9) is unbounded.
- (b) Outcome  $F_{(4.11)}$ : Let  $(\hat{\psi}, \hat{u}_y, \hat{w})$  denote the optimal solution of Problem (4.11) and denote its optimal objective value as  $\mathcal{O}_{(4.11)}$ .

The proof is by a case analysis over two versions of Problem (4.9) in which  $w > 0$  and  $w = 0$ . Note first that  $\hat{\mu} := (\hat{\psi}, \hat{u}_y, \hat{w}, \hat{w}\hat{y}, \hat{w}\hat{v})$  is a feasible solution to Problem (4.9) and has an objective value of  $\mathcal{O}_{(4.11)}$ . Suppose  $w > 0$ , then by stating  $(y, v) = (\frac{y}{w}, \frac{v}{w})$ , Problem (4.9) becomes as follows:

$$\max_{w>0} \mathcal{O}(w), \quad (\text{C.1})$$

where

$$\begin{aligned} \mathcal{O}(w) &:= \max \psi^T(b - A\hat{x}) + u_y^T(h_y - G_{xy}\hat{x}) - w\mathcal{O} \\ \text{s.t. } & B^T\psi + G_y^T u_y \leq dw + c_y, \\ & \psi, u_y \geq 0. \end{aligned}$$

Note that Problem (C.1) is equivalent to Problem (4.11) where the nonnegativity constraint for  $w$  is restricted by strict inequality. Therefore,  $\max_{w>0} \mathcal{O}(w) \leq \mathcal{O}_{(4.11)}$ .

When  $w = 0$ , Problem (4.9) can be decomposed into Problem (4.11) with  $w$  fixed at 0 (i.e., a restriction of Problem (4.11)) and

$$\min\{d^T y - v^T(k + K_x \hat{x}) : By - K_\psi^T v \geq 0, K_s^T v \leq 0, y, v \geq 0\}. \quad (\text{C.3})$$

Note that Problem (C.3) is either unbounded or zero at optimality, since it has a trivial solution with all variables at zeros. Therefore, its optimum must be zero since otherwise Problem (4.10) is unbounded. This implies that the optimal objective value of Problem (4.9) when  $w = 0$  is also bounded above by  $\mathcal{O}_{(4.11)}$ , which proves that  $\hat{\mu}$  is the optimal solution of Problem (4.9).  $\square$

## C.2 Proof of Corollary 4.4.3

The proof of Theorem 4.4.1 implies that  $\hat{\mu}$  is an extreme point of Problem (4.9) if and only if  $\hat{\mu} = (\hat{\psi}, \hat{u}_y, \hat{w}, \hat{w}\hat{y}, \hat{w}\hat{v})$  for some  $(\hat{\psi}, \hat{u}_y, \hat{w}, \hat{y}, \hat{v}) \in \mathcal{J}_2 \times \mathcal{J}_1$ . Therefore, Equation (4.15a) holds. Likewise, the proof of Theorem 4.4.1 also indicates that  $\tilde{\mu}$  is an extreme ray of Problem (4.9) if and only if  $\tilde{\mu}$  corresponds to one of the following: (i)  $(0, 0, 0, \tilde{y}, \tilde{v})$  for  $(\tilde{y}, \tilde{v}) \in \mathcal{R}_1$ , (ii)  $(\tilde{\psi}, \tilde{u}_y, 0, 0, 0)$  for  $(\tilde{\psi}, \tilde{u}_y, 0) \in \mathcal{R}_2$ , or (iii)  $(\tilde{\psi}, \tilde{u}_y, \tilde{w}, \tilde{w}\hat{y}, \tilde{w}\hat{v})$  for  $(\hat{y}, \hat{v}) \in \mathcal{J}_1$  and  $(\tilde{\psi}, \tilde{u}_y, \tilde{w}) \in \mathcal{R}_2$  with  $\tilde{w} > 0$ . Thus, Equations (4.15b)-(4.15d) hold and are equivalent to the projection of the feasible region of the linear relaxation of Problem (MIP) onto the space of  $x$ .  $\square$

## C.3 Proof of Corollary 4.6.1

Built upon Theorem 4.4.1, it suffices to show that solving Problem (4.11)' is sufficient to obtain the optimal solution or unbounded ray of Problem (4.11). Note that, by defining  $(\psi', u'_y) = (\frac{\psi}{w+1}, \frac{u_y}{w+1})$ , Problem (4.11) becomes as follows:

$$\max \psi'^T(b - A\hat{x}) + u'_y{}^T(h_y - G_{xy}\hat{x}) + w \left[ \psi'^T(b - A\hat{x}) + u'_y{}^T(h_y - G_{xy}\hat{x}) - \mathcal{O} \right] \quad (\text{C.4a})$$

$$\text{s.t. } B^T\psi' + G_y^T u'_y \leq c_y, \quad (\text{C.4b})$$

$$\psi', u'_y, w \geq 0. \quad (\text{C.4c})$$

Suppose Problem (4.11)' has a finite optimum  $\mathcal{O}_{(4.11)'}$  at  $(\hat{\psi}, \hat{u}_y)$  and  $\mathcal{O}_{(4.11)'}$   $>$   $\mathcal{O}$ . Then, for any  $\alpha > 0$ ,  $(\psi', u'_y, w) = (\hat{\psi}, \hat{u}_y, \alpha)$  is feasible to Problem (C.4) and its objective value increases as  $\alpha$  increases, and thus Problem (C.4) is unbounded, so is Problem (4.11). Note that by converting  $(\psi', u'_y, w)$  to the solution of Problem (4.11) using  $(\psi', u'_y) = (\frac{\psi}{w+1}, \frac{u_y}{w+1})$ , we can see that  $(\hat{\psi}, \hat{u}_y, 1)$  is an unbounded ray of Problem (4.11). When  $\mathcal{O}_{(4.11)'}$   $\leq$   $\mathcal{O}$ , the term associated with  $w$  in Problem (C.4) can be disregarded, thus Problems (C.4) and (4.11)' have a finite optimum  $\mathcal{O}_{(C.4)}$  at  $(\hat{\psi}, \hat{u}_y, 0)$ . Otherwise, i.e., when Problem (4.11)' is unbounded with an unbounded ray of  $(\tilde{\psi}, \tilde{u}_y)$ , Problem (4.11) is unbounded by  $(\tilde{\psi}, \tilde{u}_y, 0)$ .  $\square$

## C.4 Proof of Corollary 4.6.2

Similar to the proof of Corollary 4.6.1, it suffices to show that solving Problem (4.11)'' is sufficient to obtain the optimal solution or unbounded ray of Problem (4.11). We define

$(\psi', u'_y) = (\frac{\psi}{w}, \frac{u_y}{w})$ , then Problem (4.11) becomes as follows:

$$\max w \left[ \psi'^T (b - A\hat{x}) + u'_y{}^T (h_y - G_{xy}\hat{x}) - \mathcal{O} \right] \quad (\text{C.5a})$$

$$\text{s.t. } B^T \psi' + G_y^T u'_y \leq d, \quad (\text{C.5b})$$

$$\psi', u'_y, w \geq 0. \quad (\text{C.5c})$$

The same analysis as in the proof of Corollary 4.6.1 holds; If Problem (4.11)'' has a finite optimum  $\mathcal{O}_{(4.11)''}$  at  $(\hat{\psi}, \hat{u}_y)$  and  $\mathcal{O}_{(4.11)''} > \mathcal{O}$ ,  $(\hat{\psi}, \hat{u}_y, 1)$  gives an unbounded ray of Problem (4.11). If  $\mathcal{O}_{(4.11)''} \leq \mathcal{O}$ ,  $(0, 0, 0)$  is an optimal solution of Problem (4.11). Otherwise, i.e., Problem (4.11)'' is unbounded by a feasible ray of  $(\tilde{\psi}, \tilde{u}_y)$ , Problem (4.11) is also unbounded by the feasible ray of  $(\tilde{\psi}, \tilde{u}_y, 0)$ .  $\square$

## BIBLIOGRAPHY

- [1] IEA, “Digitalisation and Energy,” Tech. rep., Paris, 2017.
- [2] Duenas-Osorio, L. and Vemuru, S. M., “Cascading failures in complex infrastructure systems,” *Structural safety*, Vol. 31, No. 2, 2009, pp. 157–167.
- [3] Dantzig, G. B. and Wolfe, P., “Decomposition principle for linear programs,” *Operations research*, Vol. 8, No. 1, 1960, pp. 101–111.
- [4] Benders, J. F., “Partitioning procedures for solving mixed-variables programming problems,” *Computational Management Science*, Vol. 2, No. 1, 2005, pp. 3–19.
- [5] Lübbecke, M. and Desrosiers, J., “Selected topics in column generation,” *Operations Research*, Vol. 53, No. 6, 2005, pp. 1007–1023.
- [6] Shahidehpoor, M. and Fu, Y., “Benders decomposition: applying Benders decomposition to power systems,” *IEEE Power and Energy Magazine*, Vol. 3, No. 2, 2005, pp. 20–21.
- [7] Glover, J. D., Sarma, M. S., and Overbye, T., *Power system analysis & design, SI version*, Cengage Learning, 2012.
- [8] Mokhatab, S., Poe, W. A., and Mak, J. Y., *Handbook of natural gas transmission and processing: principles and practices*, Gulf professional publishing, 2018.
- [9] Jünger, M., Liebling, T. M., Naddef, D., Nemhauser, G. L., Pulleyblank, W. R., Reinelt, G., Rinaldi, G., and Wolsey, L. A., *50 Years of integer programming 1958-2008: From the early years to the state-of-the-art*, Springer Science & Business Media, 2009.
- [10] Frank, S., Steponavice, I., and Rebennack, S., “Optimal power flow: a bibliographic survey I,” *Energy Systems*, Vol. 3, No. 3, 2012, pp. 221–258.
- [11] Momoh, J. A., *Electric power system applications of optimization*, CRC press, 2017.
- [12] Ela, E., Milligan, M., Bloom, A., Cochran, J., Botterud, A., Townsend, A., and Levin, T., “Overview of wholesale electricity markets,” *Electricity Markets with Increasing Levels of Renewable Generation: Structure, Operation, Agent-based Simulation, and Emerging Designs*, Springer, 2018, pp. 3–21.

- [13] Fisher, E. B., O'Neill, R. P., and Ferris, M. C., "Optimal transmission switching," *IEEE Transactions on Power Systems*, Vol. 23, No. 3, 2008, pp. 1346–1355.
- [14] Latorre, G., Cruz, R. D., Areiza, J. M., and Villegas, A., "Classification of publications and models on transmission expansion planning," *IEEE Transactions on Power Systems*, Vol. 18, No. 2, 2003, pp. 938–946.
- [15] Huneault, M. and Galiana, F., "A survey of the optimal power flow literature," *IEEE transactions on Power Systems*, Vol. 6, No. 2, 1991, pp. 762–770.
- [16] Molzahn, D. K., Hiskens, I. A., et al., "A survey of relaxations and approximations of the power flow equations," *Foundations and Trends® in Electric Energy Systems*, Vol. 4, No. 1-2, 2019, pp. 1–221.
- [17] Zohrizadeh, F., Josz, C., Jin, M., Madani, R., Lavaei, J., and Sojoudi, S., "A survey on conic relaxations of optimal power flow problem," *European Journal of Operational Research*, 2020.
- [18] Coffrin, C. and Van Hentenryck, P., "A linear-programming approximation of AC power flows," *INFORMS Journal on Computing*, Vol. 26, No. 4, 2014, pp. 718–734.
- [19] Jabr, R. A., "Radial distribution load flow using conic programming," *IEEE transactions on power systems*, Vol. 21, No. 3, 2006, pp. 1458–1459.
- [20] Bai, X., Wei, H., Fujisawa, K., and Wang, Y., "Semidefinite programming for optimal power flow problems," *International Journal of Electrical Power & Energy Systems*, Vol. 30, No. 6-7, 2008, pp. 383–392.
- [21] Gan, L. and Low, S. H., "Convex relaxations and linear approximation for optimal power flow in multiphase radial networks," *Power Systems Computation Conference (PSCC), 2014*, IEEE, 2014, pp. 1–9.
- [22] Lavaei, J. and Low, S. H., "Zero duality gap in optimal power flow problem," *IEEE Transactions on Power Systems*, Vol. 27, No. 1, 2011, pp. 92–107.
- [23] Low, S. H., "Convex relaxation of optimal power flow—Part I: Formulations and equivalence," *IEEE Transactions on Control of Network Systems*, Vol. 1, No. 1, 2014, pp. 15–27.
- [24] Low, S. H., "Convex relaxation of optimal power flow—Part II: Exactness," *IEEE Transactions on Control of Network Systems*, Vol. 1, No. 2, 2014, pp. 177–189.
- [25] Kocuk, B., Dey, S. S., and Sun, X. A., "Strong SOCP relaxations for the optimal power flow problem," *Operations Research*, Vol. 64, No. 6, 2016, pp. 1177–1196.
- [26] Kocuk, B., Dey, S. S., and Sun, X. A., "Matrix minor reformulation and SOCP-based spatial branch-and-cut method for the AC optimal power flow problem," *Mathematical Programming Computation*, Vol. 10, No. 4, 2018, pp. 557–596.

- [27] Coffrin, C., Hijazi, H. L., and Van Hentenryck, P., “The QC relaxation: A theoretical and computational study on optimal power flow,” *IEEE Transactions on Power Systems*, Vol. 31, No. 4, 2015, pp. 3008–3018.
- [28] Jabr, R. A., “A conic quadratic format for the load flow equations of meshed networks,” *IEEE Transactions on Power Systems*, Vol. 22, No. 4, 2007, pp. 2285–2286.
- [29] Coffrin, C., Hijazi, H., and Van Hentenryck, P., “Alternating current (AC) power flow analysis in an electrical power network,” March 17 2020, US Patent 10,591,520.
- [30] Baradar, M. and Hesamzadeh, M. R., “AC power flow representation in conic format,” *IEEE Transactions on Power Systems*, Vol. 30, No. 1, 2014, pp. 546–547.
- [31] Thorley, A. and Tiley, C., “Unsteady and transient flow of compressible fluids in pipelines—a review of theoretical and some experimental studies,” *International journal of heat and fluid flow*, Vol. 8, No. 1, 1987, pp. 3–15.
- [32] Osiadacz, A. J. and Control systems centre (Manchester, GB), “Simulation and analysis of gas networks,” 1987.
- [33] Weymouth, T. R., “Problems in natural gas engineering,” *Transactions of the American Society of Mechanical Engineers*, Vol. 34, No. 1349, 1912, pp. 185–231.
- [34] Ríos-Mercado, R. Z. and Borraz-Sánchez, C., “Optimization problems in natural gas transportation systems: A state-of-the-art review,” *Applied Energy*, Vol. 147, 2015, pp. 536–555.
- [35] Borraz-Sánchez, C., Bent, R., Backhaus, S., Hijazi, H., and Hentenryck, P. V., “Convex relaxations for gas expansion planning,” *INFORMS Journal on Computing*, Vol. 28, No. 4, 2016, pp. 645–656.
- [36] De Wolf, D. and Smeers, Y., “The gas transmission problem solved by an extension of the simplex algorithm,” *Management Science*, Vol. 46, No. 11, 2000, pp. 1454–1465.
- [37] Correa-Posada, C. M. and Sanchez-Martin, P., “Integrated power and natural gas model for energy adequacy in short-term operation,” *IEEE Transactions on Power Systems*, Vol. 30, No. 6, 2014, pp. 3347–3355.
- [38] Shao, C., Wang, X., Shahidehpour, M., Wang, X., and Wang, B., “An MILP-based optimal power flow in multicarrier energy systems,” *IEEE Transactions on Sustainable Energy*, Vol. 8, No. 1, 2016, pp. 239–248.
- [39] Ordoudis, C., Pinson, P., and Morales, J. M., “An integrated market for electricity and natural gas systems with stochastic power producers,” *European Journal of Operational Research*, Vol. 272, No. 2, 2019, pp. 642–654.
- [40] Singh, M. K. and Kekatos, V., “Natural Gas Flow Solvers using Convex Relaxation,” *IEEE Transactions on Control of Network Systems*, 2020.

- [41] Singh, M. K. and Kekatos, V., “Natural gas flow equations: Uniqueness and an MI-SOCP solver,” *2019 American Control Conference (ACC)*, IEEE, 2019, pp. 2114–2120.
- [42] Manshadi, S. D. and Khodayar, M. E., “A tight convex relaxation for the natural gas operation problem,” *IEEE Transactions on Smart Grid*, Vol. 9, No. 5, 2018, pp. 5467–5469.
- [43] Zlotnik, A., Chertkov, M., and Backhaus, S., “Optimal control of transient flow in natural gas networks,” *2015 54th IEEE conference on decision and control (CDC)*, IEEE, 2015, pp. 4563–4570.
- [44] Yamangil, E., Bent, R., and Backhaus, S., “Resilient Upgrade of Electrical Distribution Grids.” *AAAI*, 2015, pp. 1233–1240.
- [45] Ahmed, S., “A scenario decomposition algorithm for 0–1 stochastic programs,” *Operations Research Letters*, Vol. 41, No. 6, 2013, pp. 565–569.
- [46] Du Merle, O., Villeneuve, D., Desrosiers, J., and Hansen, P., “Stabilized column generation,” *Discrete Mathematics*, Vol. 194, No. 1-3, 1999, pp. 229–237.
- [47] Bent, R., Blumsack, S., Van Hentenryck, P., Borraz-Sánchez, C., and Shahriari, M., “Joint Electricity and Natural Gas Transmission Planning with Endogenous Market Feedbacks,” *IEEE Transactions on Power Systems*, Vol. 33, No. 6, 2018, pp. 6397–6409.
- [48] Labbé, M., Marcotte, P., and Savard, G., “A bilevel model of taxation and its application to optimal highway pricing,” *Management science*, Vol. 44, No. 12-part-1, 1998, pp. 1608–1622.
- [49] Fontaine, P. and Minner, S., “Benders decomposition for discrete–continuous linear bilevel problems with application to traffic network design,” *Transportation Research Part B: Methodological*, Vol. 70, 2014, pp. 163–172.
- [50] Scaparra, M. P. and Church, R. L., “A bilevel mixed-integer program for critical infrastructure protection planning,” *Computers & Operations Research*, Vol. 35, No. 6, 2008, pp. 1905–1923.
- [51] Wood, R. K., “Bilevel network interdiction models: Formulations and solutions,” *Wiley encyclopedia of operations research and management science*, 2010.
- [52] Jeroslow, R. G., “The polynomial hierarchy and a simple model for competitive analysis,” *Mathematical programming*, Vol. 32, No. 2, 1985, pp. 146–164.
- [53] Byeon, G., Van Hentenryck, P., Bent, R., and Nagarajan, H., “Communication-constrained expansion planning for resilient distribution systems,” *arXiv preprint arXiv:1801.03520*, 2018.

- [54] Byeon, G. and Van Hentenryck, P., “Benders Subproblem Decomposition for Discrete-Continuous Bilevel Problems,” *arXiv preprint arXiv:1902.04375*, 2019.
- [55] Byeon, G. and Van Hentenryck, P., “Unit Commitment with Gas Network Awareness,” *IEEE Transactions on Power Systems*, 2019, pp. 1–1.
- [56] Executive Office of the President, “Economic Benefits of Increasing Electric Grid Resilience to Weather Outages,” Tech. rep., 2013.
- [57] Lasseter, R., Akhil, A., Marnay, C., Stephens, J., Dagle, J., Guttromson, R., Meliopoulos, A., Yinger, R., and Eto, J., “The CERTS microgrid concept,” *White paper for Transmission Reliability Program, Office of Power Technologies, US Department of Energy*, Vol. 2, No. 3, 2002, pp. 30.
- [58] Resende, F., Gil, N., and Lopes, J., “Service restoration on distribution systems using Multi-MicroGrids,” *International Transactions on Electrical Energy Systems*, Vol. 21, No. 2, 2011, pp. 1327–1342.
- [59] Wang, Y., Chen, C., Wang, J., and Baldick, R., “Research on resilience of power systems under natural disasters: A review,” *IEEE Transactions on Power Systems*, Vol. 31, No. 2, 2016, pp. 1604–1613.
- [60] Panteli, M., Trakas, D. N., Mancarella, P., and Hatziargyriou, N. D., “Power Systems Resilience Assessment: Hardening and Smart Operational Enhancement Strategies,” *Proceedings of the IEEE*, Vol. 105, No. 7, July 2017, pp. 1202–1213.
- [61] Falahati, B., Fu, Y., and Wu, L., “Reliability assessment of smart grid considering direct cyber-power interdependencies,” *IEEE Transactions on Smart Grid*, Vol. 3, No. 3, 2012, pp. 1515–1524.
- [62] Gholami, A., Aminifar, F., and Shahidehpour, M., “Front lines against the darkness: Enhancing the resilience of the electricity grid through microgrid facilities,” *IEEE Electrification Magazine*, Vol. 4, No. 1, 2016, pp. 18–24.
- [63] Martins, L., Girao-Silva, R., Jorge, L., Gomes, A., Musumeci, F., and Rak, J., “Interdependence between Power Grids and Communication Networks: A Resilience Perspective,” *DRCN 2017-Design of Reliable Communication Networks; 13th International Conference; Proceedings of, VDE*, 2017, pp. 1–9.
- [64] Li, Z., Shahidehpour, M., Aminifar, F., Alabdulwahab, A., and Al-Turki, Y., “Networked Microgrids for Enhancing the Power System Resilience,” *Proceedings of the IEEE*, Vol. 105, No. 7, July 2017, pp. 1289–1310.
- [65] Barnes, A., Nagarajan, H., Yamangil, E., Bent, R., and Backhaus, S., “Tools for improving resilience of electric distribution systems with networked microgrids,” *CoRR*, Vol. abs/1705.08229, 2017.

- [66] Oukil, A., Amor, H. B., Desrosiers, J., and El Gueddari, H., “Stabilized column generation for highly degenerate multiple-depot vehicle scheduling problems,” *Computers & Operations Research*, Vol. 34, No. 3, 2007, pp. 817–834.
- [67] Amor, H. M. B., Desrosiers, J., and Frangioni, A., “On the choice of explicit stabilizing terms in column generation,” *Discrete Applied Mathematics*, Vol. 157, No. 6, 2009, pp. 1167–1184.
- [68] Chen, C., Wang, J., Qiu, F., and Zhao, D., “Resilient distribution system by microgrids formation after natural disasters,” *IEEE Transactions on smart grid*, Vol. 7, No. 2, 2016, pp. 958–966.
- [69] Ding, T., Lin, Y., Li, G., and Bie, Z., “A new model for resilient distribution systems by microgrids formation,” *IEEE Transactions on Power Systems*, Vol. 32, No. 5, 2017, pp. 4145–4147.
- [70] Gao, H., Chen, Y., Xu, Y., and Liu, C. C., “Resilience-Oriented Critical Load Restoration Using Microgrids in Distribution Systems,” *IEEE Trans. on Smart Grid*, Vol. PP, No. 99, 2016, pp. 1–1.
- [71] Yuan, C., Illindala, M. S., and Khalsa, A. S., “Modified Viterbi algorithm based distribution system restoration strategy for grid resiliency,” *IEEE Transactions on Power Delivery*, Vol. 32, No. 1, 2017, pp. 310–319.
- [72] Wang, Z., Chen, B., Wang, J., and Chen, C., “Networked microgrids for self-healing power systems,” *IEEE Transactions on smart grid*, Vol. 7, No. 1, 2016, pp. 310–319.
- [73] Yuan, W., Wang, J., Qiu, F., Chen, C., Kang, C., and Zeng, B., “Robust optimization-based resilient distribution network planning against natural disasters,” *IEEE Transactions on Smart Grid*, Vol. 7, No. 6, 2016, pp. 2817–2826.
- [74] Carvalho, P., Ferreira, L., and Da Silva, A. C., “A decomposition approach to optimal remote controlled switch allocation in distribution systems,” *IEEE Transactions on Power Delivery*, Vol. 20, No. 2, 2005, pp. 1031–1036.
- [75] Xu, Y., Liu, C.-C., Schneider, K. P., and Ton, D. T., “Placement of remote-controlled switches to enhance distribution system restoration capability,” *IEEE Transactions on Power Systems*, Vol. 31, No. 2, 2016, pp. 1139–1150.
- [76] Parhizi, S., Lotfi, H., Khodaei, A., and Bahramirad, S., “State of the art in research on microgrids: A review,” *IEEE Access*, Vol. 3, 2015, pp. 890–925.
- [77] McCormick, G. P., “Computability of global solutions to factorable nonconvex programs: Part I Convex underestimating problems,” *Mathematical programming*, Vol. 10, No. 1, 1976, pp. 147–175.
- [78] Kersting, W., “Radial distribution test feeders,” *IEEE Transactions on Power Systems*, Vol. 6, No. 3, 1991, pp. 975–985.

- [79] U.S. Energy Information Administration, “Annual Energy Outlook 2014,” Tech. rep., 2014.
- [80] Bialek, T., “Private Communications, San Diego Gas and Electric,” 2014.
- [81] State of Virginia Corporation Commission, “Placement of Utility Distribution Lines Underground,” Tech. Rep. House Document 30, Governor and the General Assembly of Virginia, Richmond, VA, 2005.
- [82] Sa, Y., *Reliability Analysis of Electric Distribution Lines*, Ph.D. thesis, McGill University, 2002.
- [83] PJM, “Analysis of Operational Events and Market Impacts During the January 2014 Cold Weather Events,” , 2014.
- [84] FERC, “Ruling in docket el14-45-000,” , 2015.
- [85] Liu, C., Shahidehpour, M., Fu, Y., and Li, Z., “Security-constrained unit commitment with natural gas transmission constraints,” *IEEE Transactions on Power Systems*, Vol. 24, No. 3, 2009, pp. 1523–1536.
- [86] Liu, C., Shahidehpour, M., and Wang, J., “Coordinated scheduling of electricity and natural gas infrastructures with a transient model for natural gas flow,” *Chaos: An Interdisciplinary Journal of Nonlinear Science*, Vol. 21, No. 2, 2011, pp. 025102.
- [87] Martinez-Mares, A. and Fuerte-Esquivel, C. R., “A unified gas and power flow analysis in natural gas and electricity coupled networks,” *IEEE Transactions on Power Systems*, Vol. 27, No. 4, 2012, pp. 2156–2166.
- [88] Correa-Posada, C. M. and Sanchez-Martin, P., “Security-constrained optimal power and natural-gas flow,” *IEEE Transactions on Power Systems*, Vol. 29, No. 4, 2014, pp. 1780–1787.
- [89] Correa-Posada, C. M. and Sánchez-Martín, P., “Integrated power and natural gas model for energy adequacy in short-term operation,” *IEEE Transactions on Power Systems*, Vol. 30, No. 6, 2015, pp. 3347–3355.
- [90] Alabdulwahab, A., Abusorrah, A., Zhang, X., and Shahidehpour, M., “Coordination of interdependent natural gas and electricity infrastructures for firming the variability of wind energy in stochastic day-ahead scheduling,” *IEEE Transactions on Sustainable Energy*, Vol. 6, No. 2, 2015, pp. 606–615.
- [91] Biskas, P., Kanelakis, N., Papamathaiou, A., and Alexandridis, I., “Coupled optimization of electricity and natural gas systems using augmented Lagrangian and an alternating minimization method,” *International Journal of Electrical Power & Energy Systems*, Vol. 80, 2016, pp. 202–218.

- [92] Li, G., Zhang, R., Jiang, T., Chen, H., Bai, L., and Li, X., “Security-constrained bi-level economic dispatch model for integrated natural gas and electricity systems considering wind power and power-to-gas process,” *Applied energy*, Vol. 194, 2017, pp. 696–704.
- [93] Zhao, B., Conejo, A. J., and Sioshansi, R., “Unit commitment under gas-supply uncertainty and gas-price variability,” *IEEE Transactions on Power Systems*, Vol. 32, No. 3, 2017, pp. 2394–2405.
- [94] Zlotnik, A., Roald, L., Backhaus, S., Chertkov, M., and Andersson, G., “Coordinated scheduling for interdependent electric power and natural gas infrastructures,” *IEEE Transactions on Power Systems*, Vol. 32, No. 1, 2017, pp. 600–610.
- [95] Chen, R., Wang, J., and Sun, H., “Clearing and pricing for coordinated gas and electricity day-ahead markets considering wind power uncertainty,” *IEEE Transactions on Power Systems*, Vol. 33, No. 3, 2018, pp. 2496–2508.
- [96] Ordoudis, C., Delikaraoglou, S., Pinson, P., and Kazempour, J., “Exploiting flexibility in coupled electricity and natural gas markets: A price-based approach,” *PowerTech, 2017 IEEE Manchester*, IEEE, 2017, pp. 1–6.
- [97] Gil, M., Dueñas, P., and Reneses, J., “Electricity and natural gas interdependency: comparison of two methodologies for coupling large market models within the European regulatory framework,” *IEEE Transactions on Power Systems*, Vol. 31, No. 1, 2016, pp. 361–369.
- [98] Chen, Y., Wei, W., Liu, F., and Mei, S., “A multi-lateral trading model for coupled gas-heat-power energy networks,” *Applied energy*, Vol. 200, 2017, pp. 180–191.
- [99] Wang, C., Wei, W., Wang, J., Wu, L., and Liang, Y., “Equilibrium of interdependent gas and electricity markets with marginal price based bilateral energy trading,” *IEEE Transactions on Power Systems*, Vol. 33, No. 5, 2018, pp. 4854–4867.
- [100] Ji, Z. and Huang, X., “Coordinated bidding strategy in synchronized electricity and natural gas markets,” *Energy, Power and Transportation Electrification (ACEPT), 2017 Asian Conference on*, IEEE, 2017, pp. 1–6.
- [101] Ji, Z. and Huang, X., “Day-Ahead Schedule and Equilibrium for the Coupled Electricity and Natural Gas Markets,” *IEEE Access*, Vol. 6, 2018, pp. 27530–27540.
- [102] Zhao, B., Zlotnik, A., Conejo, A. J., Sioshansi, R., and Rudkevich, A. M., “Shadow Price-Based Co-ordination of Natural Gas and Electric Power Systems,” *IEEE Transactions on Power Systems*, 2018.
- [103] Sánchez, C. B., Bent, R., Backhaus, S., Blumsack, S., Hijazi, H., and Van Hentenryck, P., “Convex optimization for joint expansion planning of natural gas and power systems,” *System Sciences (HICSS), 2016 49th Hawaii International Conference on*, IEEE, 2016, pp. 2536–2545.

- [104] Misra, S., Fisher, M. W., Backhaus, S., Bent, R., Chertkov, M., and Pan, F., “Optimal compression in natural gas networks: A geometric programming approach,” *IEEE transactions on control of network systems*, Vol. 2, No. 1, 2015, pp. 47–56.
- [105] Morales-España, G., Latorre, J. M., and Ramos, A., “Tight and compact MILP formulation for the thermal unit commitment problem,” *IEEE Transactions on Power Systems*, Vol. 28, No. 4, 2013, pp. 4897–4908.
- [106] Fischetti, M., Salvagnin, D., and Zanette, A., “A note on the selection of Benders cuts,” *Mathematical Programming*, Vol. 124, No. 1-2, 2010, pp. 175–182.
- [107] Fischetti, M., Ljubic, I., and Sinnl, M., “Redesigning Benders Decomposition for Large-Scale Facility Location,” *Management Science*, Vol. 63, 2017, pp. 2146–2162.
- [108] Allen, E. H., Lang, J. H., and Ilic, M. D., “A combined equivalenced-electric, economic, and market representation of the northeastern power coordinating council us electric power system,” *IEEE Transactions on Power Systems*, Vol. 23, No. 3, 2008, pp. 896–907.
- [109] Krall, E., Higgins, M., and O'Neill, R. P., “RTO unit commitment test system,” *Federal Energy Regulatory Commission*, 2012.
- [110] Steven Levine, P. C. A. T., “Understanding natural gas markets,” 2014, <https://www.api.org/~media/Files/Oil-and-Natural-Gas/Natural-Gas/API-Understanding-Natural-Gas-Markets.pdf>.
- [111] FERC, “Ruling in docket RM13-17-000,” , 2013.
- [112] Zavala, V. M., Kim, K., Anitescu, M., and Birge, J., “A stochastic electricity market clearing formulation with consistent pricing properties,” *Operations Research*, Vol. 65, No. 3, 2017, pp. 557–576.
- [113] Zakeri, G., Pritchard, G., Bjorndal, M., and Bjorndal, E., “Pricing Wind: A Revenue Adequate, Cost Recovering Uniform Price Auction for Electricity Markets with Intermittent Generation,” *INFORMS Journal on Optimization*, Vol. 1, No. 1, 2018, pp. 35–48.
- [114] Philpott, A., Ferris, M., and Wets, R., “Equilibrium, uncertainty and risk in hydro-thermal electricity systems,” *Mathematical Programming*, Vol. 157, No. 2, 2016, pp. 483–513.
- [115] Pritchard, G., Zakeri, G., and Philpott, A., “A single-settlement, energy-only electric power market for unpredictable and intermittent participants,” *Operations research*, Vol. 58, No. 4-part-2, 2010, pp. 1210–1219.
- [116] Morales, J. M., Zugno, M., Pineda, S., and Pinson, P., “Electricity market clearing with improved scheduling of stochastic production,” *European Journal of Operational Research*, Vol. 235, No. 3, 2014, pp. 765–774.

- [117] Dempe, S., *Foundations of bilevel programming*, Springer Science & Business Media, 2002.
- [118] Côté, J.-P., Marcotte, P., and Savard, G., “A bilevel modelling approach to pricing and fare optimisation in the airline industry,” *Journal of Revenue and Pricing Management*, Vol. 2, No. 1, 2003, pp. 23–36.
- [119] Fampa, M., Barroso, L., Candal, D., and Simonetti, L., “Bilevel optimization applied to strategic pricing in competitive electricity markets,” *Computational Optimization and Applications*, Vol. 39, No. 2, 2008, pp. 121–142.
- [120] Aussel, D., Brotcorne, L., Lepaul, S., and von Niederhäusern, L., “A Trilevel Model for Best Response in Energy Demand-Side Management,” *European Journal of Operational Research*, 2019.
- [121] Lai, C. and Xu, L., “Bilevel Fee-Setting Optimization for Cloud Monitoring Service Under Uncertainty,” *IEEE Access*, Vol. 6, 2018, pp. 9473–9483.
- [122] Yue, D. and You, F., “Game-theoretic modeling and optimization of multi-echelon supply chain design and operation under Stackelberg game and market equilibrium,” *Computers & Chemical Engineering*, Vol. 71, 2014, pp. 347–361.
- [123] Alguacil, N., Delgado, A., and Arroyo, J. M., “A trilevel programming approach for electric grid defense planning,” *Computers & Operations Research*, Vol. 41, 2014, pp. 282–290.
- [124] Borrero, J. S., Prokopyev, O. A., and Sauré, D., “Sequential interdiction with incomplete information and learning,” *Operations Research*, Vol. 67, No. 1, 2019, pp. 72–89.
- [125] Colson, B., Marcotte, P., and Savard, G., “Bilevel programming: A survey,” *4or*, Vol. 3, No. 2, 2005, pp. 87–107.
- [126] Grimm, V., Kleinert, T., Liers, F., Schmidt, M., and Zöttl, G., “Optimal price zones of electricity markets: a mixed-integer multilevel model and global solution approaches,” *Optimization methods and software*, Vol. 34, No. 2, 2019, pp. 406–436.
- [127] Ambrosius, M., Grimm, V., Kleinert, T., Liers, F., Schmidt, M., and Zöttl, G., “Endogenous price zones and investment incentives in electricity markets: an application of multilevel optimization with graph partitioning,” *Available at SSRN 3271827*, 2018.
- [128] Kleinert, T. and Schmidt, M., “Global optimization of multilevel electricity market models including network design and graph partitioning,” *Discrete Optimization*, 2019.
- [129] Sun, H., Gao, Z., and Wu, J., “A bi-level programming model and solution algorithm for the location of logistics distribution centers,” *Applied mathematical modelling*, Vol. 32, No. 4, 2008, pp. 610–616.

- [130] Arslan, O., Jabali, O., and Laporte, G., “Exact solution of the evasive flow capturing problem,” *Operations Research*, Vol. 66, No. 6, 2018, pp. 1625–1640.
- [131] Cao, D. and Chen, M., “Capacitated plant selection in a decentralized manufacturing environment: a bilevel optimization approach,” *European Journal of Operational Research*, Vol. 169, No. 1, 2006, pp. 97–110.
- [132] Garcés, L. P., Conejo, A. J., García-Bertrand, R., and Romero, R., “A bilevel approach to transmission expansion planning within a market environment,” *IEEE Transactions on Power Systems*, Vol. 24, No. 3, 2009, pp. 1513–1522.
- [133] Zare, M. H., Borrero, J. S., Zeng, B., and Prokopyev, O. A., “A note on linearized reformulations for a class of bilevel linear integer problems,” *Annals of Operations Research*, Vol. 272, No. 1-2, 2019, pp. 99–117.
- [134] Saharidis, G. K. and Ierapetritou, M. G., “Resolution method for mixed integer bilevel linear problems based on decomposition technique,” *Journal of Global Optimization*, Vol. 44, No. 1, 2009, pp. 29–51.
- [135] Moore, J. T. and Bard, J. F., “The mixed integer linear bilevel programming problem,” *Operations research*, Vol. 38, No. 5, 1990, pp. 911–921.
- [136] DeNegre, S. T. and Ralphs, T. K., “A branch-and-cut algorithm for integer bilevel linear programs,” *Operations research and cyber-infrastructure*, Springer, 2009, pp. 65–78.
- [137] DeNegre, S., “Interdiction and discrete bilevel linear programming,” 2011.
- [138] Fischetti, M., Ljubić, I., Monaci, M., and Sinnl, M., “A new general-purpose algorithm for mixed-integer bilevel linear programs,” *Operations Research*, Vol. 65, No. 6, 2017, pp. 1615–1637.
- [139] Caramia, M. and Mari, R., “Enhanced exact algorithms for discrete bilevel linear problems,” *Optimization Letters*, Vol. 9, No. 7, 2015, pp. 1447–1468.
- [140] Ben-Ameur, W. and Neto, J., “Acceleration of cutting-plane and column generation algorithms: Applications to network design,” *Networks: An International Journal*, Vol. 49, No. 1, 2007, pp. 3–17.
- [141] Fischetti, M., Ljubić, I., and Sinnl, M., “Redesigning Benders decomposition for large-scale facility location,” *Management Science*, Vol. 63, No. 7, 2016, pp. 2146–2162.
- [142] Schrijver, A., *Theory of linear and integer programming*, John Wiley & Sons, 1998.
- [143] Ehrgott, M., *Multicriteria optimization*, Vol. 491, Springer Science & Business Media, 2005.